

CATAHOULA FORMATION
OF THE TEXAS COASTAL PLAIN:
ORIGIN, GEOCHEMICAL EVOLUTION,
AND CHARACTERISTICS
OF URANIUM DEPOSITS

William E. Galloway

and

W. R. Kaiser

Assisted by

C. S. Childs, R. S. Fisher, B. D. Johnson,
S. M. Sutton, Jr., and B. R. Van Allen

Project funded by
Bendix Field Engineering Corporation
Contract No. 77-063-E

Bureau of Economic Geology
The University of Texas at Austin
Austin, Texas 78712
W. L. Fisher, Director

1979

CONTENTS

Abstract	1
Introduction	3
Objectives	8
Data and methodology	8
Source and mobilization of uranium	10
Diagenesis of fresh volcanic glass	13
Syndepositional diagenesis	13
Postdepositional diagenesis	15
Uranium mobilization	18
Summary	23
Geochemical and physical aspects of uranium transport	26
Hydrochemistry of the Catahoula aquifer	27
Early ground-water composition	27
Burial and exhumation phase hydrochemistry	29
Chita-Corrigan fluvial system	32
Gueydan fluvial system	33
Eh and pH	39
Uranium mobility	39
Flow dynamics of the Catahoula aquifer	41
Chita-Corrigan aquifer	42
Gueydan aquifer	45
Uranium Concentration I: Characteristics and habitat of Catahoula uranium deposits	50
Bruni deposit	51
Uranium and trace metals distribution	51
Major element distribution	55
Mineralogy and diagenesis	57
House-Seale deposit	60
Uranium and trace metal distribution	62
Major element distribution	66
Mineralogy and diagenesis	67
Washington-Fayette deposit	72
Uranium and trace metal distribution	72
Major element distribution	79

Mineralogy and diagenesis	79
Summary comparision of deposits	83
Uranium Concentration II: Mineralization geochemistry	85
Concentration mechanisms	85
Physical	85
Chemical	86
Deposit Mineralogy	90
Iron sulfides	90
Trace metals and organic matter	93
Paragenetic sequence	93
Summary	95
Uranium Concentration III: Deposit hydrochemistry	96
Mineral-solution equilibria	96
Uranium occurrence	103
Holiday - El Mesquite	103
Bruni	103
O'Hern	110
Piedre Lumbre	110
Summary and exploration implications	120
Conclusions	122
References	126
Appendix A: Key free energy values	134
Appendix B: Calculation of free energies of formation for montmorillonite and clinoptilolite	137

FIGURES

1.	Depositional systems and principal genetic facies of the Catahoula Formation	4
2.	Diagrammatic representation of the two principal phases of uranium cycle interpreted for Catahoula fluvial systems.	6
3.	Index map showing outcrop belt, section localities, and special-purpose study areas.	9
4.	Schematic tabulation of genetic facies, mineralogical composition, and uranium content of potential uranium source rocks in the Gueydan fluvial system.	11
5.	Schematic tabulation of genetic facies, mineralogical composition, and uranium content of potential uranium source rocks in the Chita-Corrigan fluvial system.	12
6.	Pedogenic features of tuffaceous sand and mudstones.	14
7.	Features produced by open hydrologic system diagenesis of glass.	17
8.	Lacustrine sequence showing uranium enrichment in the carbonaceous basal clay.	25
9.	Schematic uranium mobilization pathways during successive depositional, pedogenic, and diagenetic events that alter volcanic glass.	25
10.	Hydrochemistry of modern Catahoula ground waters.	30
11.	Hydrochemical facies map of select study areas of the Gueydan and Chita-Corrigan aquifer systems.	34
12.	Mode and range of total dissolved solids in all waters of each hydrochemical facies of the Chita-Corrigan and Gueydan systems.	36
13.	Schematic flow and mixing patterns for Chita Corrigan and Gueydan aquifer systems	37
14.	Published measured pH of ground-water samples from the Gueydan and Chita-Corrigan systems.	40
15.	Net sand and log-derived apparent ground-water chlorinity for a portion of the lower Chita-Corrigan fluvial system.	43
16.	Strike and dip cross sections of the Chita-Corrigan aquifer showing apparent chlorinity patterns within individual aquifer sands.	44

17.	Net sand and apparent chlorinity maps for upper and lower intervals of a portion of the Gueydan fluvial system.	46
18.	Dip cross section of the Gueydan system showing apparent chlorinity patterns within major sand sequences.	48
19.	Geologic setting of the Bruni and nearby uranium deposits.	52
20.	Core cross section of Bruni oxidation/alteration front.	53
21.	Distribution and mineralogical form of sulfur and iron along a core cross section of the Bruni front.	56
22.	Petrographic composition of Bruni host sand.	58
23.	Distribution of weight percent carbonate across Bruni alteration front.	59
24.	Geologic setting of the House-Seale and associated deposits of the northern Live Oak district.	61
25.	Geochemical and mineralogical variations within sections from walls of the House-Seale open-pit mine.	65
26.	Scanning electron microscope spectra and micrograph of uranium-bearing material, House-Seale deposit.	68
27.	Paragenetic sequence displayed by tuffaceous host sands of Bruni deposit.	70
28.	Geologic setting of the Washington-Fayette deposit.	73
29.	Uranium and trace element distribution in cores of the Washington-Fayette oxidation/alteration tongue.	74
30.	Distribution of sulfide and sulfate around the periphery of the Washington-Fayette oxidation/alteration tongue.	80
31.	Distribution of carbonate around the periphery of the Washington-Fayette oxidation/alteration tongue.	81
32.	Petrographic composition of the Washington-Fayette host sand.	82
33.	Eh-pH diagram showing the stability of $USiO_4$	87
34.	Eh-pH diagram showing the stability of benzoic acid.	88
35.	The effect of pH on the stability of UO_2 and $USiO_4$	89
36.	Pathways of iron sulfide formation.	91
37.	Eh-pH diagram showing the stability of mackinawite and elemental sulfur.	92

38.	Plot of average deposit waters on Ca-montmorillonite - Na-montmorillonite activity diagram.	100
39.	Plot of average deposit waters on Ca-montmorillonite - clinoptilolite activity diagram.	101
40.	Plot of average deposit waters on Na-montmorillonite - clinoptilolite activity diagram.	102
41.	Plot of Holiday-El Mesquite waters on Ca-montmorillonite - clinoptilolite activity diagram.	104
42.	Map of Y-axis values from Holiday-El Mesquite Ca-montmorillonite - clinoptilolite activity diagram.	105
43.	Map of Holiday - El Mesquite log IAP/Ksp values for Ca-montmorillonite.	106
44.	Map of Holiday - El Mesquite log IAP/Ksp values for calcite.	107
45.	Plot of Bruni waters on Ca-montmorillonite - clinoptilolite activity diagram.	108
46.	Map of Y-axis values from Bruni (Grid Y) Ca-montmorillonite - clinoptilolite activity diagram.	109
47.	Map of Bruni log IAP/Ksp values for Ca-montmorillonite.	111
48.	Map of Bruni log IAP/Ksp values for calcite.	112
49.	Map of the ratio Y/X axis from O'Hern Ca-montmorillonite - clinoptilolite activity diagram.	113
50.	Plot of O'Hern waters on Ca-montmorillonite - clinoptilolite activity diagram.	114
51.	Map of O'Hern log IAP/Ksp values for Ca-montmorillonite.	115
52.	Map of O'Hern log IAP/Ksp values for calcite.	116
53.	Plot of Piedre Lumbre waters on Na-montmorillonite - clinoptilolite activity diagram.	117
54.	Map of X-axis values from Piedre Lumbre Na-montmorillonite - clinoptilolite activity diagram.	118
55.	Map of Y-axis values from Piedre Lumbre Ca-montmorillonite - clinoptilolite activity diagram.	119
56.	Family tree of Catahoula uranium deposits based on the various likely geochemical histories.	124

TABLES

1.	Uranium content of various depositional facies, Catahoula fluvial systems.	19
2.	Analytical and petrologic data, Bruni samples.	54
3.	Analytical and petrologic data, House-Seale deposit.	63
4.	Analytical and petrologic data, Washington-Fayette deposit.	75
5.	Summary of paragenetic sequence.	94
6.	Average concentration mg/l.	97
7.	Negative log average activity.	97
8.	Saturation ratios, average log IAP/Ksp values.	99

tr
tic

th
cl
sh
ef
gl
de
as
si
C
l
d
d
c
i

CATAHOULA FORMATION OF THE TEXAS COASTAL PLAIN:
ORIGIN, GEOCHEMICAL EVOLUTION, AND CHARACTERISTICS
OF URANIUM DEPOSITS

W. E. Galloway and W. R. Kaiser

ABSTRACT

The Catahoula Formation is composed of ancient fluvial sediments that controlled a wide range of water-sediment interactions responsible for uranium mobilization, transportation, and concentration.

Uranium was released from volcanic glass deposited within the Catahoula through early pedogenic and diagenetic processes. Soil development produced plasmic clay cutans, oxide nodules, and vacuoles; open hydrologic system diagenesis produced shard-moldic porosity and clinoptilolite pore-filling cement. Pedogenesis was the most efficient process for mobilizing uranium. Original uranium content in fresh Catahoula glass is estimated to have averaged at least 10 ppm; about 5 ppm was mobilized after deposition and made available for migration. Uranium was transported predominantly as uranyl dicarbonate ion by oxidizing neutral to mildly basic, bicarbonate- and silica-rich ground waters. Uranium transport is continuing today in parts of the Catahoula aquifer in oxidizing (+240 to +300 mV) and neutral to highly basic (pH 7 to 11) ground waters. The chemistry of modern Catahoula ground waters reflects downflow ionic evolution and localized mixing with compositionally diverse waters discharged vertically from underlying aquifers.

Chlorinity mapping reveals modern ground-water flow patterns, suggests hydrodynamic interpretation of alteration-front geometry, and provides clues to flow dynamics extant during earlier aquifer evolution. Isochemical contours reproduce geometries

reminiscent of alteration fronts, reveal vertical discharge of saline waters across aquitards and up fault zones, and demonstrate updip movement of sulfide-rich waters apparently intruded into shallow aquifers along faults.

Six uranium deposits representative of the spectrum of Catahoula ores were studied. Uranium-bearing meteoric waters were reduced by reaction with pre-ore stage pyrite formed by extrinsically introduced fault-leaked sulfide (for example, Bruni deposit) or intrinsically by organic matter (for example, Washington-Fayette deposit). Uranium was concentrated in part by adsorption on Ca-montmorillonite cutans, amorphous TiO_2 , and/or organic matter followed by uranyl reduction to U^{4+} in amorphous uranous silicates. Field and geochemical evidence shows that clinoptilolite, a potential adsorber of uranium, is not correlative with mineralization. Calcite is pervasive throughout host sands but shows no spatial or temporal relationship to uranium mineralization.

Waters presently associated with Catahoula uranium deposits are oxidizing, alkaline, high-ionic-strength waters and are not appropriate models for the primary mineralizing waters, which are postulated to have been reducing, acid, low- to moderate-ionic-strength waters. The presence of marcasite and uranium together at the alteration front strongly supports an acid pH during Catahoula mineralization. Maximum adsorption and minimum solubility of uranium occur at approximately pH 6 in carbonate-rich waters.

Solution and mineral equilibria were used to test activities and mineral saturation against the occurrence of uranium in four deposits. Log activity ratios of individual waters more highly supersaturated with respect to montmorillonite, taken from montmorillonite-clinoptilolite activity diagrams, show a positive correlation with uranium mineralization. High Ca^{2+} , Mg^{2+} , $\text{Al}(\text{OH})_4^-$, and H^+ activities promote the formation of montmorillonite relative to clinoptilolite. High saturation ratios for montmorillonite show fair correlation with mineralization. The mineral-solution equilibria approach is a potential method of geochemical exploration.

INTRODUCTION

The physical geology and hydrologic framework of the Catahoula Formation of the Texas Coastal Plain has been described previously (Galloway, 1977). This new report is the product of a second phase in an inclusive study of the distribution, genesis, and potential of uranium resources in the Catahoula Formation, and emphasizes both the geochemical and hydrologic habitats of known uranium deposits and the geochemical evolution of uranium within a coastal plain aquifer system. Much of the following discussion presumes familiarity with details of the preceding report. Only a few salient conclusions will be reviewed.

The Catahoula Formation of the Texas Coastal Plain consists of deposits of two major ancient fluvial systems. The Gueydan fluvial system is centered in the Rio Grande Embayment (fig. 1) and hosts the known uranium reserves of the Catahoula. The Chita-Corrigan fluvial system consists of the deposits of several major and minor rivers that emptied primarily into the Houston Embayment (fig. 1). The two depositional sub-basins are separated by the San Marcos Arch, a passive, stable platform of the central portion of the Coastal Plain (fig. 1). Each fluvial system contains characteristic channel fill, crevasse splay, overbank, and lacustrine facies, which have been described in detail (Galloway, 1977, p. 11-23).

The Gueydan and Chita-Corrigan depositional systems are also major aquifer systems. Like other regionally confined aquifers of the Coastal Plain, both aquifer systems evolved from a syndepositional (water table) phase, through an early postdepositional (semi-confined) phase, to an extended burial phase, during which the aquifer was further confined by overlying deposits and flow restricted. Exhumation of updip recharge areas during Pleistocene sea level fluctuation and valley incision has imposed modifications on the ground-water flow systems of the Coastal Plain.

The similar evolutionary patterns of Coastal Plain aquifers, combined with geologic attributes of the Catahoula depositional systems and their contained uranium deposits, suggest a generalized uranium cycle of mobilization, migration, and accumulation consisting of two distinct phases (Galloway, 1977, p. 45-46).

The *primary mineralization* phase included four events, which are, in terms of geologic time, essentially contemporaneous (fig. 2).

1. Uranium was released from volcanic ash by reactions occurring at shallow depths soon after deposition.

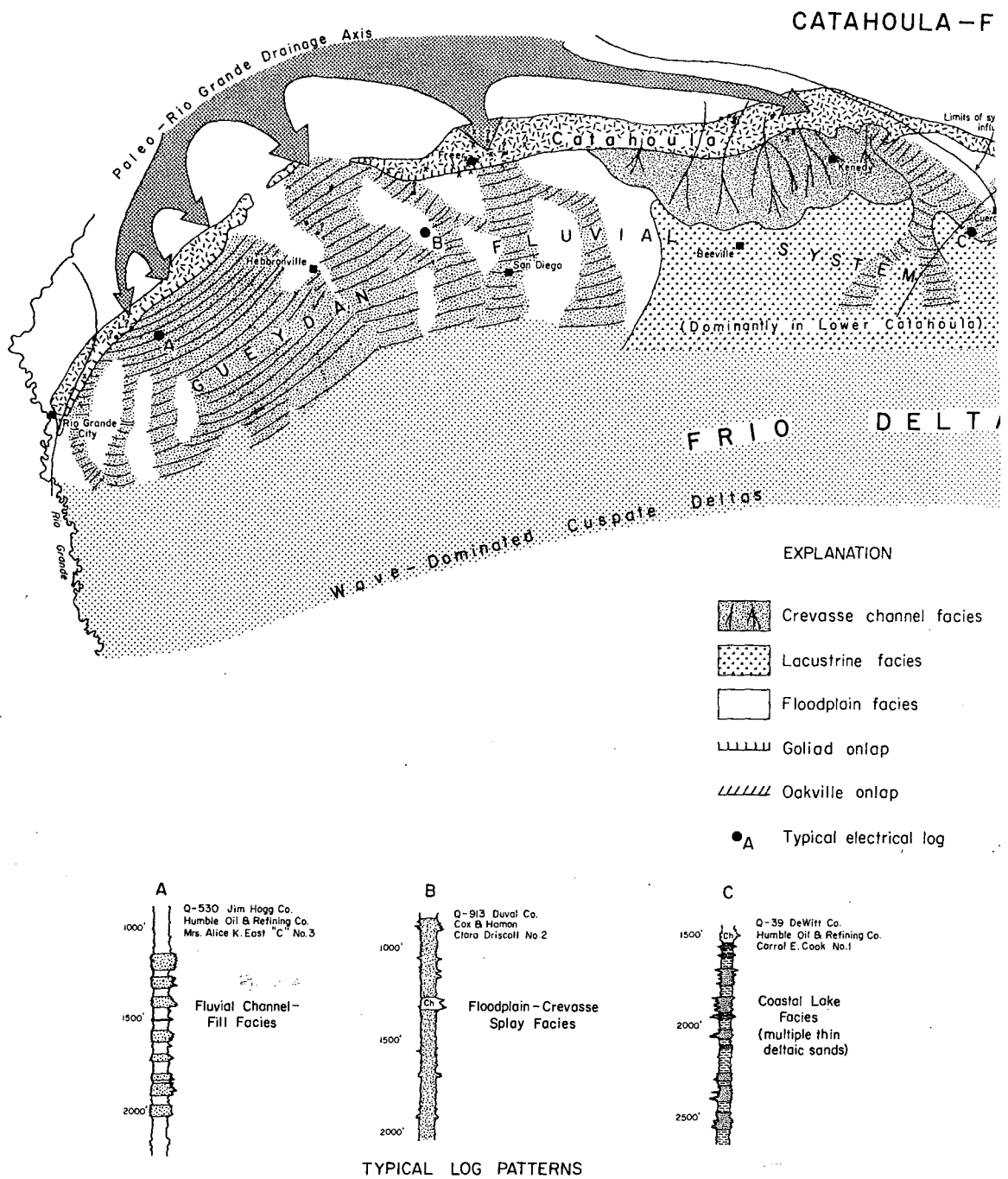
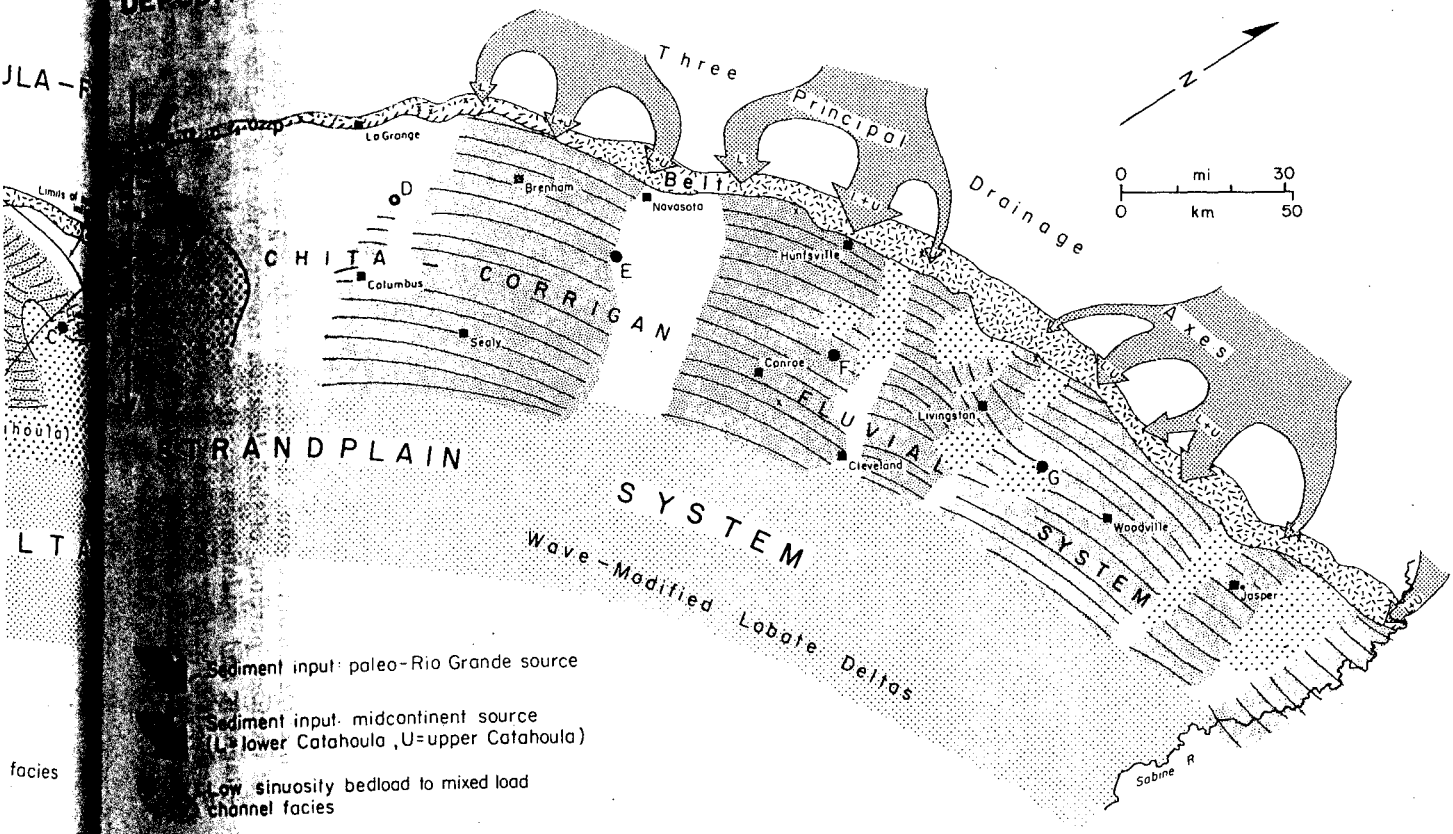
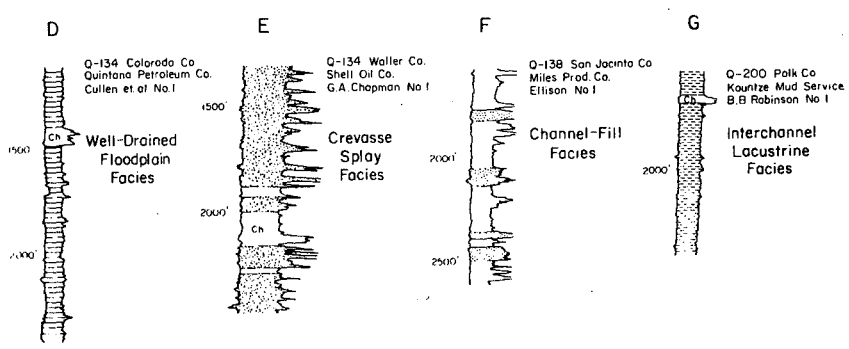


Figure 1. Depositional systems and principal genetic facies of the Cataboula. The Gueydian fluvial system occupies the Rio Grande Embayment and interfingers with beds of the Chita-Corrigan fluvial system along the western flank of the San Marcos Arch. Both systems grade downdip into facies of the Frio delta system.

DEPOSITIONAL SYSTEMS



- Sediment input: paleo-Rio Grande source
- Sediment input: midcontinent source (L=lower Catahoula, U=upper Catahoula)
- Low sinuosity bedload to mixed load channel facies
- Sinuous to meandering mixed load channel facies
- Uranium deposit or show



Electrical logs typical of thick sections of major genetic facies types are shown by A through G. Patterned portions of the log are interval of the particular facies labeled; unpatterned intervals represent other facies interbedded with the principal facies type. After Galloway (1977), figure 6.

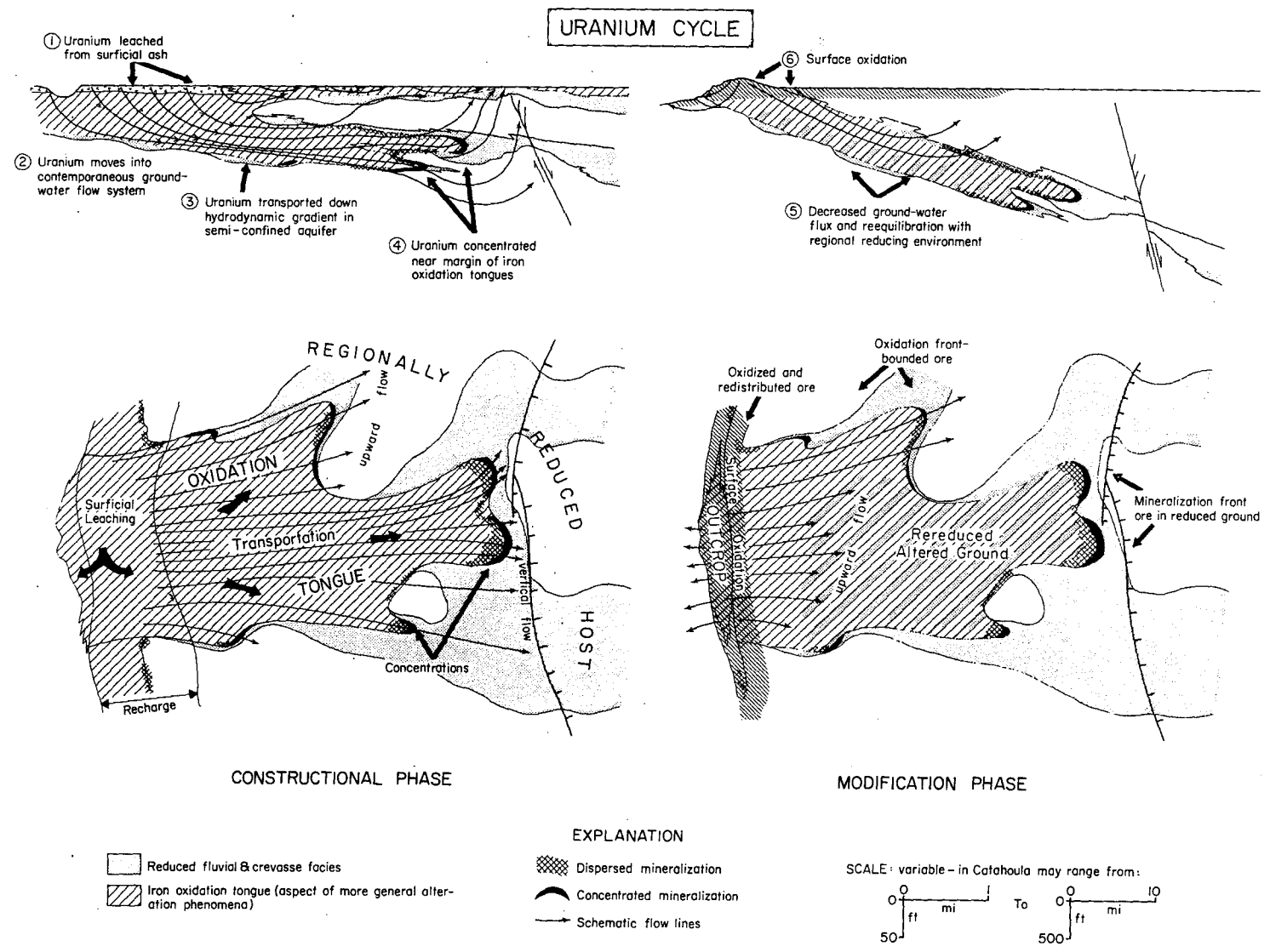


Figure 2. Diagrammatic representation of the two principal phases of uranium cycle interpreted for Catahoula fluvial systems. Constructional events include primary mobilization, migration, and concentration of uranium within a semi-confined aquifer system contemporaneous with or soon after deposition of volcanic ash in the ground-water recharge area. Development of an extensive oxidation tongue is the most recognizable aspect of more general alteration phenomena.

concentration of uranium. Modification of the deposits includes re-reduction of oxidized portions of the alteration tongue where the aquifer becomes stagnant, and oxidation, minor remobilization, and destruction of shallow deposits by surface oxidation at or above the ambient water table. Note that the scale on which the cycle operates can vary in proportion to the size of the aquifer system. After Galloway (1977), p. 22.

2. Mobilized uranium entered the ground-water flow system in areas of regional ground-water recharge.

3. Reactive, oxidizing ground water containing dissolved uranium migrated through semi-confined aquifers, producing salients of altered ground within regionally reduced portions of the aquifer system.

4. Uranium and other metals were concentrated along the interface between altered and unaltered portions of the aquifers as flow traversed the abrupt Eh and associated pH gradients extant at this boundary.

In this report the term *alteration* is used to describe the entire range of diagenetic and geochemical changes that accompany migration of uranium-rich ground waters. Thus the alteration front defines the boundary (whether sharp or diffuse) between altered and unaltered portions of the aquifer. Alteration is most commonly and easily defined on the basis of the oxidation state of iron because a sharp matrix Eh gradient commonly separates altered from unaltered ground. However, oxidation features must be considered an ephemeral record of alteration. The oxidation state of a volume of sediment, as manifested by color or presence or absence of iron sulfide minerals, can be readily modified by other epigenetic processes that do not involve the entire spectrum of alteration phenomena, including the transport and concentration of uranium. The ambient oxidation front may not coincide with the primary mineralization front, the term used in this report to describe the actual locus of uranium concentration and preservation.

The *modification phase* includes later events that have modified and obscured primary mineralization patterns (fig. 2):

1. Postmineralization changes in the flow system--caused by diagenesis and compaction of permeable units as well as bounding aquitards, continued structural development, and increasing confinement of downflow portions of the aquifer beneath younger sediments--tended to reduce or restrict flux within the aquifer. Upward intrusion of deeper reactive reducing waters (commonly along fault zones) may have caused re-equilibration of stagnant portions of the aquifer system with the generally reduced subsurface environment.

2. Outcrop recession and valley incision, particularly during the Pleistocene, exposed portions of primary mineralization fronts to near-surface oxidation or to rejuvenated flux of shallow, oxidizing ground water. Uranium was locally remobilized or stabilized as uranyl minerals such as autunite.

Development of an extensive oxidation tongue is the most recognizable aspect of more general alteration phenomena that accompany migration and the scale on which the cycle operates can vary in proportion to the size of the aquifer system. After Galloway (1977), figure 30.

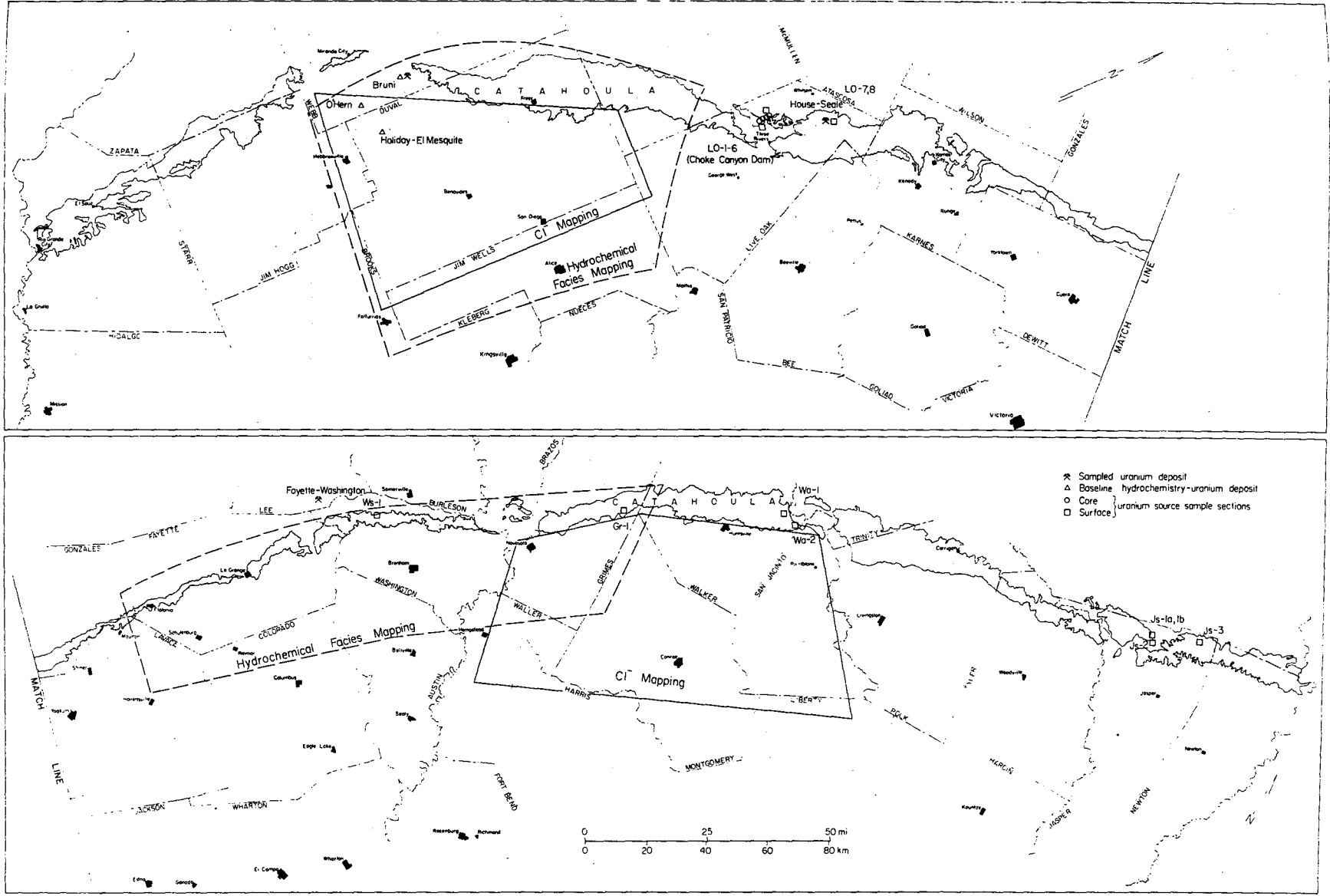
Objectives

The generalized uranium cycle provides a basis for regional evaluation of resource potential and explains (and thus to some extent also predicts) broad patterns of mineralization. The goal of the second phase of research has been to more specifically define several elements of the general uranium cycle by analysis of the diagenetic, geochemical, and hydrologic habitat of principal Catahoula uranium source and host facies. Specific objectives include:

1. Interpret the early diagenetic history of siliceous volcanic ash and quantify uranium mobilization during each diagenetic event. Inherent in this task is a determination of original uranium content of the ash.
2. Test the hypothesis that distribution and geometry of alteration fronts primarily record physically controlled ground-water flow phenomena. Interpretation of modern patterns of ground-water movement through a complex fluvial aquifer such as the Catahoula can be compared with the areal and vertical patterns observed in preserved alteration fronts.
3. Describe the geochemistry of uranium concentration along the margins of alteration tongues. This objective incorporates several interrelated facets, including (a) establishment of geologic processes or factors responsible for host preparation; (b) reconstruction of the hydrochemistry of the mineralizing ground waters; and (c) determination of processes that concentrate uranium and localize it spatially along the alteration boundary.
4. Examine the spectrum of postmineralization processes that may obscure primary mineralogic and geochemical trends or may redistribute the uranium.

Data and Methodology

The primary analytical data base consists of sampled outcrop, open-pit, and core sections selected to provide representative or best available coverage of principal source and host rock facies (fig. 3). All samples and interpreted data were placed in their depositional and structural context on the basis of the regional framework and facies studies. Laboratory analyses and conventional petrographic and x-ray diffraction studies provided basic geochemical and mineralogical data. Selected samples were studied by microprobe, scanning electron microscopy, and radioluxography.



6

Figure 3. Index map showing the Catahoula outcrop belt, principal sample section localities, and special-purpose study areas.

Hydrochemical data were obtained from the Texas Water-Oriented Data Bank, National Uranium Resource Evaluation (NURE) Program geochemical surveys, and baseline water quality data provided by mine operators in mining applications to the Texas Railroad Commission or to the Department of Water Resources. Chlorinity studies utilized electric logs available in the files of the Department of Water Resources, supplemented by additional logs purchased from commercial sources. Activities and chemical equilibria of dissolved species were calculated utilizing a modified version of the WATEQ program (Truesdell and Jones, 1974). Eh-pH diagrams were constructed following the methods outlined by Garrels and Christ (1965).

SOURCE AND MOBILIZATION OF URANIUM

Initial work suggested that uranium in the Catahoula Formation was derived from siliceous volcanic ash deposited in various environments of both the Gueydan and Chita-Corrigan fluvial systems. Analyses indicated that tuffaceous samples were commonly depleted in uranium relative to average extrusive volcanic materials of similar siliceous composition. Further, two lines of evidence suggested early mobilization of uranium (Galloway, 1977, p. 38-42):

1. Most volcanic glass deposited within the Catahoula was thoroughly altered by early pedogenic and shallow diagenetic processes.
2. Average remnant uranium in tuffaceous samples correlates with original depositional environment. Environments such as paleosoils characterized by intensive leaching and oxidation were most depleted in uranium whereas facies such as lacustrine sequences that experienced minimal leaching and early diagenesis of volcanic glass contained highest average uranium values.

To further document the early leach hypothesis, and to quantify original uranium content of the glass and effectiveness of possible mobilization processes, samples were collected from the best exposures or cores representative of principal depositional and diagenetic environments of both systems. From this suite, 129 samples were analyzed for trace uranium content following nitric acid leach and total fusion extraction methods. Texture, mineralogy, and minor sedimentary and diagenetic features were described by x-ray diffraction analysis, binocular microscope observation and thin section petrography (figs. 4 and 5).

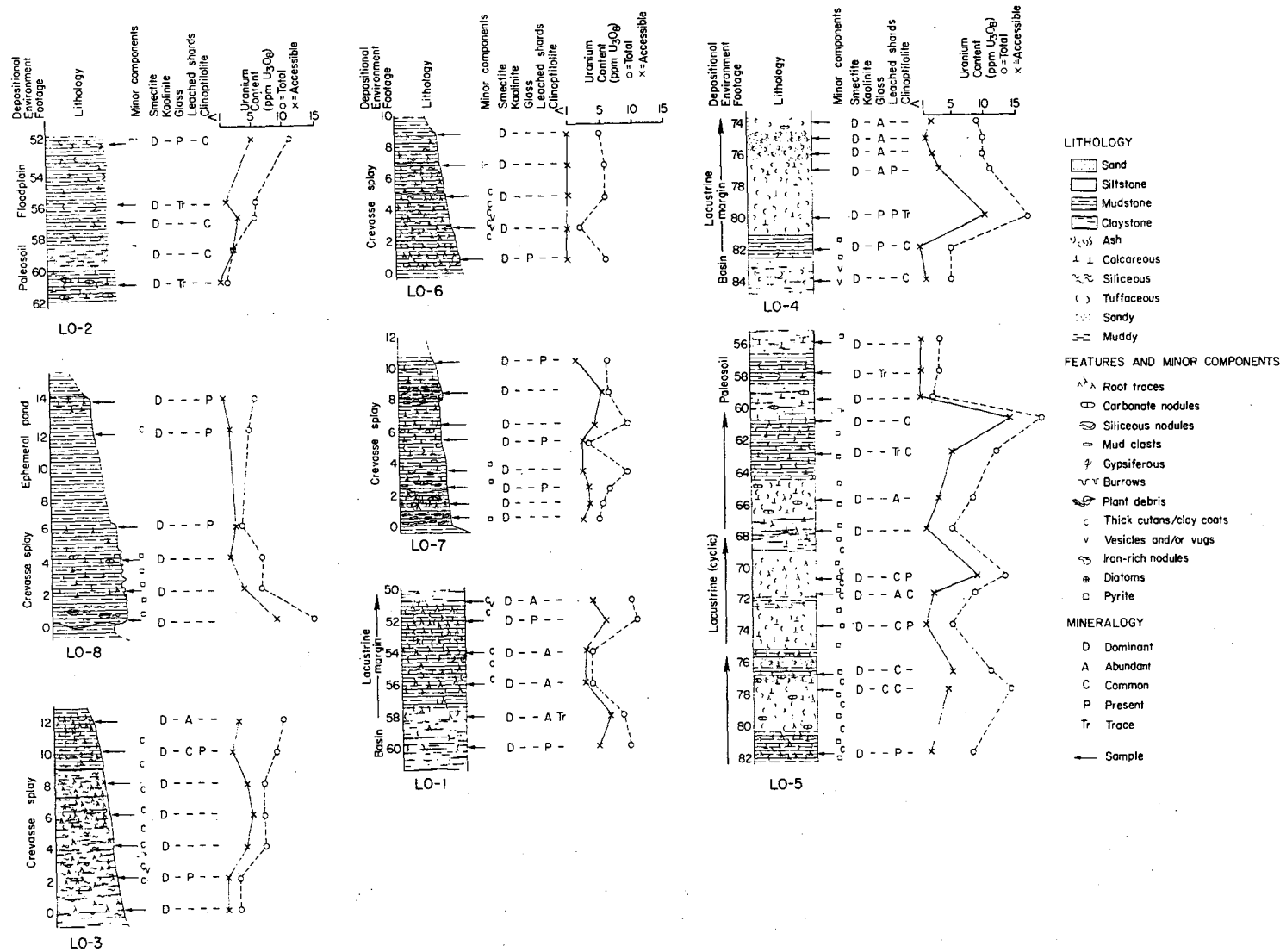


Figure 4. Schematic tabulation of genetic facies, mineralogical composition, and uranium content of potential uranium source rocks in the Gueydan fluvial system. Accessible uranium is leached with hot nitric acid. Total uranium is measured after sample fusion. For section locations see figure 3.

Diagenesis of Fresh Volcanic Glass

Paragenesis and distribution of a variety of authigenic minerals present in tuffaceous silt, mud, and claystones of the Catahoula document two major diagenetic episodes: (1) Syngenetic and very early postdepositional diagenesis of fresh ash locally produced a variety of features, including pedogenic montmorillonite and kaolinite clay coats or cutans and colloidal masses, diffuse and discrete micrite nodules, and diffuse silica nodules, as well as complete argillation of the glass particles. (2) Postdepositional diagenesis in an open hydrologic system produced characteristic sequences of authigenic montmorillonite, leached glass shards, clinoptilolite, and calcite.

Syndepositional Diagenesis

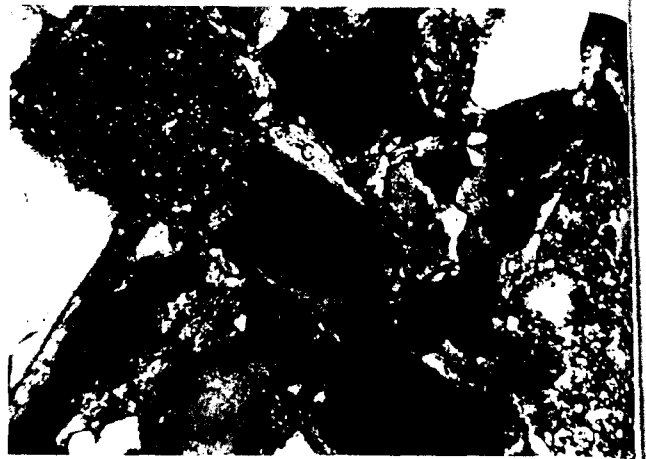
Syndepositional diagenetic features and minerals are the product of pedogenesis (soil formation processes), repeated flushing of newly deposited sediment by meteoric water within the vadose zone, or by flux of chemically concentrated waters generated by local evaporative conditions or ponding. Such processes are quite rapid, and may modify or completely alter the texture and mineralogy of original volcanogenic sediments within a few tens to a few thousand years (Davies and Almon, 1977; Hay, 1977).

Samples of Gueydan and most Chita-Corrigan paleosoils as well as intensely altered crevasse splay and floodplain sediments consist of massive, homogenized, disturbed silt or sand in a clay matrix. Matrix clay is submicroscopic, and pedogenic features such as cutans (fig. 6A), papules, and clay-filled root traces (fig. 6B) show that much of the clay is syngenetic. Extremely oxidized soils (fig. 4, LO-2) contain submicroscopic zeolite (clinoptilolite), and common micrite and silica nodules, and typically are red or brown, even if entombed within a generally reduced, pyritic section. Calcite occurs as replacement nodules or layers (fig. 6C) and more rarely as dispersed intergranular cement. Early calcite is characteristically finely crystalline; staining of thin sections shows it to be iron-poor, but possibly magnesium-bearing.

Paleosoils in the Gueydan and most of the Chita-Corrigan fluvial system have many features characteristic of vertisols (Fitz Patrick, 1971). Pedogenic processes active within such soils, which are characteristically developed on volcanic debris in arid to semi-arid areas, include (1) weathering of the parent material to produce



A



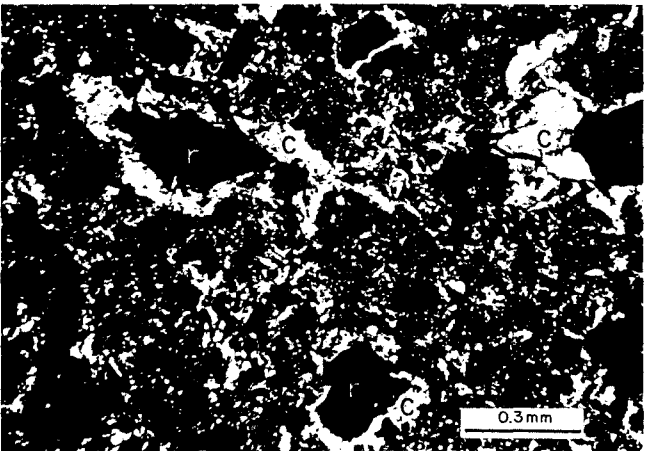
B



C



D



E



F

Figure 6. Pedogenic features of tuffaceous sand and mudstones. A. Thick clay coats or cutans (c) surrounding detrital framework grains of a crevasse splay sand bed. Cutanic clay was physically washed into pore spaces as colloidal alumino-silicate gel during early dissolution of fine glass from surrounding tuff units. B. Under crossed polars, the coats show strong birefringence, indicating alignment of the submicroscopic clay particles parallel to the grain surface. C. Massive, blocky-weathering paleosol horizon. Nearly all bedding has been thoroughly homogenized by root disturbance and thorough argillation of the original ash, Lower Catahoula, Live Oak County. D. Pervasively root-disturbed tuffaceous mudstone. Root casts and molds range from 1 cm to a few mm in diameter. E. Thick clay cutans (c) lining walls of hollow root tubules (r) in a thoroughly pedogenically altered tuff. Crossed nicols. F. Micrite nodules (m) scattered through a paleosol horizon within a crevasse splay unit.

abundant colloidal montmorillonite, which can then be washed about and coat grains or pores to form cutans; and (2) precipitation of calcium carbonate as dispersed cement, crusts, or nodules.

Small, ephemeral lakes in and around crevasse and levee deposits of the Gueydán were also typified by intense argillation and precipitation of minor microcrystalline clinoptilolite (fig. 4, LO-8). Authigenesis of zeolites within both soils and lake bed deposits containing volcanic ash has been noted by Hay (1977).

Significant kaolinite enrichment in paleosoil deposits is first encountered in the Chita-Corrigan fluvial system in Walker County (compare Ws-1 with Wa-2). Farther eastward, kaolinite becomes the dominant clay mineral, particularly in highly vegetated lacustrine margin sediments (fig. 5, Wa-1, Js-2). Abrupt vertical changes in clay mineralogy from nearly pure kaolinite to pure montmorillonite in lithologically similar sequences (for example, fig. 4, Wa-1) indicate a diagenetic origin for the kaolinite. Pedogenic features, such as cutans, indicative of early physical transport of colloidal alumino-silicate gels or clay particles by percolating water, also occur in kaolinitic samples. Examination of sections containing abundant kaolinite shows that vegetation (as indicated by the abundance of root tubules) was dense; detrital organic matter is preserved locally.

Weathering of volcanic ash in a wide range of humid climates produces andosols, which are characterized by allophane, an amorphous alumino-silicate gel (Fitz Patrick, 1971). Further intensification of leaching by organic acid-rich waters, particularly in highly saturated environments such as the margins of interchannel lakes, could strip virtually all cations and transform early-formed montmorillonite to kaolinite (Ahschuler and others, 1963; Huang and Keller, 1972). Kaolinite-rich sequences are notably free of carbonate and clinoptilolite; suggesting efficient cation leaching, and probably slightly acidic conditions.

In summary, syngenetic processes included widespread destruction and argillation of volcanic glass to form montmorillonite or kaolinite, precipitation of microcrystalline calcium carbonate, and rarely, precipitation of clinoptilolite.

Postdepositional Diagenesis

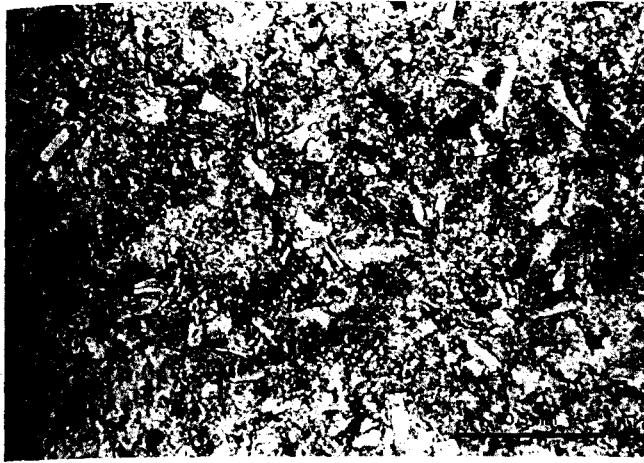
With continued burial (perhaps to several hundred feet), ash-rich units that had escaped argillation and retained some permeability were flushed by chemically evolving circulating meteoric waters. Further water-rock reactions resulted in (1) solution of finest ash particles and authigenesis of montmorillonite rims on remaining

framework grains, (2) complete solution of large glass shards leaving pores or shard molds (fig. 7B), and (3) precipitation of euhedral clinoptilolite available pore space (fig. 7C). Diagenetic montmorillonite is the dominant mineral component of many samples; zeolite rarely constitutes more than a few percent of the rock volume. Sparry calcite cement (fig. 7D) and opal also characterize this sequence.

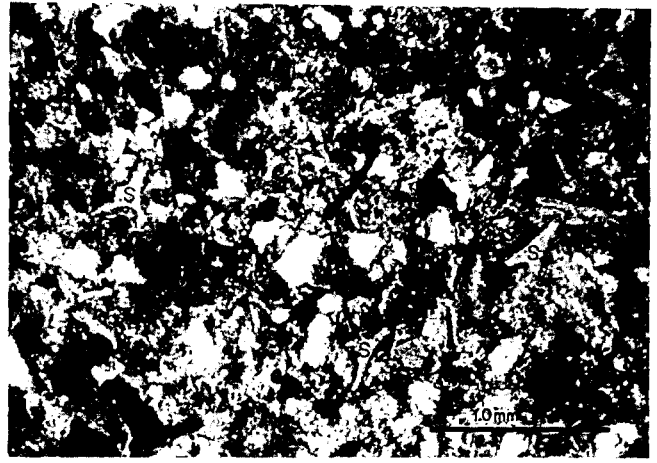
The three diagenetic facies (fresh glass with montmorillonite rims, dissolved glass, and clinoptilolite) occur in a consistent spatial relationship. Fresh glass is characteristically separated from clinoptilolite-bearing samples by a transition zone of leached glass (fig. 4, Lo-4). This diagenetic sequence typifies the alteration of volcanic glass in open hydrologic systems and has been described by several authors, including Hay (1977) and Walton (1975, 1978), in comparatively simple flow systems within thick volcanic ash deposits. Water flowing through volcanic deposits dissolves glass, particularly the finest silt- and clay-sized material, becoming progressively enriched in silica and alumina. Concomitantly, hydrolysis of the silica and alumina raises the pH of the ground water. As additional sediment accumulates and cumulative contact time of ground water with glass increases, a series of diagenetic zones evolve and then migrate upflow within the tuffaceous aquifer. Waters initially become saturated with respect to montmorillonite and opal, which precipitate in the first zone. As pH climbs above 9, silica solubility increases rapidly and the remaining coarse glass shards are etched and dissolved. With the abruptly increased charge of silica and aluminate, the solubility product of clinoptilolite is exceeded and precipitation of the zeolite ensues in the third zone.

Formation of both montmorillonite and clinoptilolite indicates complete dissolution of glass and at least local transport of the soluble products within moving ground water. Release of uranium would certainly be expected. Clinoptilolite is rare in Chita-Corrigan sequences, perhaps indicating rapid flushing and dilution, limiting supersaturation with respect to clinoptilolite.

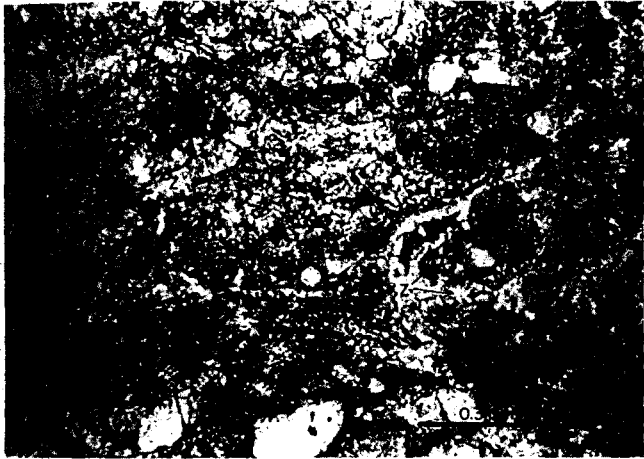
Permeable, ash-rich units are prime candidates for thorough leaching and subsequent formation of zeolite. Paleosols and other units argillized by syngenetic destruction of ash have low permeability and rarely contain good examples of leached or zeolitized shards. In contrast, lacustrine-margin tuffs, which were typically subjected to minimal syngenetic destruction of glass, provide the best examples of zeolite formation (fig. 4, LO-5). Similarly, tuffaceous sequences that overlie highly permeable sand facies commonly show abundant glass dissolution and zeolitization.



A



B



C



D

Figure 7. Features produced by open hydrologic system diagenesis of glass. A. Coarse glass shards embedded within authigenic montmorillonite rims and matrix, which appear dusty or powdery in the figure. B. Dissolved shard molds. Glass has been thoroughly leached from the sample, and former shards (s) are outlined by their clay rims. C. Root pores lined with authigenic clinoptilolite (z). Clinoptilolite fills available pore space, whether primary or moldic. D. Sparry calcite cement (Ca) filling intergranular pore space. Thick clay coats (c) partially filled vesicles within the pumice fragment. Crossed nicols.

Because flux of ground water in a Coastal Plain fluvial aquifer such as the Catahoula is spatially variable and time dependent, distribution of the various open-system diagenetic facies is highly complex. Extensive sampling would be necessary to outline the three-dimensional distribution of diagenetic facies within even a single local aquifer. Patterns are further complicated by local facies changes and structural discontinuities, and consequent cross-stratal flow and ground-water mixing. Waters supersaturated with respect to clinoptilolite may move laterally or vertically into beds containing no preserved shards. Zeolite would then precipitate in available intergranular pore space; or, if mixed with waters of differing composition, zeolite precipitation might be delayed or precluded. Despite local complexities, however, observed distribution and paragenesis are consistent with the open-system hydrologic model developed in more lithologically homogeneous ash sequences.

Uranium Mobilization

The extent of uranium mobilization must be assessed within the context of numerous interdependent variables, including original abundance of glass or other uranium-bearing phases in the unit, depositional environment, and diagenetic history. The analyzed samples were selected as representative of a variety of depositional and diagenetic facies. Original glass content is impossible to determine for most samples because of the inherent pervasive alteration. However, all contain compositional or textural features indicative of high initial glass content. Splits of each sample were analyzed using hot concentrated (50 percent by volume) nitric acid leach and total fusion extraction methods to give two values for trace uranium content as summarized in table 1. *Total uranium* (measured by sample fusion) is the sum of the *accessible uranium* (measured by acid leach), which includes loosely bound uranium in surficial sites on other solid phases and uranium in clinoptilolite, and *bound uranium*, which includes uranium tightly bound within intra-granular sites.

Dissolution of the glass is required for mobilization of the uranium (Zielinski, 1977), thus uranium within original or remaining glass is dominantly bound. Diagenetic alteration of the glass can lead to uranium mobilization with one of three consequences:

1. Uranium is flushed from the source unit. Both total and accessible uranium values will be low for the sample suite.

Table 1. Uranium content (ppm U_3O_8) of various depositional facies, Catahoula fluvial systems.

		Common ←————— Vadose flushing —————→ Rare High ←————— Weathering intensity —————→ Low				
		Crevasse splay/ lacustrine delta plain			Lacustrine	
		Paleosoils	Floodplain/ backswamp	Margin	Basin	
GUEYDAN SYSTEM	Total U_3O_8					
	Average	2	6	7	9	5
	Median	2	6	6	9	6
	Accessible U_3O_8					
	Average	1	2	3	4	2.5
	Median	< 1	2	3	3	3
	Bound U_3O_8					
	Average	1	4	4	5	2.5
	Median	> 1	4	3	6	3
	Number of Samples	5	21	3	22	6
CHITA - CORRIGAN SYSTEM	Total U_3O_8					
	Average	3	5	7	7	11
	Median	3	5	5.5	7.5	12
	Accessible U_3O_8					
	Average	1	1	2.5	2.5	8
	Median	1	1	2.5	2.5	6
	Bound $U_3O_8^*$					
	Average	2	4	3	4	5
	Median	2	4	3	5	5.5
	Number of Samples	10	9	18	18	17

* Total U_3O_8 was measured on only a representative selection of the total sample suite. Thus the addition of accessible U_3O_8 values for the total suite to calculated values for the subset does not necessarily equal the total U_3O_8 value.

2. Uranium is freed from the glass but is trapped in precipitating mineral phases and returned to a bound state. Total uranium remains high and accessible uranium remains generally low.

3. Mobilized uranium is loosely trapped by other diagenetic or detrital phases within the host unit. Averaged total uranium is thus not depleted, but all or most of the uranium occupies accessible sites. Extent of redistribution is indeterminate, but must be sufficiently localized that little net depletion of the depositional or diagenetic facies results. Sample to sample variation may be increased.

Only uranium efficiently flushed from the source unit can contribute to formation of ore deposits. Thus functional source rocks will be characterized by low total uranium content. Efficiency of uranium mobilization can be estimated by comparison of average total uranium content of the sample suite with the inferred uranium content of the original source lithology. It is important to note that volcanic ash in the Catahoula was characteristically reworked and impure. Thus uranium content of a pure, fresh glass separate probably exceeded that of the impure, tuffaceous source units.

Review of uranium content in the sample suites (expressed as ppm U_3O_8) leads to several observations:

1. The intensity of syngenetic weathering and periodic leaching by oxidizing vadose meteoric water is a dominant control on bound, total, and accessible uranium within sample suites. Average and median uranium contents for each of five major environmental groupings within the Gueydan and Chita-Corrigan fluvial systems are significantly different (table 1) and are proportional to the intensity of weathering and periodic flushing by oxidizing water in the vadose zone characteristic of each environment. For example, total U_3O_8 from five highly weathered Gueydan paleosol samples averaged 2 ppm compared with an average content of 9 ppm in 22 relatively unweathered lacustrine-margin samples.

Details of uranium concentration within several sections further document the relationship (figs. 4 and 5).

Lo-2: A highly oxidized paleosol zone capping a fluvial channel shows nearly complete uranium depletion relative to overlying floodplain muds.

Lo-8: Highly oxidized mud and claystone deposited in an ephemeral pond capping a crevasse channel fill contain moderate amounts of uranium; slight enrichment may account for the high accessible and consequent high total uranium value in the base of the channel.

Lo-3: Uranium content decreases downward through a sequence of three crevasse splay depositional units. The depleted lowest unit also exhibits the greatest abundance of pedogenic weathering features such as iron oxide nodules, cutans, and vacuoles.

Lo-6: A homogeneous sequence of crevasse splay muds has been stripped of all accessible uranium but retains moderate total uranium content averaging 5 to 6 ppm.

Lo-7: Texturally heterogeneous crevasse channel deposits exhibit considerable variation in uranium content, ranging from 3 to 9 ppm total U_3O_8 .

Lo-1, 4, and 5: Three lacustrine sequences, which include both lake basin and progradational lake margin deposits, display a wide range in uranium content, but are notable for the unusually high values found in a few samples and high average uranium content. Lo-5 is particularly interesting because three cycles of upward-increasing total and accessible uranium content correspond to three thin, progradational, lacustrine-margin cycles. The entire sequence is capped by a thoroughly leached and uranium-depleted paleosoil.

A series of sections from the Chita-Corrigan fluvial system displays similar relationships among depositional setting, early weathering, and preserved uranium content (fig. 5).

Wa-2: Thick, highly weathered paleosoil exhibited uniformly low uranium content. Intensity of syngenetic leaching is indicated by the abundance of kaolinite, particularly in the upper three samples.

Ws-1 and Gr-1: Two sections of vegetated crevasse splay deposits are characterized by low available uranium and low to moderate total uranium content.

Js-1a and 1b: Two sections of stratigraphically equivalent interchannel lake margin tuffaceous silt, mud, and claystone display systematic vertical variations in available and total uranium content. Total uranium ranges from moderate to high.

Wa-1 and Js-2: Thick interchannel backswamp and lake sequences from two areas exhibit similar patterns of trace uranium content. The thick lake-basin clay and mud contain moderate to high uranium. The capping progradational backswamp mudstone and interbedded muddy sand sequence, which exhibits abundant root traces and other pedogenic features, contains significantly less uranium.

2. Destruction of glass by diagenetic alteration effectively releases uranium. In sections from the Gueydan system, samples with abundant fresh glass average 10 ppm total uranium; an average of 7 ppm of this uranium is bound. Significantly, none of the samples consist exclusively of fresh, unaltered ash. Typical Catahoula samples contain at least 50 percent clay, much of which is the diagenetic product of solution of the finest glass debris. Uranium in clays would probably occupy accessible sites. Thus 7 ppm is a *minimal* original average uranium content of pure fresh volcanic glass. The actual primary uranium content of unaltered tuffs would reasonably have been several ppm greater.

Thorough argillation of all the glass by weathering and/or diagenesis reduced total uranium content to an average of 6 ppm in the sample suite. Remaining bound uranium averages only 3.5 ppm. In thoroughly weathered and oxidized soil zones typical of the bulk of updip Catahoula interchannel facies, total uranium content is even lower (Lo-2; Lo-5, top); presence of syngenetic zeolite has little effect on uranium loss (Lo-2, Lo-8).

Diagenetic alteration of glass in open hydrologic systems may further release uranium during shard dissolution. Samples showing common leached shards are highly variable but average 6.5 ppm U_3O_8 . Bound uranium averages 4 ppm. Samples with well-developed pore-filling clinoptilolite average about 10 ppm total uranium although individual values vary widely. Only 5 ppm, which is slightly more than the total, is retained in sites where it is not leached by acid. The additional uranium is principally in an available form, suggesting that some enrichment occurs during or after zeolite precipitation by sorption (Doi and others, 1975). It should be noted, however, that differences of 1 or 2 ppm are within analytical error, and further, that there is considerable variability among samples in each diagenetic facies.

In summary, significant depletion of uranium from samples showing complete destruction of glass by argillation is clearly documented by the data presented in the profiles (fig. 4). Further modest loss of uranium during open-system dissolution of glass is strongly suggested by the data. Effect of zeolitization is more problematical. Open hydrologic system diagenesis seems to produce primarily local redistribution with

freed uranium trapped by zeolite, clay, opal, or other alteration products. A complex interplay of depositional and diagenetic factors probably accounts for cyclic patterns of uranium concentration observed in sections such as Lo-5.

3. Uranium release processes, although somewhat different in mineralogical products, effectively mobilized uranium in the more humid climatic regime of the Chita-Corrigan fluvial system. Equivalent diagenetic facies of the Gueydan and Chita-Corrigan systems produced comparable average uranium contents, with the significant exception of the lacustrine basin sections (Wa-1, Js-2). Comparison of backswamp with lake-basin and margin samples from both fluvial systems grouped into kaolinitic and montmorillonite-dominated populations (based on semiquantitative x-ray analysis) shows average and median bound uranium content to be 3.5 ppm and 3 ppm, respectively. Likewise, available uranium averages 2 ppm in kaolinitic samples and 4 ppm in montmorillonite-rich samples. In general, uranium was thoroughly leached from tuffs by argillation during early diagenesis, assuming original uranium content was comparable.

4. Uranium was locally concentrated in organic-rich lacustrine muds of the Chita-Corrigan fluvial system. One section (fig. 8, Js-3) exhibits available uranium content of 21 and 30 ppm in two kaolinitic lake-basin samples. Uranium values decrease systematically upward through the overlying lake-margin mud and silt. Association of uranium concentration with carbonaceous debris in lacustrine mudstone, as well as anomalously high uranium content noted in additional lacustrine samples (Galloway, 1977, p. 41) suggests the possibility of syngenetic mineralization within local organic-rich lake basins of the Chita-Corrigan system. Uranium was probably sorbed by organic material (Doi and others, 1975).

Summary

Results of detailed examination of trace uranium content in fine-grained, tuffaceous Catahoula sediments of both component fluvial systems confirm earlier interpretations that uranium was mobilized during or soon after deposition. More detailed examination shows that:

1. Original uranium content of the glass-rich tuffs averaged at least 7 ppm U_3O_8 and was probably higher; 10 ppm is a more reasonable figure. Such high values agree with recent analyses of uranium content in siliceous volcanic rocks of West Texas and other areas (Henry, 1978, personal communication).

2. Syndepositional weathering and early diagenesis mobilized, on the average, over half of the original uranium present in the ash. Some of the uranium was trapped after minimal redistribution in disseminated sites, possibly in diagenetic clay or zeolite, but tremendous quantities of uranium were made available for large-scale migration within the Catahoula and underlying aquifers.

3. Leaching and mobilization of uranium were equally efficient in both semi-arid and subhumid regimes found along the middle Tertiary Texas Coastal Plain.

4. Uranium mobilization is a multistage process; however, not all stages are equally effective. Volcanic ash initially deposited on the Texas Coastal Plain and subsequently reworked by the Catahoula fluvial systems contained 7 ppm to 10 ppm uranium. An unknown but potentially significant quantity of uranium was adsorbed, along with other volcanic aerosols, on the highly reactive surface of the glass particles (Henry and Tyner, 1978; Rose, 1977). Such adsorbed uranium was readily leached by fresh water flushing (Taylor and Stoiber, 1973) and would constitute the first pulse of dissolved uranium to enter extant ground-water flow systems (fig. 9). Pedogenic weathering, vadose flushing, and very early diagenetic argillation of the unstable glass released the major pulse of dissolved uranium, probably within the first few tens to thousands of years after deposition. A succession of such pulses followed deposition of each new ash fall. Finally, a subordinate long-term charge of dissolved uranium released as ash was argillized and leached in open hydrologic systems. However, the amount of uranium released by this mechanism appears comparatively small and may in part have been rapidly sorbed by other alteration products present downflow from the glass-solution zone (fig. 9).

The average tuffaceous Catahoula mudstone retains a median uranium content of about 6 ppm; of this total, about 4 ppm remains mineralogically bound. Assuming the sample suite is representative of the Catahoula,* at least 1 ppm, and more likely 4 or

*The sample suite is in fact highly biased toward the uranium-rich lacustrine facies. However, quantification of the relative proportion of different facies and appropriate weighting of analytical results is extremely difficult because outcrop exposures are rare.

Figure 8. Lacustrine sequence showing uranium enrichment in the carbonaceous basinal clay. For section location see figure 3.

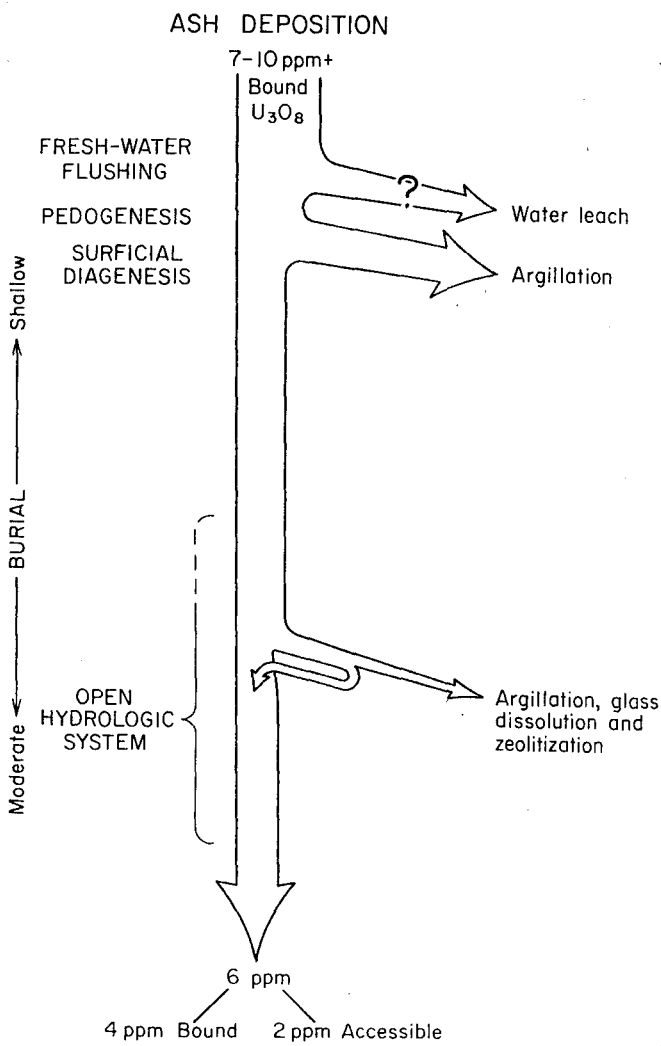
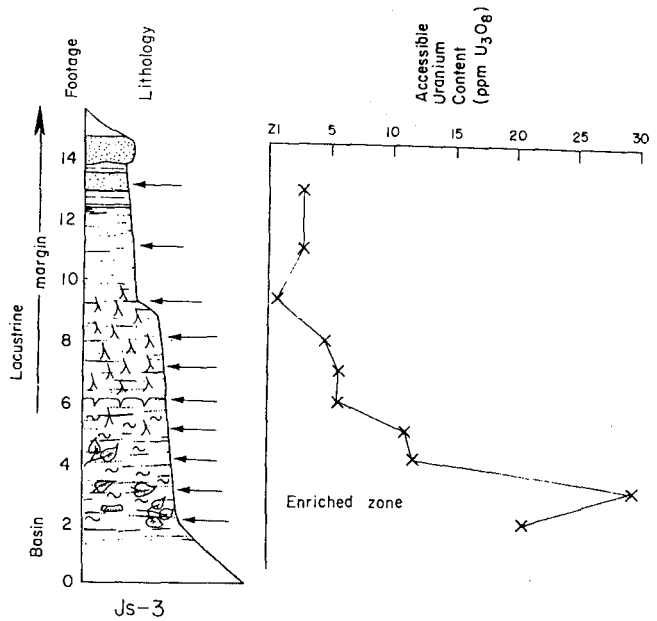


Figure 9. Schematic uranium mobilization pathways during successive depositional, pedogenic, and diagenetic events that alter volcanic glass. An unknown but possibly substantial amount of uranium is washed from the ash surface with the first flushing by fresh water. Pedogenic argillation is the most effective uranium mobilizer, and highly altered paleosols are thoroughly depleted in uranium. Solution of glass in an open hydrologic system frees small amounts of uranium, but part of this uranium may be rapidly trapped in the zeolitic facies that forms immediately downflow from the zone of glass dissolution.

more ppm of U_3O_8 was released for ore formation. Though proportionally modest, the quantity of mobilized uranium is staggering. One simplistic volumetric approximation gives 16 billion pounds of U_3O_8 per ppm mobilized from glass in the updip Catahoula section of Texas.

GEOCHEMICAL AND PHYSICAL ASPECTS OF URANIUM TRANSPORT

Uranium that is dissolved during weathering or diagenesis of volcanic ash must be transported to sites of accumulation within local or regional ground-water flow systems. Development of highly enriched, stratigraphically isolated mineralization fronts requires large-scale transport (miles or tens of miles) within semi-confined aquifers (Galloway, 1977). Such coherent flow systems may, however, develop very soon after deposition and shallow burial of permeable conduit facies. Thus, initial migration and redistribution of uranium was controlled by the early hydrochemistry and physical flow patterns that characterized the Catahoula aquifer during periods of active uranium mobilization. Modern hydrochemistry and flow dynamics may not accurately preserve physical and chemical attributes of earlier evolutionary phases of the aquifer history.

The principal questions about uranium transport include:

1. What was the geochemistry of the uranium-bearing ground waters that were responsible for primary mineralization? Mechanisms, and consequently, sites of mineralization are determined by evolutionary changes in hydrochemistry or by localized mixing of different water masses. Interactions between the uranium-charged ground waters and the rock matrix produce alteration phenomena that may guide exploration.

2. To what extent are the location, geometry, and total uranium content of mineralization fronts determined by physical aspects (flow geometry, relative flux) of ground-water flow? Regional and local ground-water flux is molded by the distribution, trend, and relative permeability of various aquifer facies and by structural features. These features can be mapped during exploration and may provide regional or local guides for efficient exploration or resource evaluation.

3. What geochemical or physical factors control uranium redistribution in the evolving aquifer following the primary mineralization episode? Uranium was released

from source ash units very early and primary deposits (as will be shown below) were emplaced very early. Anomalous geochemical zonations and radiometric disequilibrium suggest, however, geologically recent modification of some primary trends.

Hydrochemistry of the Catahoula Aquifer

Uranium in the Catahoula Formation (as well as in other sandstone hosts) is interpreted by most workers as having been transported by oxidizing, neutral to weakly basic, bicarbonate-rich ground waters. Such waters are typical of uranium-bearing areas today, and uranyl carbonate complexes are demonstrably efficient in cool, dilute aqueous systems (Hostetler and Garrels, 1962). A closer examination of the modern hydrochemistry and geochemical evolution of uraniferous aquifers, such as the Catahoula, seems in order.

A terrigenous coastal plain aquifer undergoes four significantly different but transitional phases in its flow history (Galloway, 1977, p. 35-36; Galloway and others, 1979), including a syndepositional water table phase, an early postdepositional semi-confined phase, a confined burial phase, and locally, an exhumation phase. Hydrochemistry of the syndepositional and early postdepositional phases can only be interpreted from general principles and preserved diagenetic features. The modern ground-water system provides an accurate portrayal of the burial phase, modified by local superimposed flow systems developed by exhumation and valley incision.

Early Ground-Water Composition

The early geochemistry of Catahoula waters was primarily the product of subaerial weathering of abundant volcanic glass in subarid to subhumid climatic regimes. Shallow, unconfined ground waters below the water table, as well as vadose waters, would have been conditioned by the abundance of readily soluble constituents present on and in ash. Consequently, the qualitative geochemistry of the early waters can be reasonably deduced.

Shallow ground waters of the Gueydan and most of the Chita-Corrigan systems were initially oxidizing. Red or bleached colors and absence of organic debris (even though root zones are abundant) document early, thorough oxidation of nearly all shallow Gueydan sediments. Preservation of plant debris indicates that local, shallow-reducing conditions did exist within lacustrine and some interchannel facies of the fluvial systems.

Hydration and solution of fresh ash controlled pH of the syndepositional phase waters. Hydrolysis of silica and alumina released by alteration of glass consumes hydrogen, which is replaced in solution by alkali and alkaline earth ions, leaving hydroxyl ions to accumulate. Vertisols have pH ranging up to 8.5; andosols developed on fresh ash are slightly acidic and display a pH of about 6 (Fitz Patrick, 1971). Their more acidic character is consistent with increasing abundance of organic material, thorough leaching, and observed lack of carbonate nodules. Basic waters percolating through Gueydan soils thus efficiently oxidized organic substances to CO_2 and enriched the water in bicarbonate (HCO_3^-). Chita-Corrigan soils--particularly in the East Texas Coastal Plain where excess ground water produced a shallow water table and permanent interchannel lakes--evolved shallow, downward percolating waters that ranged from slightly acidic to moderately basic.

Flushing of fresh ash likely released Na^+ , Ca^{2+} , Cl^- , and SO_4^{2-} sorbed on the surface of ash particles (Taylor and Stoiber, 1973). Additional Ca^{2+} was rapidly released by dissolution of fine ash, and readily reacted with dissolved bicarbonate to form pedogenic and shallow diagenetic microcrystalline carbonate. The abundance of soluble constituents available from fresh ash suggests that early, shallow ground waters may have had temporary, but substantial charges of dissolved solids, particularly in seasonally dry portions of the coastal plain. Less abundant but important early additions to the ground water likely included fluoride, phosphate, magnesium, and various metals.

In summary, syndepositional ground waters of the Gueydan fluvial system of South Texas were oxidizing, bicarbonate-rich, mildly basic to neutral, and contained a substantial dissolved load of sodium, calcium, chloride, sulfate, and possibly phosphate or other ions. In such waters, uranium would readily form uranyl-dicarbonate complexes, but high pH would favor some hydroxide complexing, and nearly all available phosphate would complex uranium (Langmuir, 1978). Chita-Corrigan waters were generally similar, but more dilute (because of the increased or more continuous availability of fresh recharge), and were neutral to slightly acidic in organic-rich environments.

Ground waters circulating through semi-confined aquifers entered the realm of open hydrologic system diagenesis. Overall chemistry would not have changed dramatically, but pH would continue to rise, and further increases in dissolved sodium, potassium, and silica would occur (Hay and Sheppard, 1977). If its solubility product was exceeded within the flow system, clinoptilolite precipitated. Waters remained oxidizing until reduced matrix was encountered. Reducing sinks within the aquifer

matrix existed in abundance within the Chita-Corrigan; organic debris and syngenetic iron sulfide nodules are still abundant. Intrinsic reductants were less abundant in the Gueydan; discharge of waters from deeper horizons provided mobile, extrinsic reductants to portions of the aquifer (as will be discussed in the section on uranium concentration). Uranium migrated as a mix of carbonate, hydroxide, and possibly, phosphate complexes, until flow entered reducing portions of the aquifer and dissolved oxidants within the uranium-charged ground water were consumed.

Burial and Exhumation Phase Hydrochemistry

The range of ground-water compositions that evolved during regional burial of the Catahoula aquifer, as well as possible local perturbations resulting from Pleistocene incision of the Gulf Coastal Plain, is portrayed by modern hydrochemical patterns. Two large areas of the Catahoula aquifer, one centered in the Gueydan, the other in the Chita-Corrigan fluvial system, provide examples for the two aquifer systems. Concepts of regional aquifer hydrochemical evolution upon which this analysis is based are reviewed by Back (1960) and Tóth (1972).

Principal anion-cation composition of ground waters can be graphically displayed on trilinear Piper diagrams* (fig. 10), which show relative proportions of major ionic species. Such plots are useful for recognition and areal delineation of principal hydrochemical facies.

Modern ground waters of the Gueydan fluvial system are dominated by sodium bicarbonate-chloride and sodium chloride compositions (fig. 10A). Deeper waters for the same system are almost exclusively sodium chloride waters, with the exception of a few sodium sulfate waters (fig. 10B). Waters of the Chita-Corrigan fluvial system display a much greater compositional range. Calcium bicarbonate, calcium bicarbonate-chloride, calcium-sodium bicarbonate-chloride, and sodium bicarbonate waters are all common in shallow portions of the aquifer (fig. 10C). Sulfate waters are notably absent. Analyses of waters from intermediate depths are not available, but deep waters are sodium chloride brines (fig. 10D).

In spite of limited data and local variability within a complex aquifer such as the Catahoula, hydrochemical facies display regional patterns in both the Gueydan and

*For a discussion of Piper diagrams and their construction, see Hem (1970).

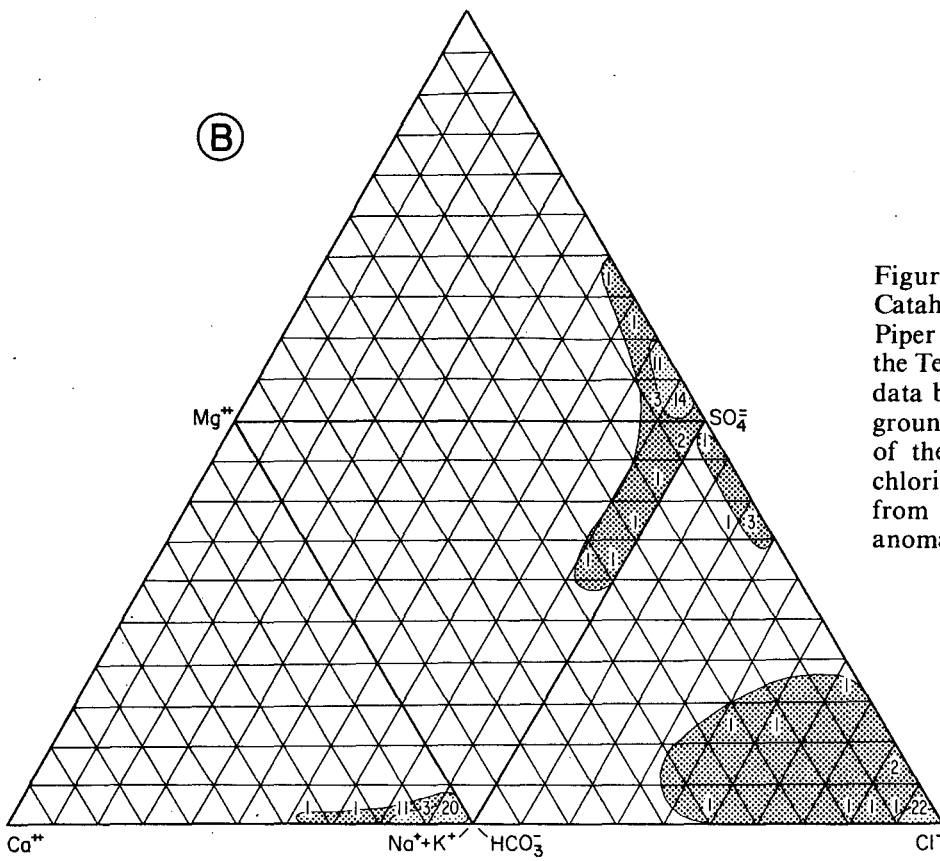
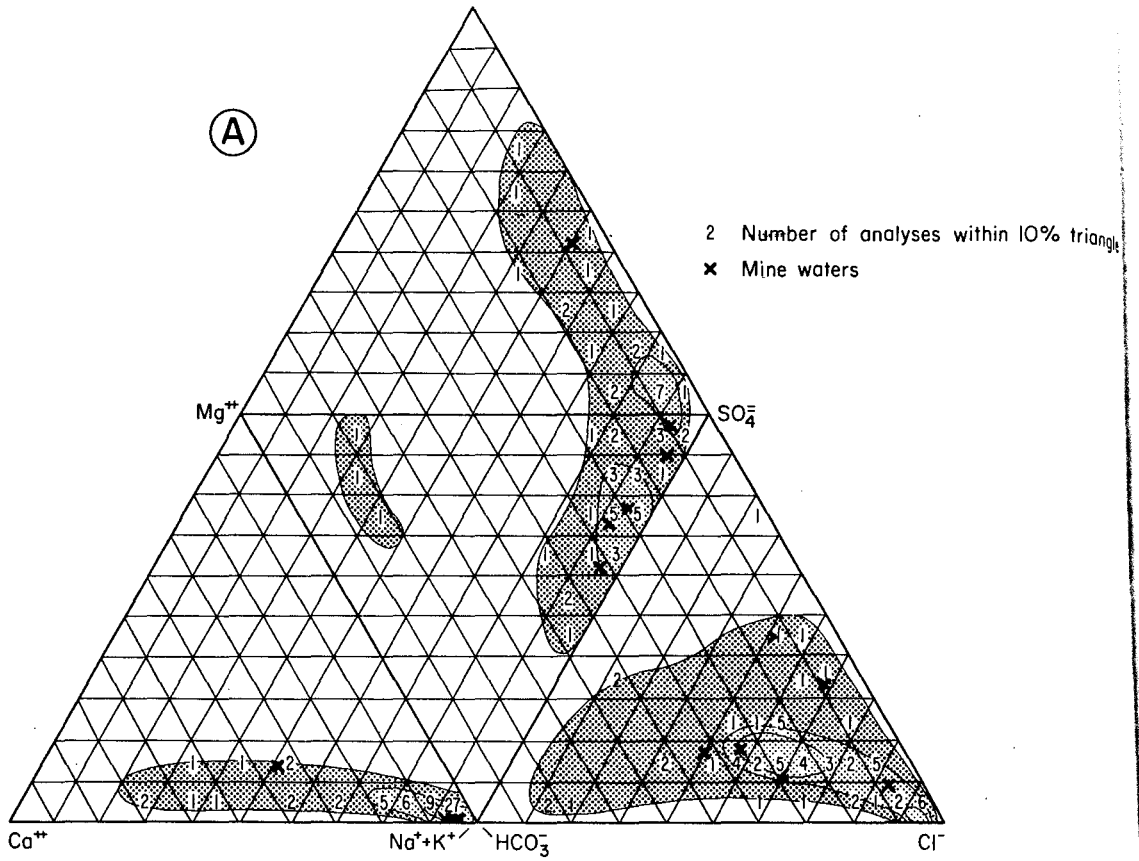


Figure 10. Hydrochemistry of modern Catahoula ground waters portrayed on Piper diagrams. Analyses tabulated from the Texas Department of Water Resources data bank, and other sources. A. Shallow ground waters (less than 1,500 ft or 500 m) of the Gueydan fluvial system. Sodium chloride waters dominate. B. Deep waters from the Gueydan system. Note the five anomalous sodium sulfate waters.

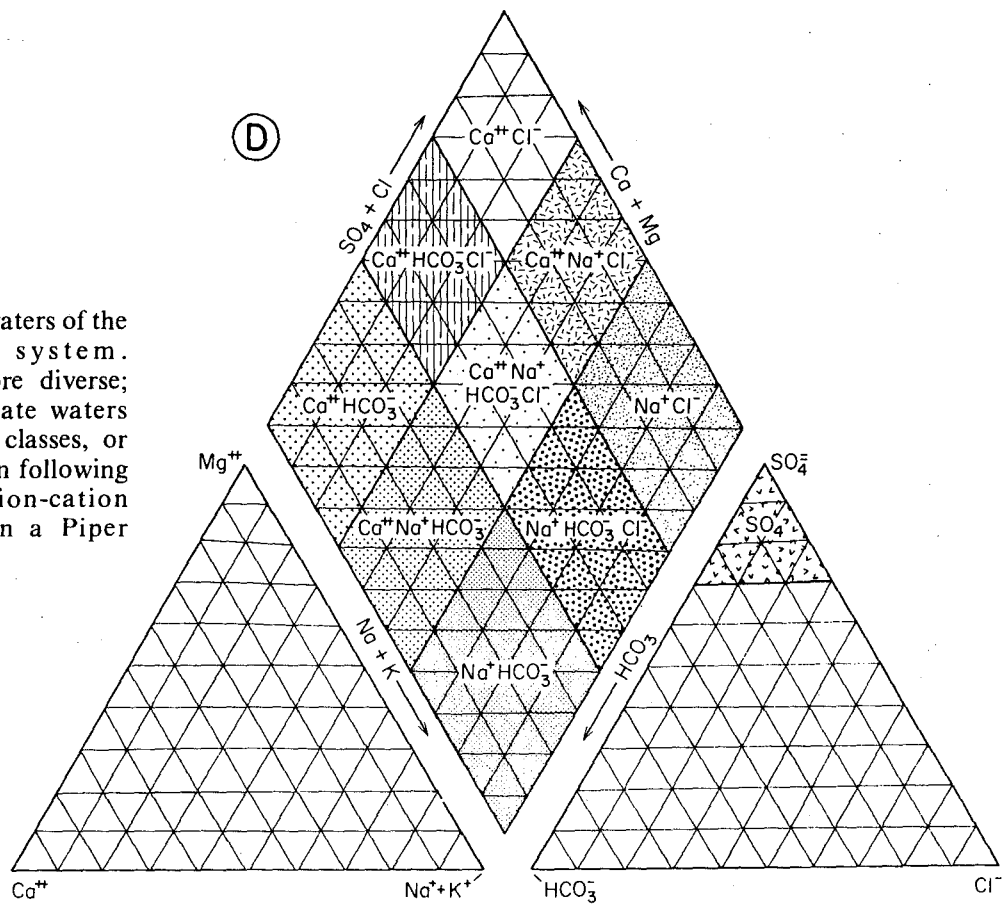
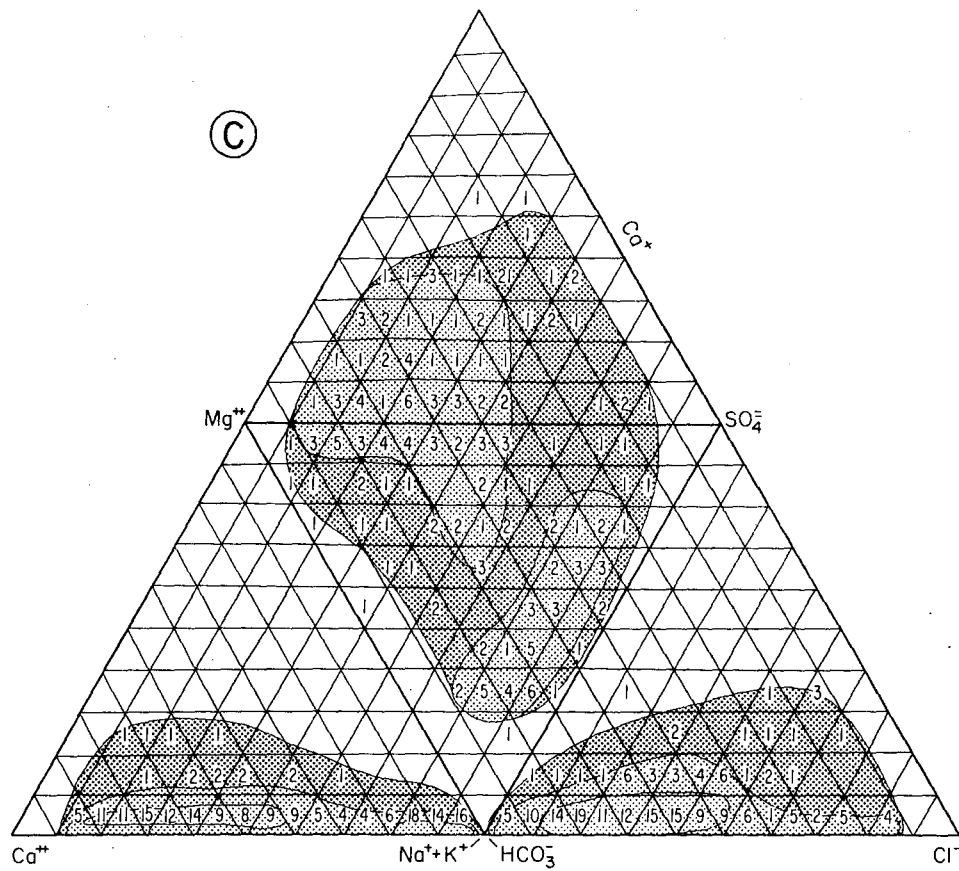


Figure 10 (cont.). C. Ground waters of the Chita-Corrigan fluvial system. Hydrochemistry is much more diverse; calcium to sodium bicarbonate waters dominate. D. Compositional classes, or hydrochemical facies, shown in following figures based on major anion-cation compositions as plotted on a Piper diagram.

Chita-Corrigan systems (fig. 11). Although more complex, the Chita-Corrigan displays evolutionary patterns of hydrochemical facies common to many aquifers, and is described first.

Chita-Corrigan Fluvial System: Regional ground-water systems in subsiding basins typically display a downflow evolution from calcium to sodium and from bicarbonate to chloride, concomitant with increasing total dissolved solids (TDS) content (Galloway and others, 1979). Evolution of waters is believed dominated by (1) exchange of calcium for sodium on clays, (2) leaching of chloride from sediment, and (3) mixing with discharging saline connate waters. This common evolutionary pattern is developed in the central portion of the map area (fig. 11B), which corresponds to a major fluvial channel axis of the Chita-Corrigan system (fig. 1). Shallow, low-TDS calcium bicarbonate waters grade downdip into mixed calcium-sodium and finally sodium bicarbonate facies. TDS contours show a concomitant increase in dissolved solids, but as expected, the pattern is highly lobate in plan view. Fresh, low-TDS water extends much farther downdip along the permeable fluvial channel axes (fig. 11B). Increased TDS is primarily a result of increasing chloride and associated cation content.

Marginal portions of the map area, which contain only minor fluvial channel axes, display complex hydrochemical facies mosaics. Water compositions are highly variable both within small areas and at different stratigraphic positions in the same well. Hydrochemical facies patterns must be generalized to fit the majority of analyses. Average TDS is higher than in the central area; even the scattered calcium bicarbonate waters are more saline. There is a general downflow decrease in the calcium/sodium ratio, but chloride content increases rapidly, and mixed chloride-bicarbonate waters dominate shallow and intermediate portions of the aquifer.

Attempts to fit the hydrochemical patterns into a simple downflow evolutionary sequence are less satisfactory. Figure 12 illustrates the problem. Whereas average TDS increases systematically in the highly transmissive central fluvial belt (path A), TDS increases abruptly from calcium bicarbonate to the surrounding calcium-sodium bicarbonate-chloride waters and then stabilizes (path B). The downflow sodium bicarbonate-chloride waters show no further increase in average TDS or in chlorinity. However, the downflow evolution of these waters can be explained by discharge and mixing moderate salinity sodium chloride waters into slowly circulating Catahoula waters. Ground waters in underlying aquifers, particularly Yegua and Sparta waters, do contain appropriate sodium chloride waters, and shallow portions of the Catahoula aquifer are appropriately located over probable discharge zones for these aquifers.

Similar deeper waters must also be discharging into and mixing with Catahoula waters in the central area. However, in the central area (path A) the Catahoula aquifer is highly transmissive and the intrastratal coastward-circulating flow system dominates the hydrochemistry. In marginal areas (path B) flux within the Catahoula aquifer is restricted and localized. Discharge of hydrochemically "mature" waters from underlying aquifers has a proportionally greater effect on hydrochemistry of the shallower aquifer system.

Discharge of ground waters from deeper aquifers into the shallow Catahoula aquifer can also explain anomalous high-TDS calcium bicarbonate-chloride and calcium-sodium chloride waters that are scattered through the fresh, calcium bicarbonate facies (fig. 11B). Vertical discharge of saline, mixed sodium-calcium, bicarbonate-chloride, and sulfate-bearing waters from the underlying Jackson aquifer is likely along a belt coincident with the present outcrop and shallow subsurface portions of the Chita-Corrigan system. These waters mix with the calcium bicarbonate waters, but their effect is apparent only in local, stagnant portions of the shallow Catahoula aquifer (fig. 12).

Processes that control the complex hydrochemical facies patterns of the modern confined Chita-Corrigan aquifer are summarized schematically in figure 13. The present hydrochemistry is a composite of simple downflow chemical evolution of ground waters combined with mixing of waters of differing composition discharging from underlying confined aquifers. Although the same principles would have operated to control hydrochemistry of the Chita-Corrigan aquifer during earlier stages in its evolution, relative proportions and areas of mixing as well as nature of the downflow evolution have undoubtedly changed.

Gueydan Fluvial System: The variety of hydrochemical facies in the Gueydan aquifer is limited. Most samples consist of sodium chloride or sodium bicarbonate-chloride waters (fig. 11A). TDS is moderate to high, even in the shallowest portions of the aquifer system. Freshest waters occupy broad lobes coincident with major sand axes in the southern and central part of the map area.

A simple downdip evolution of bicarbonate to chloride waters prevails. However, the generally high chlorinity of all water samples suggests either (1) a highly abbreviated shallow evolutionary sequence, perhaps because of the dry climate or (2) appreciable mixing of the shallow waters with chloride-rich waters discharged from below. Although part of the answer may lie with the dry climate, other South Texas aquifers, such as the Carrizo, contain bicarbonate-dominated ground waters. There is, on the other hand, abundant evidence for past and present discharge of deep waters to

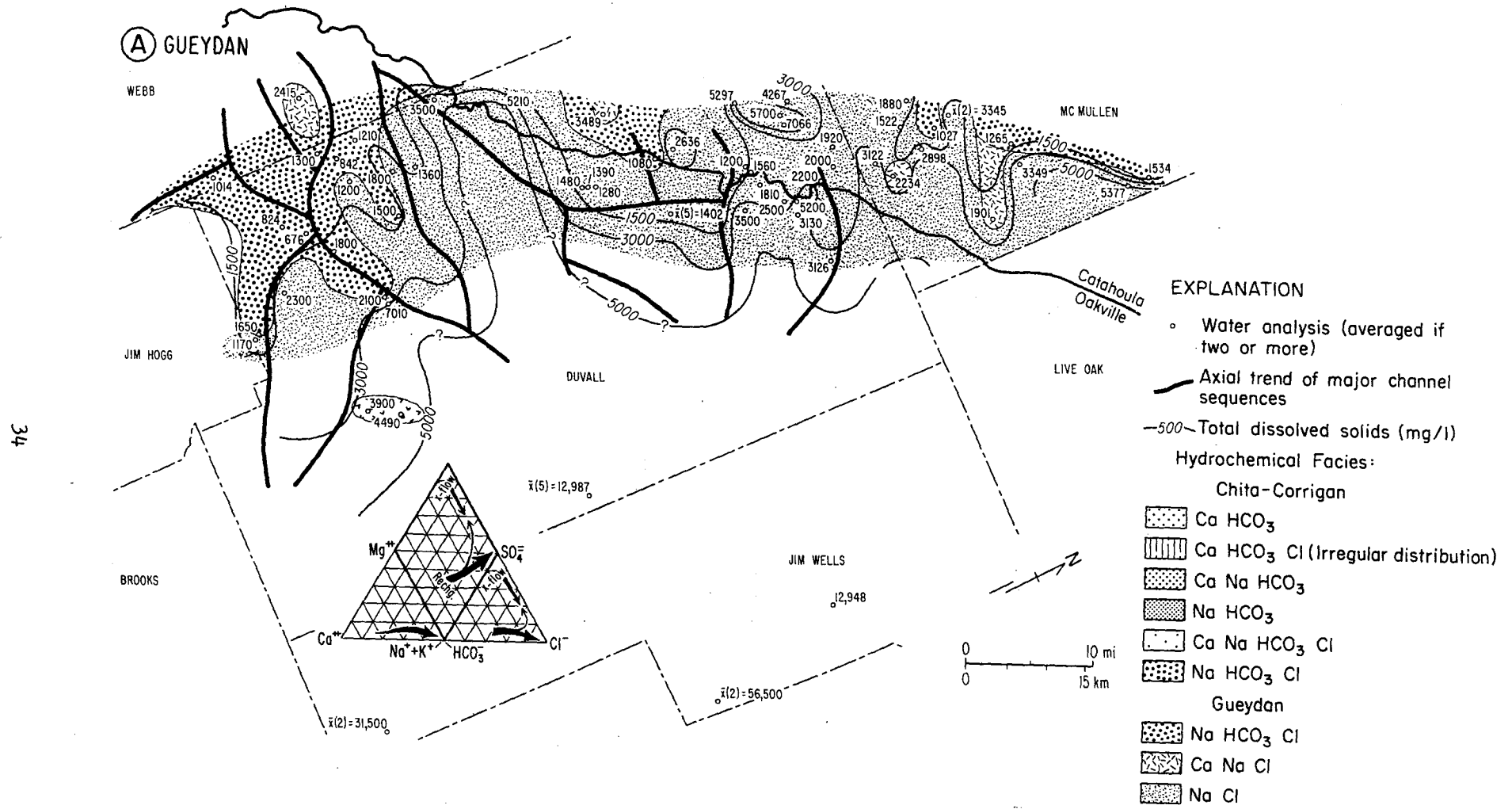


Figure 11A. Hydrochemical facies map of select study areas of the Gueydan aquifer system. Small Piper diagrams suggest downflow evolutionary trends responsible for areal patterns described in the text. The major compositional difference between waters of the Gueydan and Chita-Corrigan aquifer systems is particularly striking.

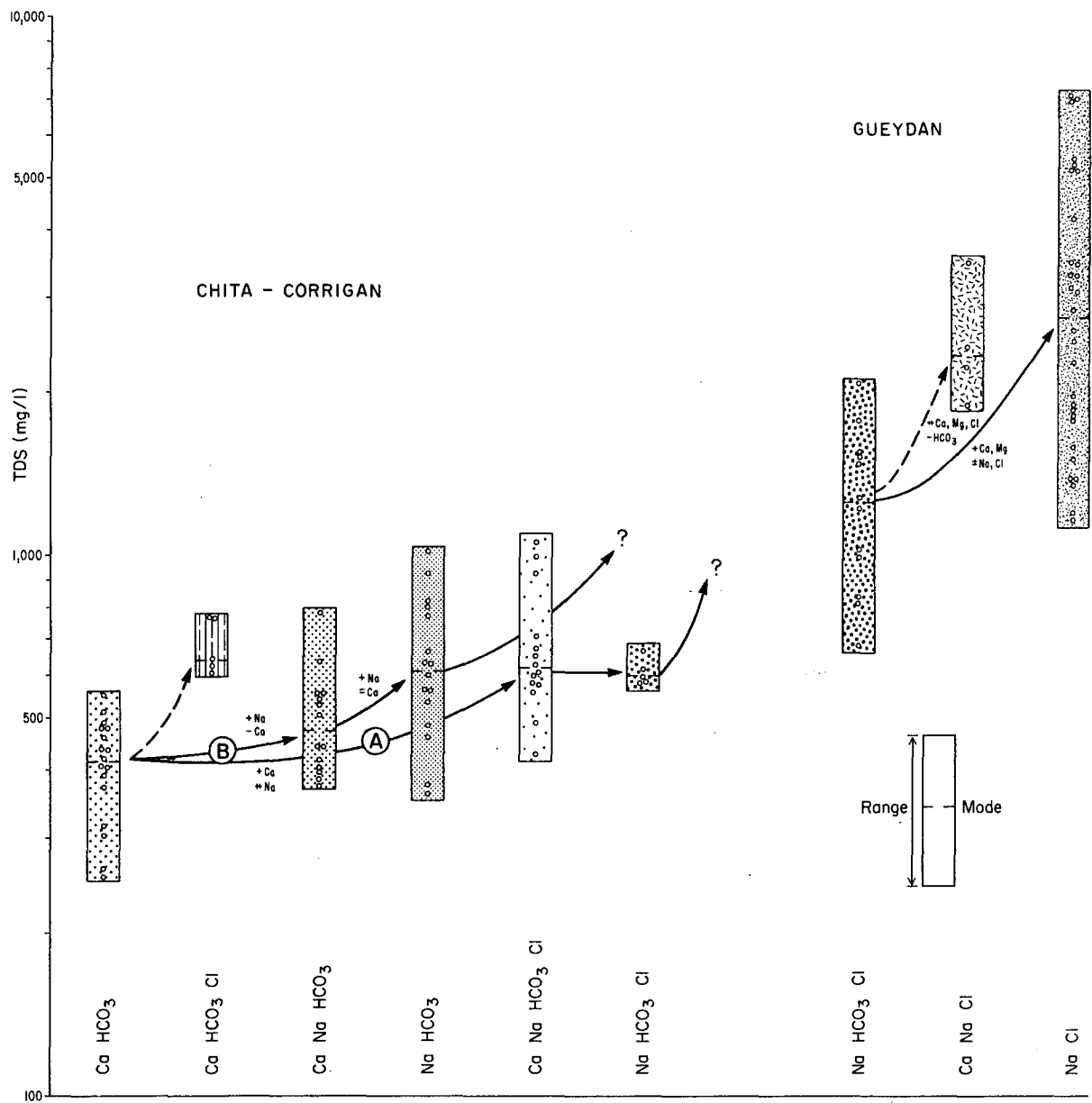


Figure 12. Mode and range of total dissolved solids (TDS, vertical scale) in all waters of each hydrochemical facies of the Chita-Corrigan and Gueydan systems. Downflow evolution or mixing with waters discharged from underlying aquifers should always cause a net increase in TDS. Suggested evolutionary or mixing paths, and the anion or cation changes necessary are shown by the labeled arrows. Path B (Chita-Corrigan) is a simple downflow evolution involving increasing chloride content and exchange of calcium for sodium in matrix clay. Path A requires net increase of calcium and sodium as well as chloride. Both Gueydan pathways necessitate absolute increase in sodium and calcium content; thus, mixing with more saline waters is strongly indicated. For explanation of symbols see figure 11.

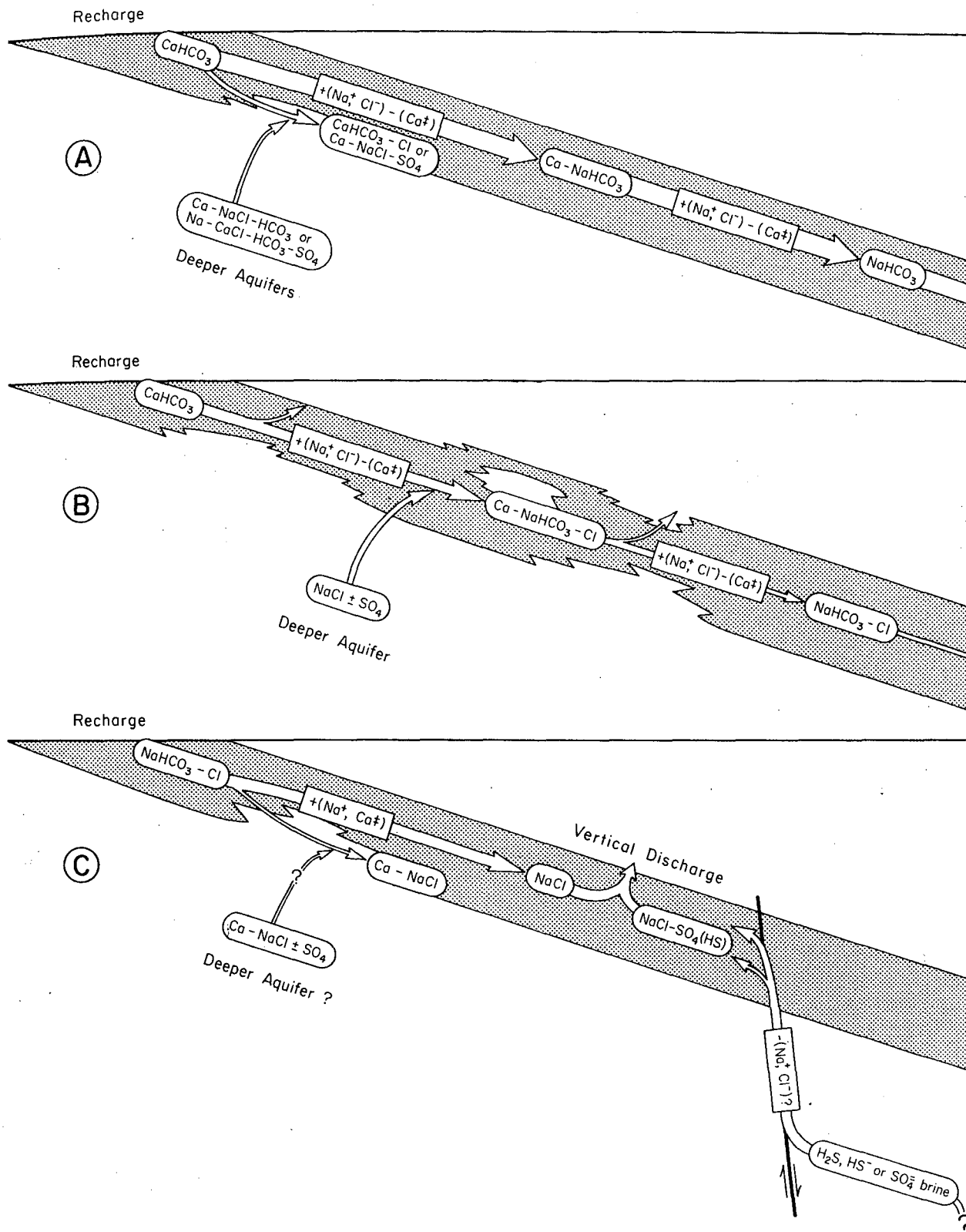


Figure 13. Schematic flow and mixing patterns interpreted for (A) highly transmissive portions of the Chita-Corrigan aquifer system, (B) low transmissivity portions of the Chita-Corrigan, and (C) within the Gueydan aquifer system.

the surface and into the Catahoula aquifer. Chalcedony and carbonate knobs paralleling fault zones are common in the Catahoula outcrop belt in the map area and are interpreted to indicate loci of ground-water discharge (Galloway, 1977; Lindemann, 1963). The Yegua and possibly other aquifers possess TDS trends indicating probable vertical discharge along this belt. Extremely saline waters locally occur at shallow depths within the Catahoula (fig. 11, north-central Duval County, for example). Such high salinities indicate mixing with deeper brines, and are associated with fault zones. The most likely interpretation is that shallow Gueydan waters have been modified by mixing with discharged sodium chloride brines. The widespread dissemination of chloride waters suggests this mixing is not primarily a result of recent contamination by petroleum development in the area.

Two anomalous water types occur locally within the Catahoula aquifer. Calcium-sodium chloride waters, which commonly display high-TDS content, can be explained by vertical discharge and mixing of a calcium-rich water (fig. 12). A second set of waters containing moderate to high measured sulfate content are scattered throughout shallow to deep portions of the aquifer. One area of such sulfate waters is indicated by two deep wells in southern Duval County (fig. 11A). Both wells lie near a zone of deep-seated growth faulting, and both produce waters from a depth of about 2,000 ft (600 m). Actual form of the dissolved sulfur is questionable. At the reducing and basic Eh-pH conditions typical of the deep Gueydan aquifer, HS^- is the more likely species. Conventional sampling procedures would result in subsequent oxidation to sulfate. These waters are also characterized by very low bicarbonate, low chloride, and low calcium content. Their moderate-TDS and extreme sulfur content are an enigma in that only the underlying Carrizo aquifer contains fresh water, and it is bicarbonate rich (Payne, 1975). Association of the sulfur-rich waters with faulting and their anomalous TDS certainly suggest vertical discharge and mixing of chemically different water masses.

Although compositionally different from Catahoula waters of East Texas, Gueydan waters also present a complex mosaic of chemically evolving waters circulating within the aquifer and mixing with varying proportions of waters discharged from deeper aquifers. The effect of vertically discharged waters is increased because of the drier climate and lesser meteoric recharge, low overall transmissivity of the Catahoula aquifer, segmentation of potential recharge areas by faulting and local topographic (and hence water table) reversals, and coincidence of the shallow Gueydan section with probable discharge zone of several underlying aquifers. Processes currently active in the aquifer probably illustrate the range of processes active

in earlier stages of its development, but present chemical composition is at best a qualitative image of earlier hydrochemical facies patterns.

Eh and pH: Modern ground waters of the Gueydan aquifer range from near neutral to highly basic. Data are sparse and measured pH in ground waters only approximates in situ pH (Hem, 1970), but evidence for systematic geographic variations exists. Waters in a relatively sandy portion of the Gueydan fluvial system (Duval County) characteristically exhibit measured pH values of 7 to 9 (fig. 14). Gueydan waters in Live Oak County, an area of abundant ash, exhibit a maximum pH range from 6.5 to 11. Chita-Corrigan waters in Fayette and Washington Counties are characterized by values between 7 and 8 (fig. 14). Detailed sampling around leach mining sites shows that pH varies greatly within the same sand body.

No direct Eh measurements of Catahoula ground waters have been published. Eh calculated from the NO_3^- - NH_4^+ pair using baseline water analyses around four shallow uranium deposits gives a range from +240 to +300 mV, suggesting slightly oxidizing waters recharge the aquifer. However, the reduced nature typical of much of the subsurface Catahoula and common presence of H_2S in many ground-water samples (Nichols and others, 1977) indicate rapid downflow reduction of the shallow waters.

Uranium Mobility: Few data on trace metal distribution in the Catahoula aquifer have been published. Nichols and others (1977) provide systematic data for the northern part of the Gueydan system (Beeville-Crystal City quadrangles). Background uranium content ranges from a few hundredths of a ppb to several tens of ppb. Molybdenum content ranges from a few ppb to tens of ppb. Very high values of dissolved U and Mo (up to a few ppm) occur locally within mineralized ground where oxidized waters intrude.

Uranium transport thus is locally continuing in parts of the Catahoula aquifer during the burial and exhumation phases and is particularly active where shallow flow systems were rejuvenated by Pleistocene valley incision and outcrop erosion. Moderate changes in water table elevation or slope may be reflected by flow modification at considerable depth, and this "stirring" has probably mobilized or remobilized more uranium in shallow portions of the aquifer than has occurred since the early postdepositional flow phase. A variety of uranyl complexes is likely present, although various carbonate complexes should dominate. Phosphate complexes could assume importance at the pH range of 4.5 to 7.5 (Langmuir, 1978) but data on phosphate content of the ground waters are lacking.

MEASURED pH

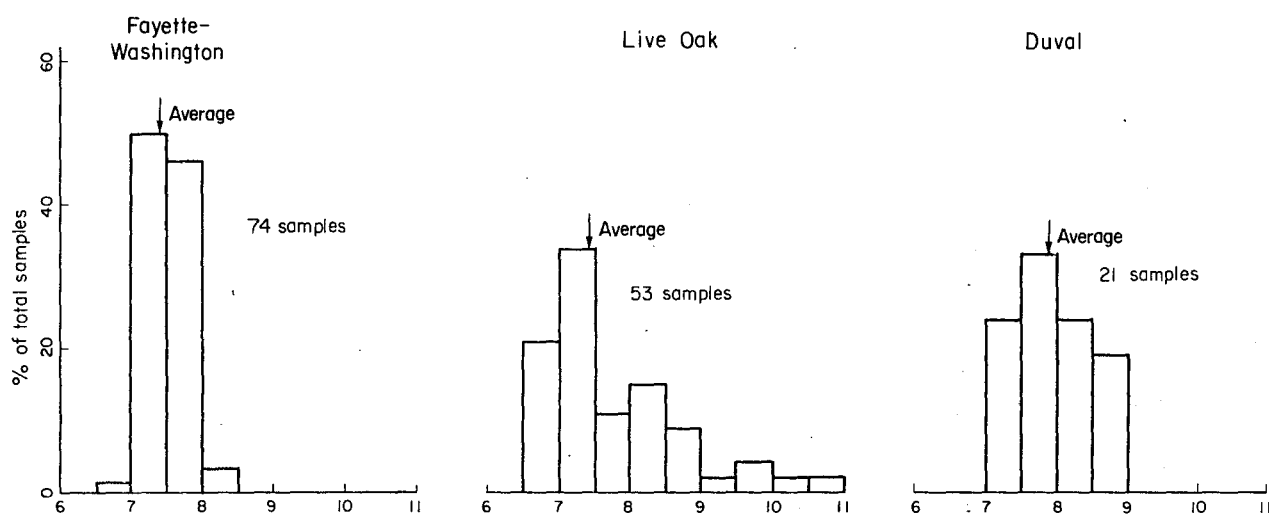


Figure 14. Published measured pH of ground-water samples from the Gueydan (Duval and Live Oak Counties) and Chita-Corrigan (Fayette-Washington Counties) systems. Highest values occur in Live Oak County where abundant volcanic glass is still preserved in the Catahoula.

Initial investigation revealed regional variations in extent and intensity of Catahoula ground-water flux (Galloway, 1977, p. 32-34), which are related to depositional and structural features. Isochemical contours for Catahoula ground waters display geometries reminiscent of matrix alteration patterns and provide a guide to relative ambient transmissivity of various parts of the aquifer system. Detailed delineation of modern flow patterns may therefore provide further criteria for reconstruction of flow dynamics extant during earlier phases of aquifer evolution.

Chloride provides a particularly useful "tracer" because chlorinity increases systematically downflow in most systems by leaching of soluble chlorides from lithologic components within the aquifer or by mixing with chloride-rich basinal waters (Hem, 1970). Many authors have noted the systematic increase in chloride attendant with increased residence time of a ground water in the subsurface (Chebotarev, 1955; Back, 1960; Tóth, 1972). Thus, the assumption that low-chloride content outlines areas of recharge and active flux, whereas abrupt increase in chloride content indicates stagnation (with consequent high residence time and mixing) or discharge seems well documented.

Chloride content can be interpreted from resistivity logs. Turcan (1966) described a method for calibration of chloride content to resistivities measured on mechanical logs; his method was applied to the existing log data base in two study areas and chlorinity maps and cross sections were constructed. Details of the calibration are discussed in Turcan (1966), and Payne (1970) provides an example of its application. Although the chlorinities calculated should be considered at best semiquantitative, the wide range of observed chlorinity and utilization of many wells allow delineation of meaningful patterns.

Two cautions are in order. These maps provide a view of ground-water flux as it exists today in a confined, leaky aquifer that has been modified by exhumation of the outcrop recharge area. Observations must be extrapolated back to earlier phases of the aquifer's history with care. Secondly, the chlorinity patterns bear striking resemblance to alteration patterns. In fact, they should, because both alteration and chloride leaching are controlled by interactions between a recharging, reactive ground water and the aquifer matrix. Thus, both mirror variations in ground-water flux and variations in the distribution of reactants within the reservoir. However, chloride content is in no way proposed as an indicator or control of uranium mineralization.

Chita-Corrigan Aquifer: The Chita-Corrigan System can be regionally subdivided into upper and lower intervals. Detailed maps of sand distribution and average chlorinity were constructed for an area covering one of the major fluvial complexes of the system. Figure 15 is the map of the lower interval and is used for discussion. Perusal of this map reveals several significant observations:

1. The sand-rich core area of the fluvial complex is well flushed, and displays a broad lobe of very fresh, low-chloride water (area A).

2. The margin of the lobe is digitate with salients of fresh water corresponding to dip-oriented sand belts and embayments of high-chloride water occupying muddier, interchannel facies (areas marked B).

3. Chlorinity increases abruptly along the downflow margin of the fresh-water tongue, suggesting vertical discharge of lower Catahoula waters. Localized vertical discharge of waters from the lowest sands into upper sands of the same stratigraphic interval is indicated by areas of upward freshening such as occur between the two sites labeled B. Here contours reflect only the freshest upper sands, but mixing with the more saline waters from the lowest sands has increased their chloride content from 250 to 500 mg/l.

4. Downflow convergence or divergence of sand axes has a focusing or defocusing effect as ground-water flow refracts into these permeable conduits. Flow convergence results in highly elongate, downflow tongues of low-chloride water (area C). Divergence is indicated by updip embayments or islands of brackish water (area D).

5. Distribution and orientation of permeable elements may modify flow patterns sufficiently to leave stagnant saline islands embedded within the regionally flushed section (area E).

Maps necessarily provide an averaged view of water chlorinity within several hundred feet of aquifer section. Similar analysis of chlorinity utilizing log response can be made on cross sections (fig. 16). Examination of salinity sections reveals additional relationships between the stratigraphic and structural configuration and inferred flux of fresh water.

6. Laterally continuous mudstone beds form the principal aquitards, vertically segregating fresh-water-bearing sands. Separation may be local, or may extend for tens of miles in the dip or strike direction.

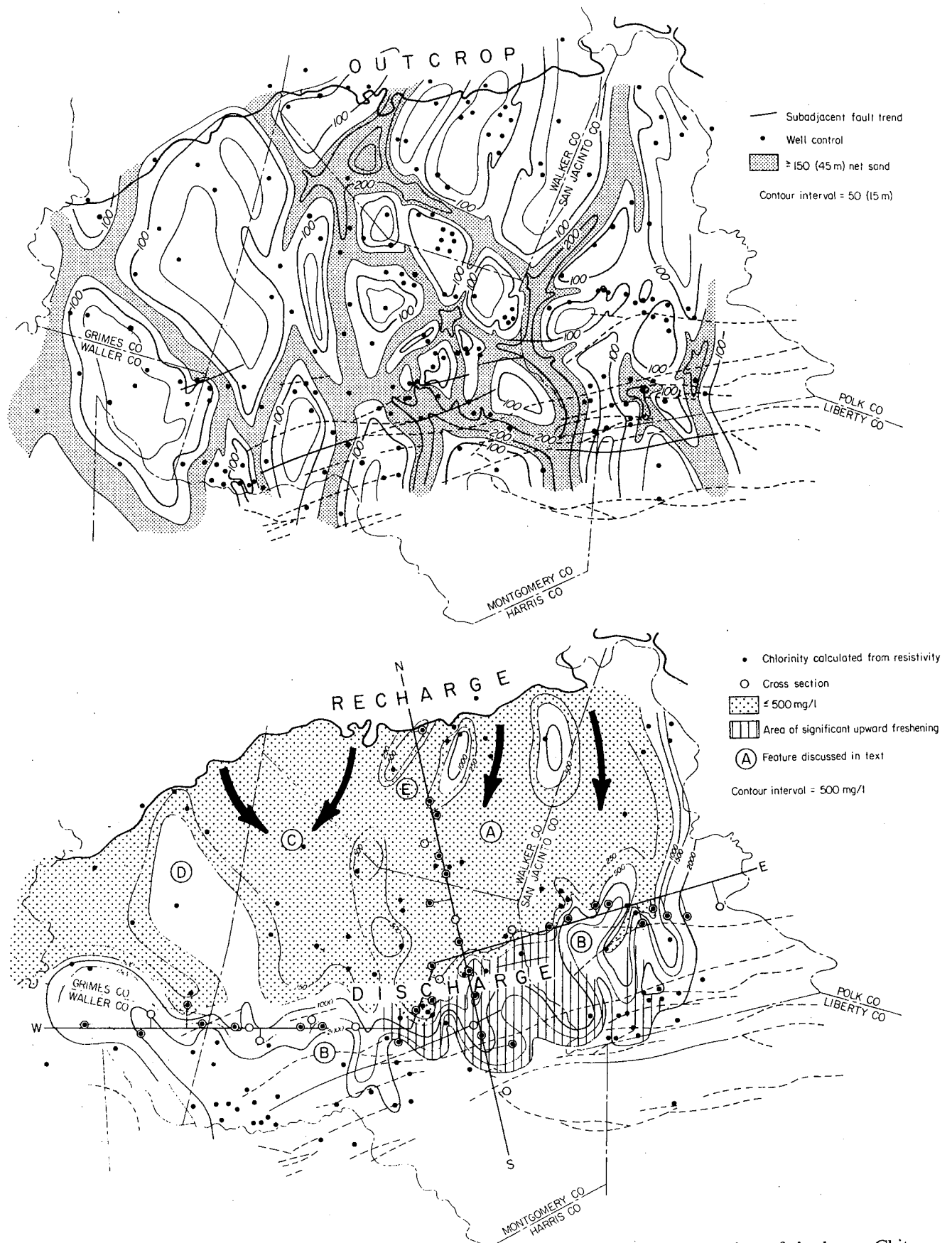


Figure 15. Net sand and log-derived apparent ground-water chlorinity for a portion of the lower Chita-Corrigan fluvial system. Lower chloride contents and, by inference, most active ground-water flux coincide with dip-oriented fluvial axes defined by sand distribution patterns. Lettered features are described in text.

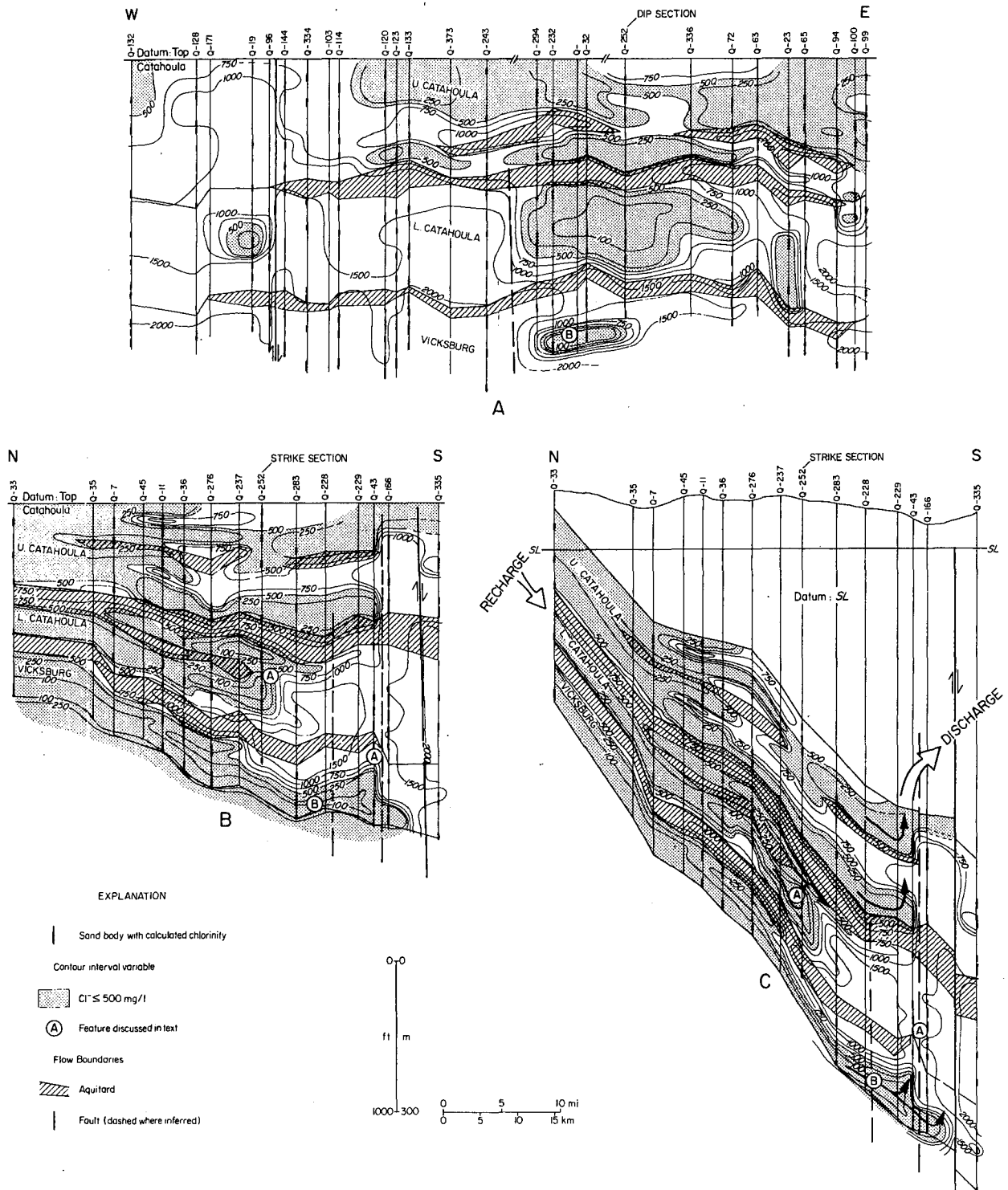


Figure 16. Strike and dip cross sections of the Chita-Corrigan aquifer showing apparent chlorinity patterns within individual aquifer sands. Lettered features illustrate several flow features discussed in the text. A. Strike section. B. Dip section hung on the top of the Catahoula. C. Dip section within sea level datum. See figure 15 for location of sections.

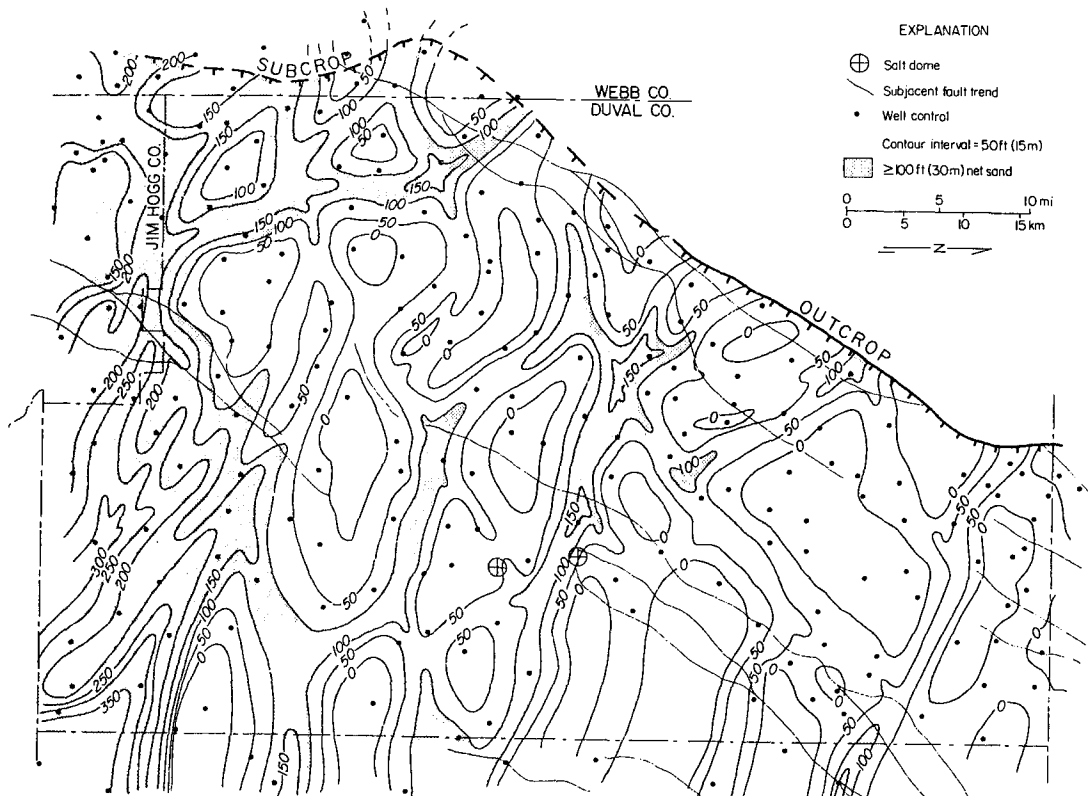
7. Vertical discharge of ground water is indicated by upward bulges of contours at the toes of fresh-water plumes (fig. 16, A areas) and occurs along the downflow margins of bounding mudstone aquitards or near fault zones.

8. The Vicksburg aquifer, which lies immediately below the Catahoula and is separated from it by a laterally continuous marine mudstone aquitard, contains a lobe of fresh water that extends more than 10 mi (16 km) downdip beyond comparably fresh waters in the lower Catahoula aquifer. Thus, the normal tendency for the base of low-chloride water to climb section in the regional downflow direction can be reversed in unusually permeable, confined aquifers, provided that ultimate discharge is possible. Structural discontinuities probably become increasingly important in localizing discharge of deeply buried, confined aquifers.

Study of chlorinity patterns reveals many geometric features typical of alteration fronts. Numerous observed complexities, such as isolated unaltered islands within altered ground, vertical and lateral isolation of individual alteration tongues, alteration chimneys, and structural control of alteration pattern are potentially explicable by physical aspects of ground-water flux. Closer examination of such physical flow phenomena is thus useful, not only for better understanding of present hydrologic processes, but for recognition and prediction of analogous geometric alteration patterns.

Gueydan Aquifer: An area of extensive well control centered in Duval County was mapped in a similar fashion. The Catahoula section was subdivided into upper and lower portions, and each mapped separately; both sets of maps are shown in figure 17 and a typical dip cross section is illustrated in figure 18.

Comparison of chlorinity patterns in the Gueydan study area with those of the Chita-Corrigan reveals several similarities as well as major differences. Tongues of fresh water (fig. 17, A areas) extend downdip from shallow outcrop or subcrop recharge zones, particularly in the area of maximum channel sand developed at the southern end of Duval County. Recharge of the Gueydan aquifer is complicated, however. The Gueydan section is overlapped by a thin veneer of Goliad gravel across much of the southern part of the map area. In addition, the lower Gueydan interval is truncated at its updip extent by upper Gueydan. Both relationships are shown in the cross section (fig. 18). Meteoric recharge entering the Gueydan in the southern part of the area must traverse the Goliad cover, and parts of the lower Gueydan can only be recharged from overlying sands of the same unit. In the northern area, recharge



UPPER GUEYDAN

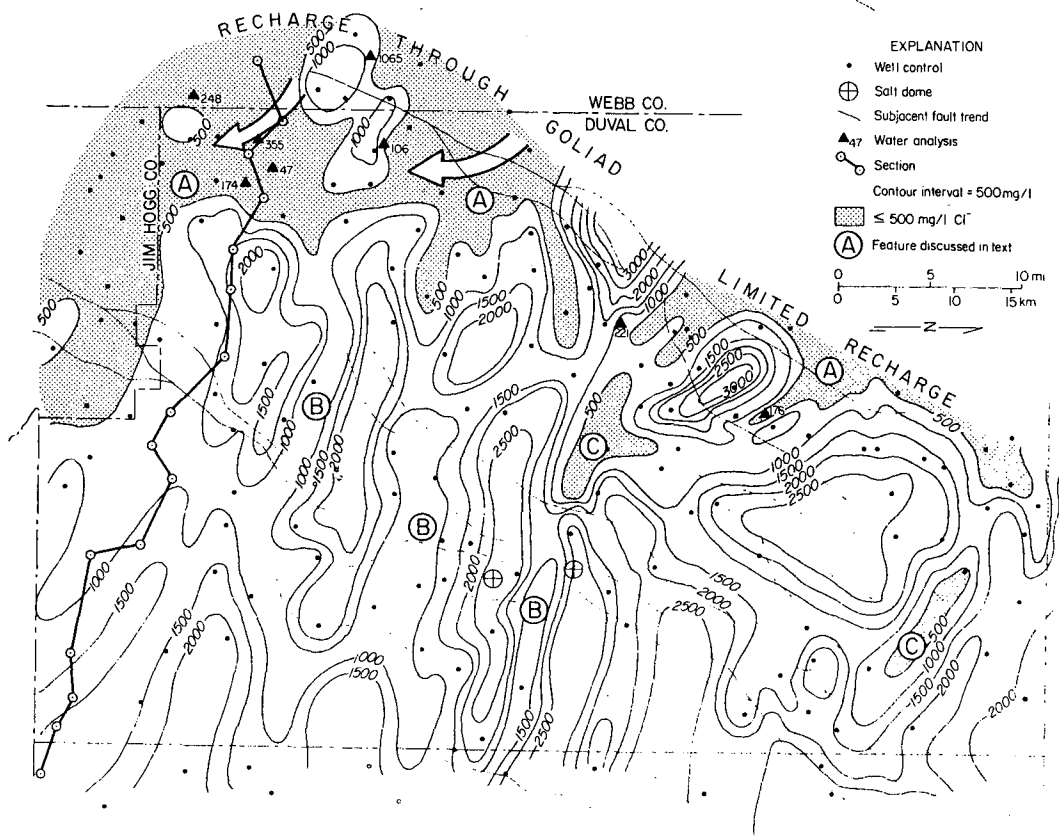
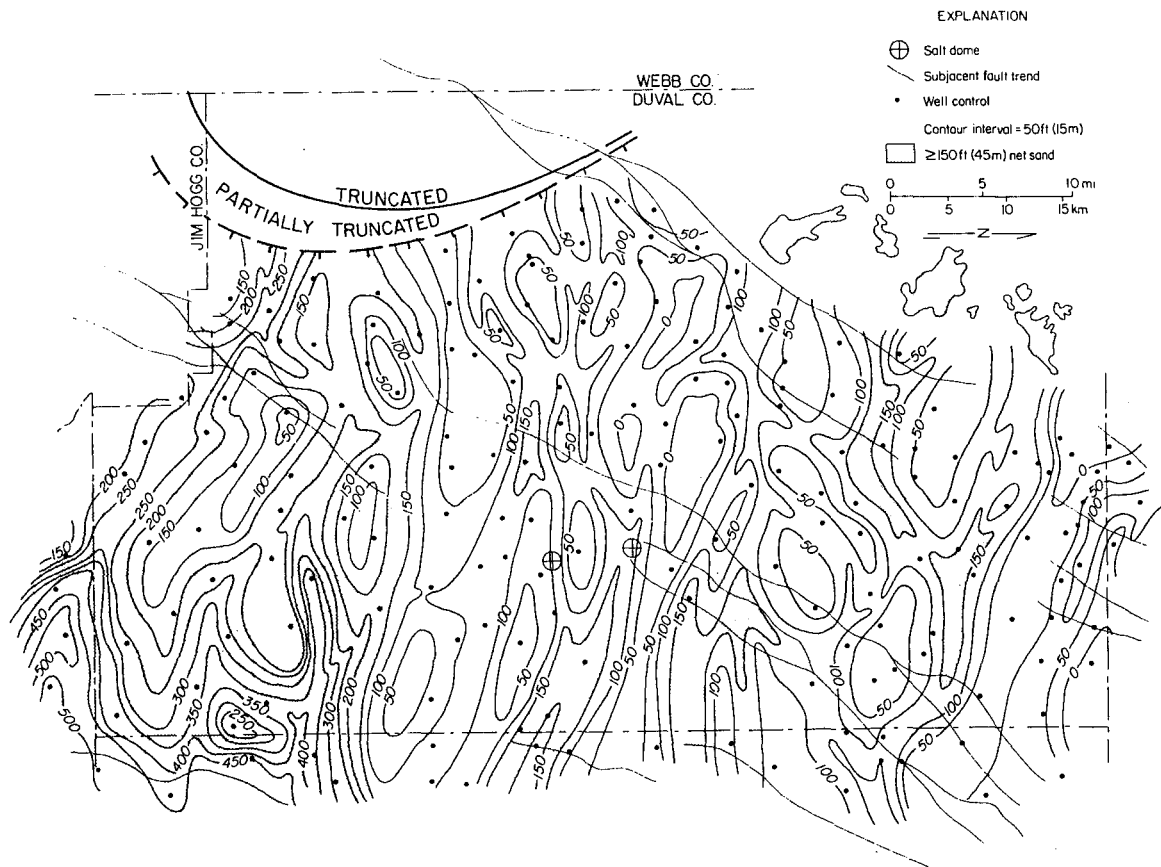
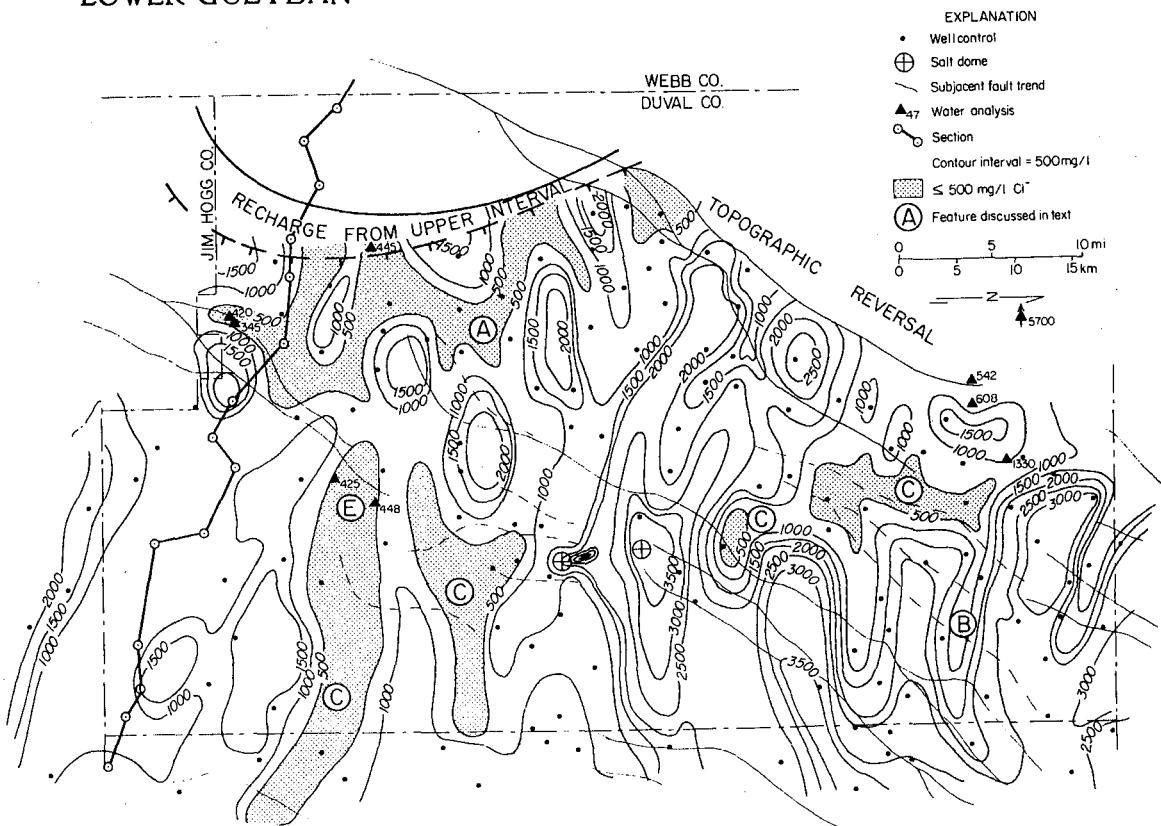


Figure 17. Net sand and apparent chlorinity maps for upper and lower intervals of a portion of the Gueydan fluvial system. Letters mark features interpreted in the text. For location of study area see figure 3.



LOWER GUEYDAN



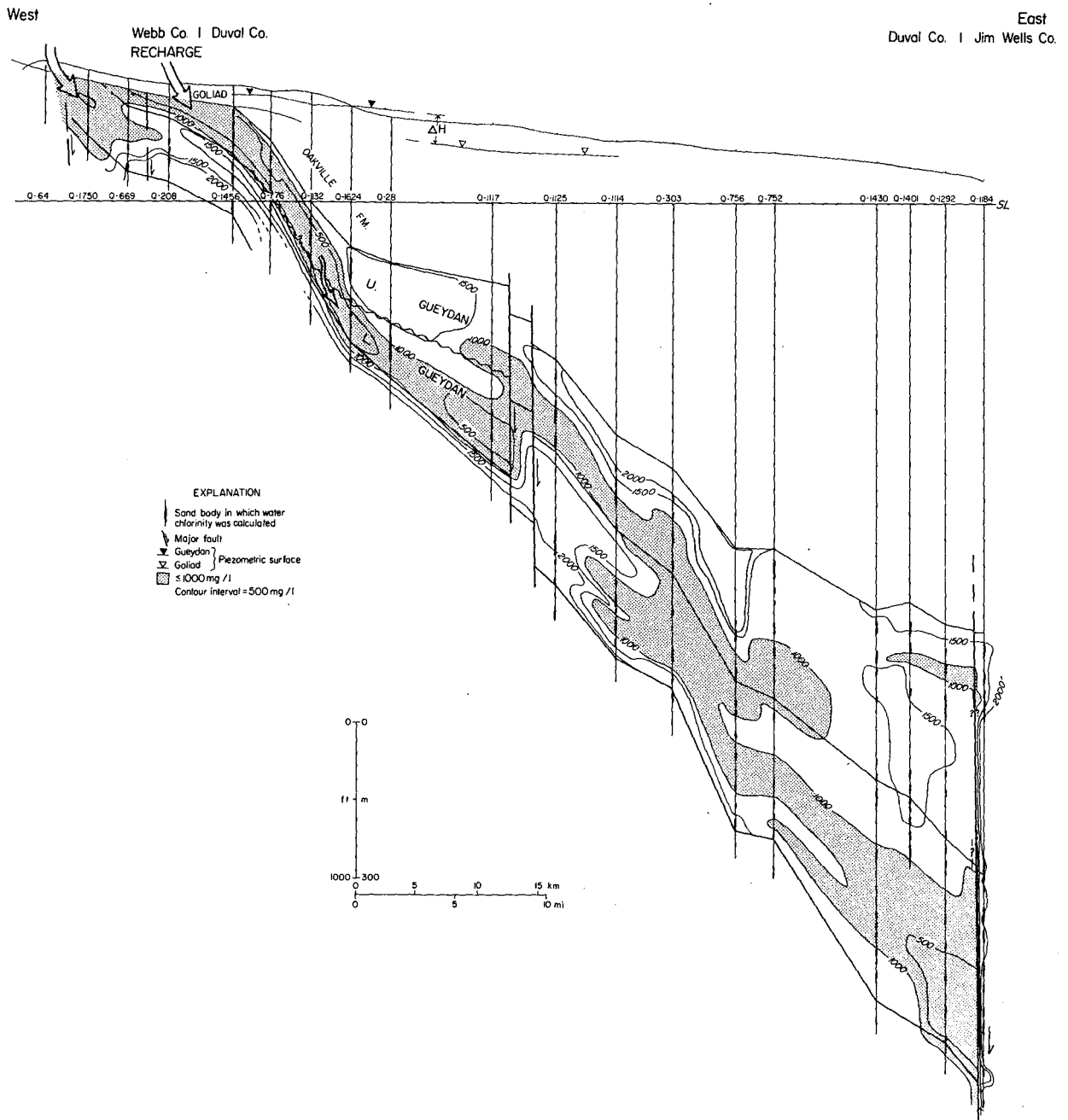


Figure 18. Dip cross section of the Gueydan system showing apparent chlorinity patterns within major sand sequences. Note truncation of the lower Gueydan by upper Gueydan fluvial sands near the updip end of the section. Lettered features discussed in text. Section located on figure 17.

potential along the outcrop is limited by westward topographic slope and by complex faulting. The upper Gueydan section could be recharged through capping Oakville sands, and presence of very shallow, low-chloride tongues suggests this does occur.

The fresh-water tongues associated with shallow recharge are limited by closure of the 500 to 1000 mg/l contours at shallow depths. Ribbon-like projections of moderate chlorinity waters coincident with the principal sand-axes extend downdip across the map (B areas). Localized masses of apparent low-chloride water locally occur within these banners, sometimes at considerable depth (C areas). The limited analytical data available are consistent with these patterns. The two wells located at E on the lower Gueydan isolith map are particularly significant. Both yielded low-chloride sulfate water from approximately 2,000 ft (600 m). Other plumes of apparent low chloride may be equally rich in dissolved sulfur species. Several such plumes originate near fault zones and suggest updip movement of the anomalous water within the Gueydan sands.

Examination of a cross section through the Duval area further suggests fault-discharge and updip flow for the anomalous water masses (fig. 18). A particularly striking example occurs at the east margin of the section. In addition, the section illustrates downward flux of meteoric water from the upper to lower Catahoula where sand bodies of the two intervals are superposed. Although such downward flux would seem at first contradictory, examination of aquifer geometry provides a logical explanation. Upper Gueydan sands trend nearly strike parallel in the area of superposition; continued flow down regional coastward hydrodynamic gradient thus necessitates cross-stratal flow into the underlying dip-oriented sands. Appropriate stratigraphic configuration thus might explain downwelling alteration tongues into lower sand bodies.

At moderate depths a significant head differential exists between the Gueydan aquifer and the overlying Goliad aquifer and vertical leakage is probable (note different elevations of the respective potentiometric surfaces plotted on fig. 18).

The data only provide a basis for speculation about the source and nature of discharging waters: (1) Waters mixing with the shallow Gueydan contain chloride and dissolved sulfur species. Possible sources include the Yegua, Sparta, and Queen City aquifers. (2) Waters discharged into deeper parts of the aquifer are low in chloride, but may be extremely rich in dissolved sulfur. The only source of low-chloride water beneath the Gueydan in the areas where the plumes are mapped is the Carrizo aquifer, and low-chloride plumes that lie along the updip fault zones occur in a likely area of

Carrizo discharge. However, similar plumes located in the southeastern part of Duval County are underlain only by waters containing several thousand mg/l chloride. The extended extrapolation of the chlorinity maps beyond the shallow calibration points does make geochemical quantification of these deep plumes highly tenuous. Deeper sources might include overpressured muds of the Wilcox (Eocene) several thousand feet below the Gueydan, but the low chloride content remains unexplained. (3) Fault zones are loci for discharge and mixing of deep connate waters. Where deep, pressured waters discharge into shallow aquifers, they tend to back-flush the aquifer and retain their geochemical integrity. Such waters move through the most permeable conduits that would allow head release into shallower aquifers or to the surface.

In summary, the observed ground-water flow patterns have several implications for the habitat of uranium mineralization in the Gueydan. Flow directions of shallow ground waters may not be coincident with patterns deduced from geometry and polarity of alteration fronts. Extensive areas may have been intruded by one or more generations of reactive waters superimposing diagenetic features not related to mineralization and obscuring primary alteration patterns. Radiometric disequilibrium is likely in areas of active ground-water flux. Certainly, the local geochemistry of modern ground waters in the Gueydan fluvial system differs in significant detail from the waters extant during the primary mineralization phase.

URANIUM CONCENTRATION I: CHARACTERISTICS AND HABITAT OF CATAHOULA URANIUM DEPOSITS

Understanding the concentration processes and subsequent modification of primary deposits necessitates thorough description of the physical geology, mineralogy, and geochemistry of known deposits. Available samples and data for three significantly different Catahoula deposits, the Bruni (Webb-Duval district), House-Seale (Live Oak district), and an unnamed discovery from Washington and Fayette Counties (fig. 3), represent three major points on the spectrum of Coastal Plain uranium deposits.

Bruni Deposit

The Bruni uranium deposit (fig. 3) is typical of numerous small to large mineralization-front deposits found in the Webb-Duval district. Bruni has been the subject of intensive mineralogical and isotopic analysis (Goldhaber and Reynolds, 1977; Spirakis and others, 1977; Reynolds and Goldhaber, 1978; Goldhaber and others, 1978). Samples examined in this study contribute additional details about the composition and habitat of the deposits.

Uranium mineralization in the Bruni lies along a continuous, linear boundary between oxidized, altered sediment and gray, sulfide-rich, reduced, unaltered ground within a proximal crevasse splay sand sequence approximately 45 ft (14 m) thick. The mineralization front (and coincident oxidation front) has been traced at least 2 mi (3 km) by drilling, and trends northeast-southwest subparallel to the margin of a mapped belt of channel-fill sands (fig. 19). Modern ground-water flow is to the southeast across the front, essentially coincident with the inferred flow during development of the mineralization front. Thus, mineralization remains in a physical hydrologic setting generally similar to that responsible for ore formation.

Uranium and Trace Metals Distribution

Uranium distribution approximates a C-shaped roll pattern and occurs along the margin of the oxidation salient or tongue within reduced ground (fig. 20). Molybdenum is concentrated slightly farther from the oxidation front within reduced ground (fig. 20, cores c and d, and table 2); selenium is concentrated within the oxidized tongue (cores a and c, table 2 and fig. 20). The zoned concentration of selenium, uranium, and molybdenum is characteristic of alteration front deposits and reflects the Eh gradient extant at the time of uranium concentration (Harshman, 1974; Vasil'eva, 1972). By analogy with electrical current flux, which is from negative to positive poles, the ratio of Mo to Se can be used to define front polarity. Thus, Mo/Se is greater than 1 on the unaltered (downflow) side and is less than 1 on the upflow, or altered side of the mineralization front. Uranium is concentrated in TiO_2 (anatase) and chemically complex U-Ca-Si phases (Reynolds and others, 1977).

Copper and lead occur in some uranium deposits (Harshman, 1974). Copper averages 6 ppm in oxidized samples and 8.5 ppm in reduced samples. Lead averages 4 ppm in oxidized samples and increases to 6 ppm in reduced ground. The distributions suggest possible slight enrichment in reduced, argillaceous sediment (fig. 20).

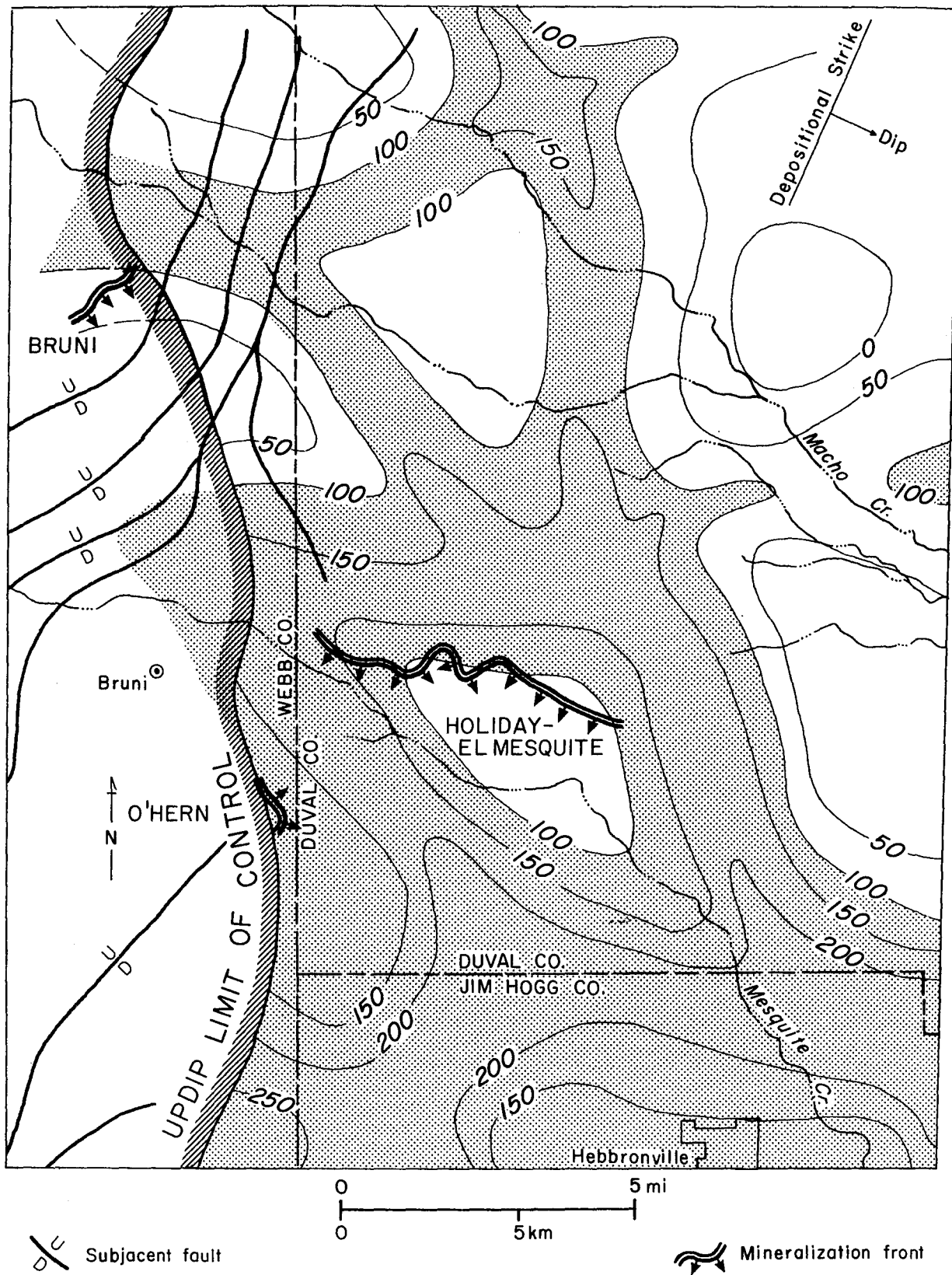


Figure 19. Geologic setting of the Bruni and nearby uranium deposits. Contours show net Catahoula sand.

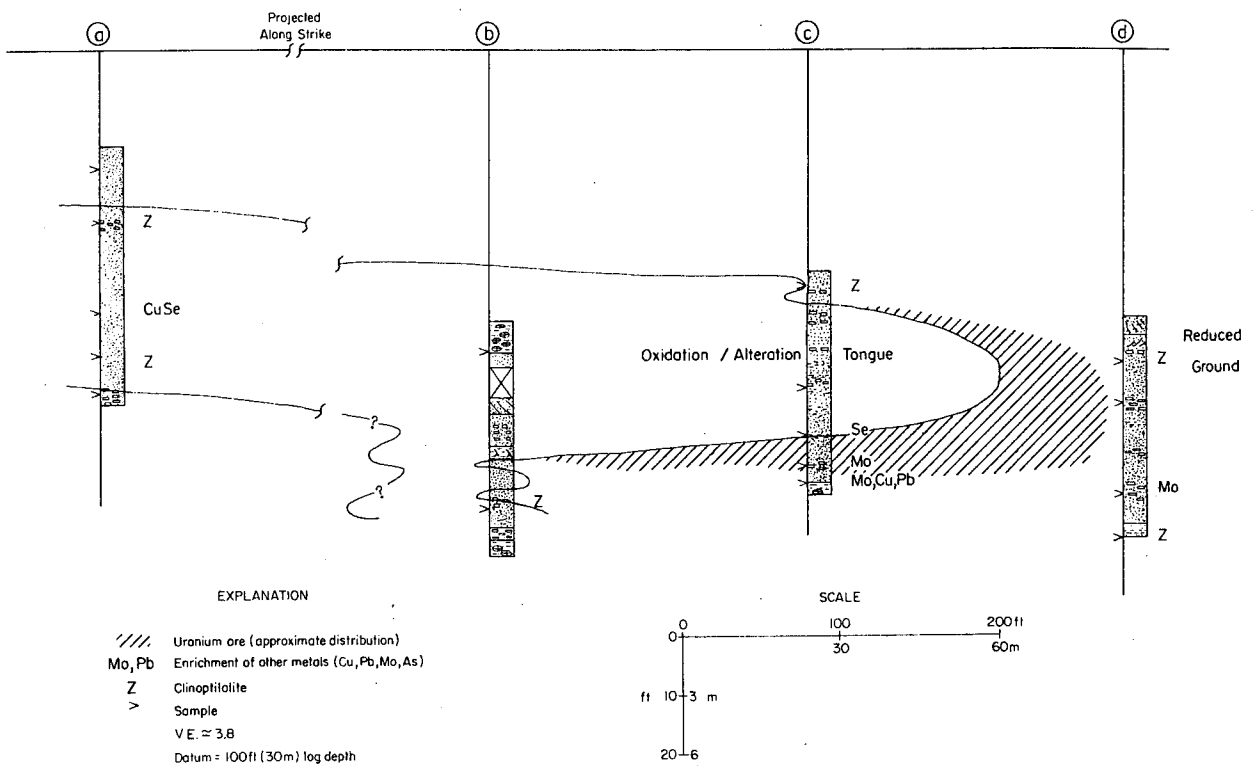


Figure 20. Core cross section of Bruni oxidation/alteration front. Distribution of uranium mineralization, trace metal enrichment and presence of clinoptilolite indicated by cross-hatching and symbols. For explanation of symbols, see figure 11.

Table 2. Analytical and petrologic data, Bruni samples.

Sample No.	Fe Ox. state	Metals (ppm)						Major components (percent by weight)						Mineralogy		
	o= Ox. r= Re.	U ₃ O ₈	Mo	Se	Cu	Pb	Fe ₂ O ₃	FeS ₂	Pyritic S	SO ₄	CO ₃	Organic C	Clinopt.Kaol.	Montmorillonite Na	Ca	
B-150	o	2	1	<0.1	4	7	-	-	-	0.02	11	-	Ab	Ab	Ab	D
B-175	o	7	2	<0.1	5	4	-	-	-	0.03	8	-	Tr	Ab	Ab	D
C-139	o/r	<1	2	<0.1	5	2	-	-	-	0.03	10	-	Tr	Ab	Ab	D
C-156	o	7	2	9	6	3	-	-	-	0.04	6	-	Ab	Ab	Ab	D
C-164	o	2,400	2	292	6	4	-	-	-	0.08	13	-	Ab	-	-	-
C-169	r	128	38	1	8	6	-	-	-	0.10	10	-	Ab	-	-	-
C-172	r	12	9	0.2	16	17	-	-	-	0.02	6	-	Ab	Ab	Ab	D
D-152	r	2	2	0.1	8	2	-	-	-	0.05	10	-	Tr	Ab	Ab	D
D-174	r	4	4	<0.1	6	6	-	-	-	0.06	7	-	Ab	Ab	Ab	D
D-182	r	2	1	<0.1	5	6	-	-	-	0.02	9	-	R	Ab	Ab	D
A-119	r	11	1	0.2	7	2	-	-	-	0.02	15	-	Tr	Ab	Ab	D
A-128	o	11	1	14	7	4	-	-	-	0.02	7	-	R	Ab	Ab	D
A-143	o	8	<1	435	12	3	-	-	-	0.02	10	-	Ab	Ab	Ab	D
A-150	o	4	<1	10	5	3	-	-	-	0.02	13	-	Tr	Ab	Ab	D
A-157	r	12	1	0.5	8	8	-	-	-	0.02	9	-	Ab	Ab	Ab	D

- = not analyzed
 Ab = absent
 Tr = trace

R = rare
 C = common
 A = abundant
 D = dominant

Major Element Distribution

Iron, sulfur, and organic carbon typically occur in varying abundance in and around most uranium deposits, and their distribution, form, and isotopic composition provide considerable information about ore genesis. In the Bruni deposit, iron is enriched in the clay-sized fraction, but there is no indication of depletion in oxidized sediments (Goldhaber and Reynolds, 1977).

Distribution of sulfur is quite different, however. Sulfate content is uniformly low, ranging between a few hundredths to a tenth of a percent (table 2). Reduced sulfur, in the form of iron sulfide, is abundant on the unaltered side of the mineralization front. Abundances range from a few tenths to as much as several percent (fig. 21) and are systematically distributed relative to the mineralization front. Figure 21 summarizes iron and sulfur data reported in a series of papers (Goldhaber and Reynolds, 1977; Goldhaber and others, 1978; Reynolds and Goldhaber, 1978). Several geochemical/mineralogical domains are present along the transect of the mineralization front.

1. The updip area (core 1) contains no sulfide. Iron is present dominantly as hematite or as detrital iron-titanium oxides.

2. The alteration tongue is outlined by limonitic sand encased in a matrix of pyritic and marcasitic gray sediment.

3. The mineralized nose of the tongue is characterized by irregular patches of marcasitic sand. Local mud lenses commonly contain relatively little iron sulfide (cores 4 through 7).

4. A broad, pyrite-rich tongue of sediment extends updip toward the alteration front (cores 8 and 9).

Pyrite appears at the expense of detrital iron-titanium oxides by sulfidization of the iron. Sulfur isotopes confirm two sulfide populations. Marcasite contains light sulfur ($\delta^{34}\text{S}/\infty = -10$ to -30), whereas pyrite is rich in heavy sulfur ($\delta^{34}\text{S}/\infty = +10$ to $+30$). Light sulfur is commonly produced by either biogenic or abiogenic fractionation processes associated with uranium concentration along an alteration front (Cheney and Trammell, 1973; Granger and Warren, 1969; Austin, 1970). Isotopically heavy sulfur, in contrast, is associated with oil field brines (Goldhaber and others, 1978). The observed patterns can be explained by sequential epigenetic reduction followed by epigenetic alteration and mineralization of originally oxidized fluvial sediments (Goldhaber and Reynolds, 1977; Goldhaber and others, 1977, 1978). Recognition of such geochemically opposed epigenetic events by mineral and geochemical zonation and distributional patterns has been discussed by Shmariovich (1973). Mineralogical

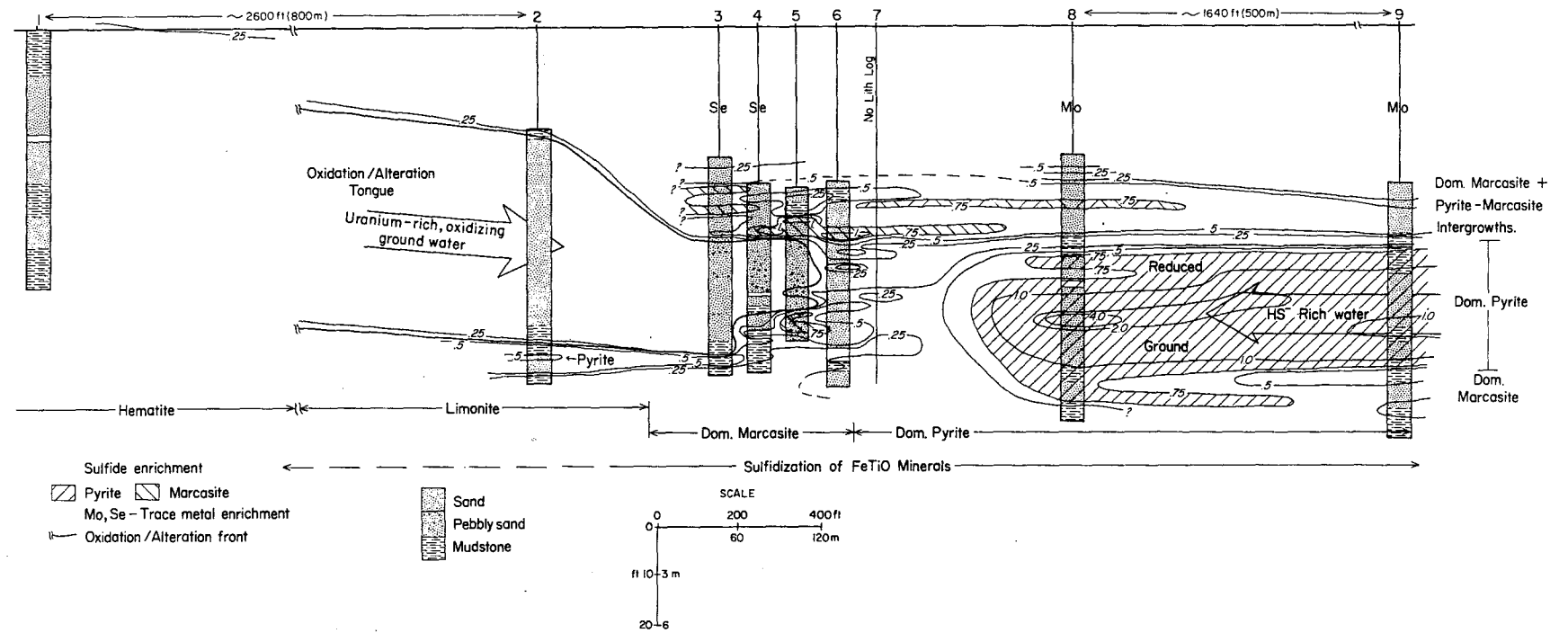


Figure 21. Distribution and mineralogical form of sulfur and iron along a core cross section of the Bruni front: Contours show lateral variation of weight percent of iron sulfide in the plane of section. Areas of sulfide enrichment include isolated marcasitic pods near the nose of the front and a broad pyritic core within the host sand down-dip from the alteration front. Marcasite is enriched in isotopically light sulfur; pyrite is enriched in isotopically heavy sulfur. Iron is present only in the oxidized state in the upflow direction. Limonite occurs within the alteration tongue; hematite dominates core 1, and is interpreted to represent primary oxidation imposed at the time of deposition of the crevasse splay sediments. Back-flux of reducing, sulfide-rich waters sulfidized detrital iron-titanium oxides to form the pre-ore pyrite, which was later oxidized by down-dip-flowing oxidizing, uranium-charged meteoric water. Section and data from Goldhaber and Reynolds (1977), Reynolds and Goldhaber (1978), and Goldhaber and others (1978).

and isotopic gradients indicate that the reactive, sulfidizing fluids moved updip at least several hundred feet beyond the present alteration front. Epigenetic alteration by meteoric ground water followed, intruding the presently observed limonitic alteration tongue into the reduced core of the sand. Both processes redistributed sulfur and formed iron sulfides, which can be distinguished by mineralogy and isotopic composition in the Bruni deposit. Such a complex history is not surprising in the context of common cross-stratal flow and mixing of geochemically diverse water masses typical of the Gueydan. Organic carbon content in and around the deposit is low. Data reported in Goldhaber and Reynolds (1977) indicate that total organic carbon (TOC) is below the detection limit in all oxidized samples analyzed, but averages 0.05 percent in unaltered sediments.

Mineralogy and Diagenesis

Host sands of the Gueydan deposit are plagioclase-rich volcanic litharenites (fig. 22). They provide a mineralogically immature reactive substrate and, as expected, display a complex diagenetic history, only part of which is related to uranium mineralization. The clay fraction of the sands, as well as the surrounding mudrocks, consists entirely of Ca-montmorillonite (based on x-ray identification methods of Jonas and Roberson, 1965).

Diagenetic features observed in thin section include

1. Clay skins and cutans.
2. Micritic and microspar calcite cement, nodules, and matrix replacement.
3. Dissolved detrital feldspar (dominantly plagioclase) and glass shards.
4. Sparse clinoptilolite laths in intergranular pore space.
5. Calcium carbonate mosaic spar replacing grains and as intergranular cement. Staining shows that low-Mg, iron-free calcite is the dominant phase.

Calcium carbonate is the only volumetrically important diagenetic cement. Spar-replaced grains and mosaic constitute the major carbonate phase. Detrital micrite grains are ubiquitous and consist of reworked pedogenic nodules and crusts. Carbonate distribution around Bruni mineralization is complex and bears little obvious correlation to alteration (fig. 23).

The multiplicity of geochemical and mineralogical features provides the basis for integrating the diagenetic and mineralization history of the deposit:

1. Deposition of the host sand in a crevasse splay marginal to a main fluvial channel complex followed by pedogenic development of thin clay cutans and micrite nodules and bands.

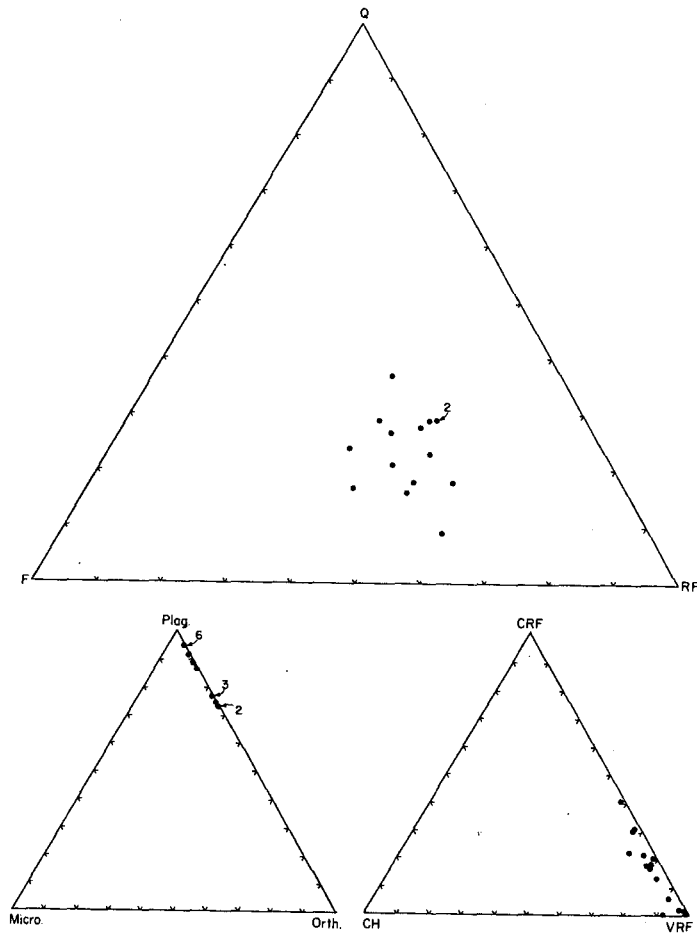


Figure 22. Petrographic composition of Brunu host sand. The average sample is a feldspathic volcanic litharenite (classification of Folk, 1974) Q - quartz; F - feldspar; R.F. - rock fragments; Plag. - plagioclase; Micro. - microcline; Orth. - orthoclase; C.R.F. - carbonate rock fragment; Ch. - chert; V.R.F. - volcanic rock fragment.

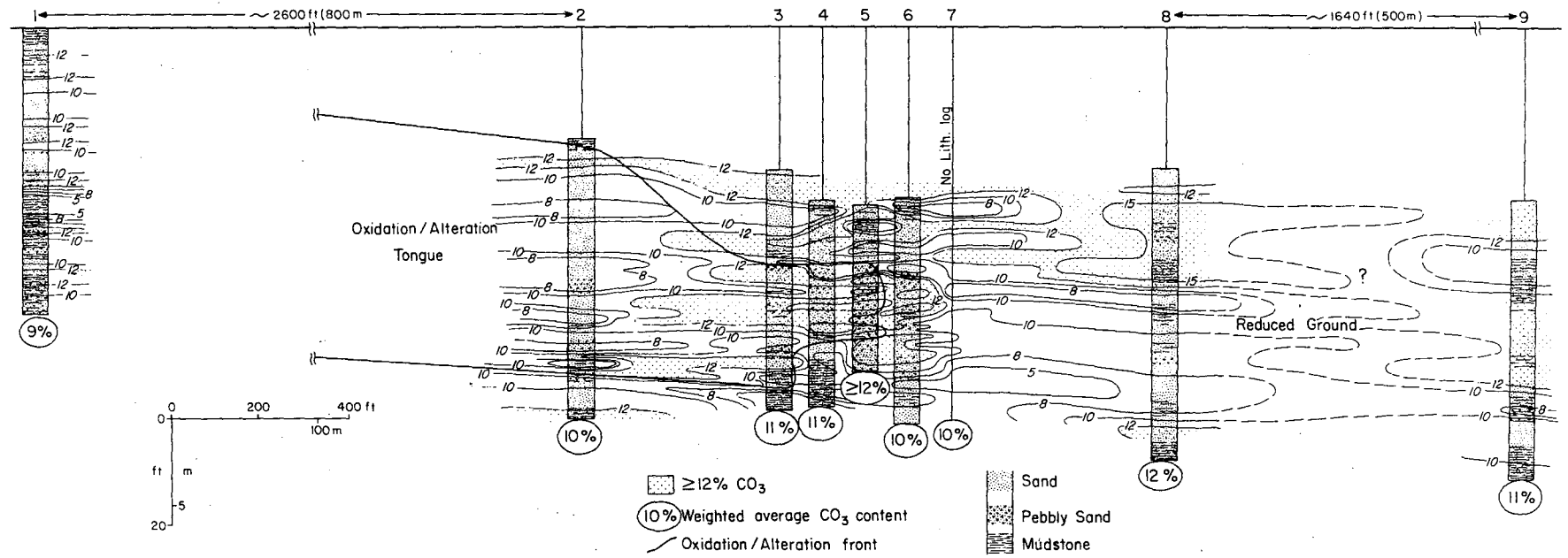


Figure 23. Distribution of weight percent carbonate across Bruni alteration front. Local complexity at nose of front likely due to greater sample density. Weighted average carbonate content for whole core shows no consistent lateral variation. Core section and data from Goldhaber and Reynolds (1977).

2. Back-flush of the local aquifer by sulfide-rich reactive, reducing waters discharged along a nearby, downdip fault zone. Detrital iron titanium minerals were replaced by pyrite.

3. Intrusion of oxidizing, uranium-enriched meteoric waters, which altered pyrite to limonite, precipitated marcasite and deposited uranium in front of the advancing alteration tongue.

4. Possible precipitation of zeolite. Exact timing of earliest clinoptilolite formation is uncertain, but minor amounts appear to predate spar cement.

5. Widespread precipitation of sparry calcite.

6. Dissolution of glass shards and precipitation of large clinoptilolite laths. Shard molds commonly occur within sparry calcite cement.

House-Seale Deposit

The House-Seale deposit is one of a number of small to medium-sized deposits that occur near the base of the Gueydan fluvial system in northern Live Oak County (fig. 24). Stratigraphic relationship and comparison of drill and outcrop sections indicate that the upper Frio clay and lower Catahoula are facies equivalents in this area, the Frio lithology forming part of the coastal lake facies. The uranium deposits occur in a zone of interfingering between a major strike-parallel fluvial axis, which intersects the outcrop in southern Karnes County (Galloway, 1977); and lacustrine ash, silt, and mud. Host beds consist of crevasse splay and lacustrine delta fine sand, ash, and tuffaceous mudstone. Mineralization occurs along a series of erratic, local fronts that individually can be traced for a few thousand feet to several miles. In the House-Seale deposit, ore is entirely surrounded by gray, pyritic sediments that extend updip for several thousand feet.

No known structural features occur near the deposits, but a major belt of growth faults extends across middle Live Oak County about 10 mi (16 km) south of the district. Faults on this trend are associated with uranium mineralization in the Ray Point district (Oakville Formation). Pre- and post-uranium mineralization iron sulfides in the Oakville deposits also suggest a deep-seated origin for the sulfur (Goldhaber and others, 1978). Several belts of sandstone within the Gueydan trend northwest from the fault zone and converge in the district. Thus, reducing waters could have migrated updip and intruded the basal Gueydan aquifer in northern Live Oak County, both before and after uranium concentration.

Present ground-water flow in the area is highly restricted; much of the aquifer appears stagnant and contains high TDS (3,000 + mg/l), sulfate-rich (up to 1,725 mg/l),

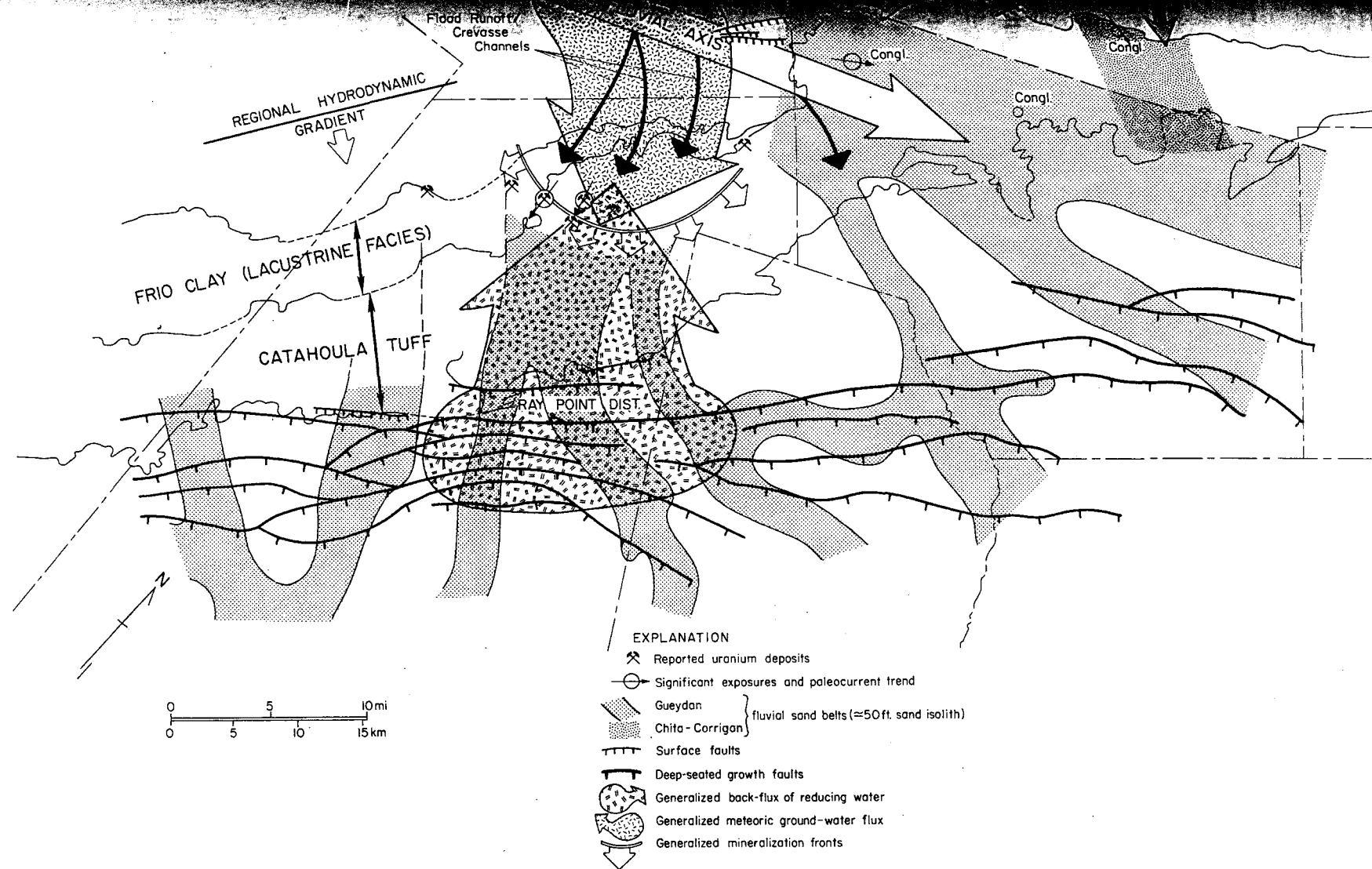


Figure 24. Geologic setting of the House-Seale and associated deposits of the northern Live Oak district. Mineralization occurs in crevasse splay facies interbedded with lacustrine deposits of the Frio and lowest Catahoula. Large arrows suggest the counterflow of reducing waters (likely bled from major faults into the dip-oriented Catahoula fluvial channels outlined by the 50-ft sand isolith) and oxidizing meteoric waters moving down regional hydrodynamic gradient. Successive flow pulses left a broadly arcuate band of mineralization fronts within the irregularly re-reduced host.

sodium and mixed calcium-sodium chloride brines. H_2S was noted in many Catahoula water samples in the area (Nichols and others, 1977). Meteoric circulation is restricted by the argillaceous, low-permeability tuffs and silts that dominate the section. Seepage into deep open pits is minimal, even during wet periods.

Uranium and Trace Metal Distribution

Samples of the deposit were limited to sections collected from the pit walls during mining operations. Two sets of samples were collected from sections spaced about 300 ft (100 m) along the mineralization front. Equivalent sections lay 60 to 80 ft (20 to 25 m) apart in the direction perpendicular to the mineralization trend. Two sections extended about 20 ft (6 m) above the ore. Data are tabulated in table 3, and illustrated in figure 25.

Uranium content averages several tens of ppm in nearly all samples from the downdip sections (fig. 25, sections H-I and H-X) and in the ore zone itself (section H-XI). Molybdenum content is high (up to a few hundred ppm) only in the downdip sections. Selenium content ranges from high to extremely high (several hundred ppm) in updip sections. Comparison of molybdenum-selenium profiles establishes the downflow polarity of the mineralization front at each transect.

The overlying sediments are also of interest. The sub-ore grade but significant uranium content of this interval in section H-I suggests stacked mineralization fronts. An appropriate downflow change in polarity is also indicated by the differing Mo/Se ratios in H-I and H-III. Apparently, similar geochemical interfaces developed at several levels, but the efficiency of uranium entrapment was much higher at the lowest interface. Alternatively, uranium content was generally greater within waters permeating the lower aquifer.

Two ore samples were studied in detail to learn something of the distribution, association, and mineralogy of the uranium. Uranium was found to be concentrated in the less than 1/16-mm sizes (2,200 to 8,100 ppm U_3O_8), but was also abundant in the range of 1/4 to 1/16 mm (1,300 to 5,300 ppm U_3O_8). Radioluxography (Dooley and others, 1977; Dooley, 1958) of sawed rock and microprobe sections shows mineralization to be nonuniformly concentrated in irregular areas a few millimeters in size. Material from these areas was studied by energy-dispersive analysis, scanning electron microscope (SEM), and microprobe analysis.

SEM spectra revealed the presence of Si, U, Al, Ca, Fe, and Mg (fig. 26A-C). Note that the increased height of the Ca peak parallels an increase for Al and decrease for U. The analyzed material coats grains, has a platy or layered

Table 3. Analytical and petrologic data, House-Seale deposit.

Sample No.	Fe Ox. state	Metals (ppm)					Major Components (percent by weight)					Mineralogy				
	o= Ox. r= Re.	U ₃ O ₈	Mo	Se	Cu	Pb	Fe ₂ O ₃	FeS ₂	Pyritic S	SO ₄	CO ₃	Organic C	Clinopt.	Kaol.	Montmorillonite Na	Ca
I-0	r	170	3	0.1	30	9	-	-	1.1	0.06	10	-	Ab	Ab	D	R
I-2	r	190	7	-	-	-	-	-	0.84	0.09	11	-	Ab	Ab	D	Ab
I-4	r	150	37	0.2	11	17	-	-	0.09	0.14	4	-	C	Tr	D	Ab
I-6	r	26	-	-	-	-	-	-	0.20	0.09	25	-	Ab	-	-	-
I-8	r	190	24	0.1	10	12	-	-	0.49	0.09	15	-	C	Ab	D	R
I-10	r	200	-	-	-	-	-	-	0.32	0.09	13	-	Ab	-	-	-
I-12	r	85	28	7	23	18	-	-	0.70	0.09	16	-	Ab	Ab	D	R
I-14	r	80	-	-	-	-	-	-	0.07	0.12	3	-	R	-	-	-
I-16	r	45	13	0.2	12	14	-	-	0.93	<0.03	11	-	Ab	Ab	D	R
I-18	r	70	6	1	15	11	-	-	0.30	0.06	14	-	Ab	Ab	D	Ab
I-20U	r	1,400	-	-	-	-	-	-	0.46	0.12	4	-	Ab	Ab	D	Ab
I-20L	r	8,000	9	18	14	37	-	-	1.3	0.12	5	-	Ab	Ab	D	Ab
I-22	r	410	59	19	10	32	-	-	0.17	0.09	4	-	Ab	Ab	D	-
I-24	r	75	2	12	9	6	-	-	0.11	0.03	2	-	Ab	-	-	-
I-26	r	480	3	4	10	6	-	-	0.26	0.03	34	-	C	-	-	-
III-0	r	12	2	2	6	8	-	-	0.06	<0.01	2	-	Ab	Tr	D	Ab
III-2	r	5	1	-	-	-	-	-	0.05	<0.01	4	-	C	Tr	D	Ab
III-4	r	12	1	3	13	10	-	-	0.17	<0.01	5	-	Ab	Tr	D	Ab
III-6	r	< 1	< 1	-	-	-	-	-	0.07	<0.03	16	0.02	C	Tr	D	Ab
III-8	r	9	2	2	10	13	-	-	0.10	<0.03	10	-	Ab	Tr	D	Ab
III-10	r	9	-	-	-	-	-	-	0.01	<0.03	-	-	C	Tr	-	-
III-12	r	6	2	5	12	22	-	-	0.05	<0.03	9	0.02	Ab	Tr	D	Ab
III-14	r	22	5	-	-	-	-	-	0.10	0.30	2	-	R	Tr	-	-
III-16	r	32	4	16	18	12	-	-	0.17	0.06	4	-	Ab	Tr	D	Ab
III-18	r	350	8	33	9	12	-	-	1.4	0.18	8	0.02	Ab	Tr	D	Ab
III-20	r	180	8	10	10	20	-	-	0.85	0.06	10	-	Ab	Tr	D	Ab
III-22	r	45	3	0.4	11	12	-	-	0.74	0.06	11	0.03	C	Tr	D	Ab

63

Table 3 (Cont'd)

Sample No.	Fe Ox. state	Metals (ppm)						Major Components (weight percent)					Mineralogy				
	o= Ox. r= Re.	U ₃ O ₈	Mo	Se	Cu	Pb	Fe ₂ O ₃	FeS ₂	Pyritic S	SO ₄	CO ₃	Organic C	Clinopt.	Kaol.	Montmorillonite		
															Na	Ca	
X-1	r	245	158	3	-	-	0.1	1.2	-	0.06	4	-	Ab	Tr	D	Ab	
X-2	r	247	49	-	10	9	1.0	1.7	-	0.04	4	0.02	C	Tr	D	Ab	
X-3	r	4,031	69	1	7	17	1.2	1.6	-	0.06	9	0.07	Ab	Ab	D	Ab	
X-4	r	1,112	24	-	-	-	1.1	1.6	-	0.04	12	-	Ab	Tr	D	Ab	
X-5	r	1,500	18	13	8	15	1.4	2.2	-	0.04	9	0.02	Ab	Tr	D	Ab	
X-6	r	325	8	-	-	-	1.1	0.9	-	0.08	20	0.11	Ab	Tr	D	Ab	
X-7	r	190	21	8	8	9	1.2	2.0	-	0.12	12	-	Ab	Tr	D	Ab	
X-8	r	118	8	2	10	16	2.4	0.8	-	0.03	3	0.01	Ab	Tr	D	Ab	
XI-1	r	25	2	660	11	3	1.9	1.0	-	0.04	15	-	C	Tr	D	Ab	
XI-3	r	24	1	328	7	10	1.8	0.2	-	0.04	11	0.04	Ab	Tr	D	Ab	
XI-4	r	20	2	-	-	-	1.9	0.3	-	0.02	9	-	C	Tr	D	Ab	
XI-5	r	34	1	560	9	9	1.6	0.2	-	0.03	15	0.02	Ab	Tr	D	Ab	
XI-6	r	120	1	-	-	-	1.7	1.2	-	0.02	7	0.03	Ab	Tr	D	Ab	
XI-7	r	225	4	3233	10	11	2.0	1.1	-	0.04	3	0.02	Ab	Tr	D	Ab	
XI-8	r	116	2	-	-	-	2.2	1.5	-	0.15	3	-	Ab	Tr	D	Ab	
XI-10	r	92	2	0.2	10	18	1.2	1.0	-	0.02	6	0.02	R	Tr	D	Ab	

76

- = not analyzed
Ab = absent
Tr = trace

R =rare
C = common
A = abundant
D = dominant

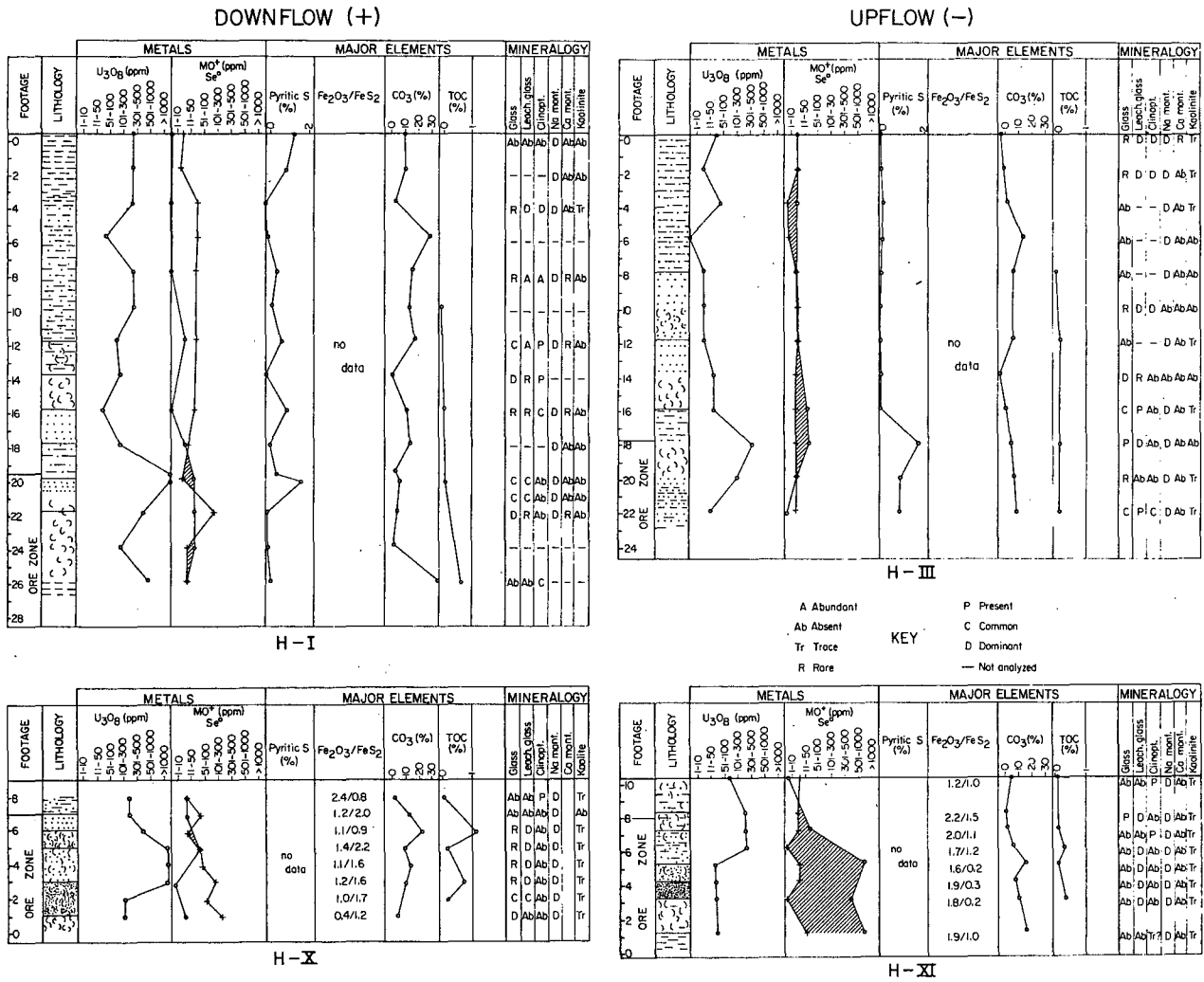


Figure 25. Geochemical and mineralogical variations within sections from walls of the House-Seale open-pit mine. Observed selenium-molybdenum ratios establish the polarity of the mineralization front. A noncommercial mineralization front appears to overlie the ore zone in sections H-I and H-III.

morphology, and is interpreted to be Ca-montmorillonite (fig. 26D). Morphologically, it is similar to infiltrated clay or clay cutans of pedogenic origin (Walker and others, 1978). Uranium is believed to be present as an adsorbed amorphous phase or associated amorphous $USiO_4$, or coffinite. Where uranium is particularly rich (fig. 26C) uranium minerals are suspected (Gavshin and others, 1973; Katayama and others, 1974), since the sorbents' capacity to adsorb must be exceeded before mineral phases form.

Microprobe analysis further shows uranium to be concentrated in matrix, which occurs as grain coats, interstitial blebs, and irregular areas completely surrounding framework grains. Matrix, identified as clay, is semi-opaque or translucent, brownish-gray, submicroscopic, low-birefringent material. Semiquantitative analysis of probed areas 30 to 40 μm in size gave uranium concentrations of 0.6 to 7 percent.

Copper and lead are slightly more abundant in samples from the upflow sections (table 3). No correlation to uranium content is evident. Ten samples were tested for arsenic, which averages 56 ppm in the downflow section and 13 ppm in the equivalent upflow section. Total arsenic correlates with uranium content of the samples.

Major Element Distribution

Iron content was determined in two sections (table 3). Average total iron shows no variation across the front. The distributions of total sulfide (sections H-I and H-III) and of FeS_2 (sections H-X and H-XI) show qualitative correlations to front polarity and positive correlation with uranium abundance. Microprobe analysis of several sulfide grains failed to detect uranium, however, so the association must be indirect. The ratio of Fe_2O_3 to FeS_2 is significantly higher (1.7 vs. 1.2 percent) in the upflow part of the ore zone. Thus, iron and sulfide may still preserve, in terms of relative abundance, alteration front polarity. However, the total depletion of sulfide and dominance of Fe^{+3} typical of oxidized altered ground has been masked by postmineralization resulfidization and reduction.

Organic carbon is present in trace amounts. Altered section samples average less than 0.03 weight percent. However, unaltered samples average about 0.1 percent, a small but significant difference. Uranium concentration shows no correlation to organic carbon content (table 3).

Carbonate, as calcite, is a ubiquitous and locally abundant component of all sections (table 3). Carbonate content shows no correlation with uranium content or with front polarity (fig. 25). In general it is less abundant in vitric tuffs, and most

abundant in argillaceous samples. Phosphate was determined in 8 samples from section H-I; contents ranged from 0.02 to 0.15 weight percent and averaged about 0.1 percent.

Mineralogy and Diagenesis

Uranium host lithologies in the House-Seale deposit include claystone, tuffaceous mudstone, muddy siltstone, and argillaceous fine sand. They are characterized by an abundance of highly altered to partially vitric volcanic glass and volcanic debris. Sands display compositions typical of Gueydan samples (see Bruni section, fig. 22). Clays are dominantly Na-montmorillonite; minor Ca-montmorillonite was detected in some samples, and traces of kaolinite occur in over half of the samples, particularly in the ore zone (table 3).

Diagenetic features include

1. Pedogenic clay cutans on detrital grains and in pores.
2. Diffuse to discrete micrite nodules and irregular masses replacing clay or mud.
3. Thin clay rims around detrital grains.
4. Leached glass shards and pumice fragments.
5. Euhedral, pore-filling clinoptilolite.
6. Calcite spar cement and grain replacement. No ferroan or high-Mg calcite was detected by staining.

Distribution of dissolved glass and clinoptilolite pore fill display definite zonation in the two longer sections (fig. 25). Fresh glass occurs locally within the ore zone. A 4- to 8-ft (2-m) section dominated by abundant dissolved shards separates fresh glass from samples containing clinoptilolite, which fills shard-molds, root tubules, and intergranular pore space. The dissolution zone is especially prominent in samples from sections H-X and H-XI. Leached shards are outlined by thin clay skins, which predate dissolution.

Petrographic relationships, mineral distribution, and geologic setting suggest the following sequence of events (fig. 27):

1. Deposition along the margin of a strike-trending fluvial channel in a crevasse splay and crevasse delta of ash and ashy fine sand.
2. Moderate pedogenic weathering of subaerial portions of the splays producing clay cutans, micrite nodules and replacement masses, and minor argillation of glass. Clay skins began to develop as open-system diagenesis was initiated during early burial.

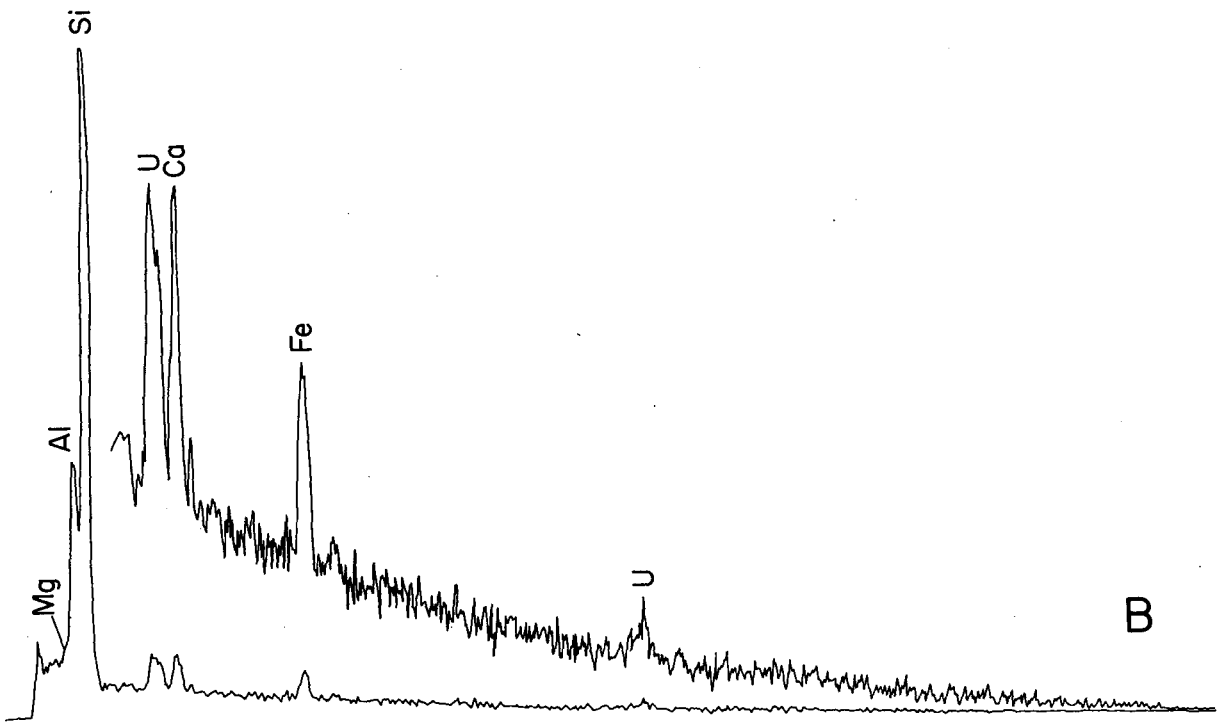
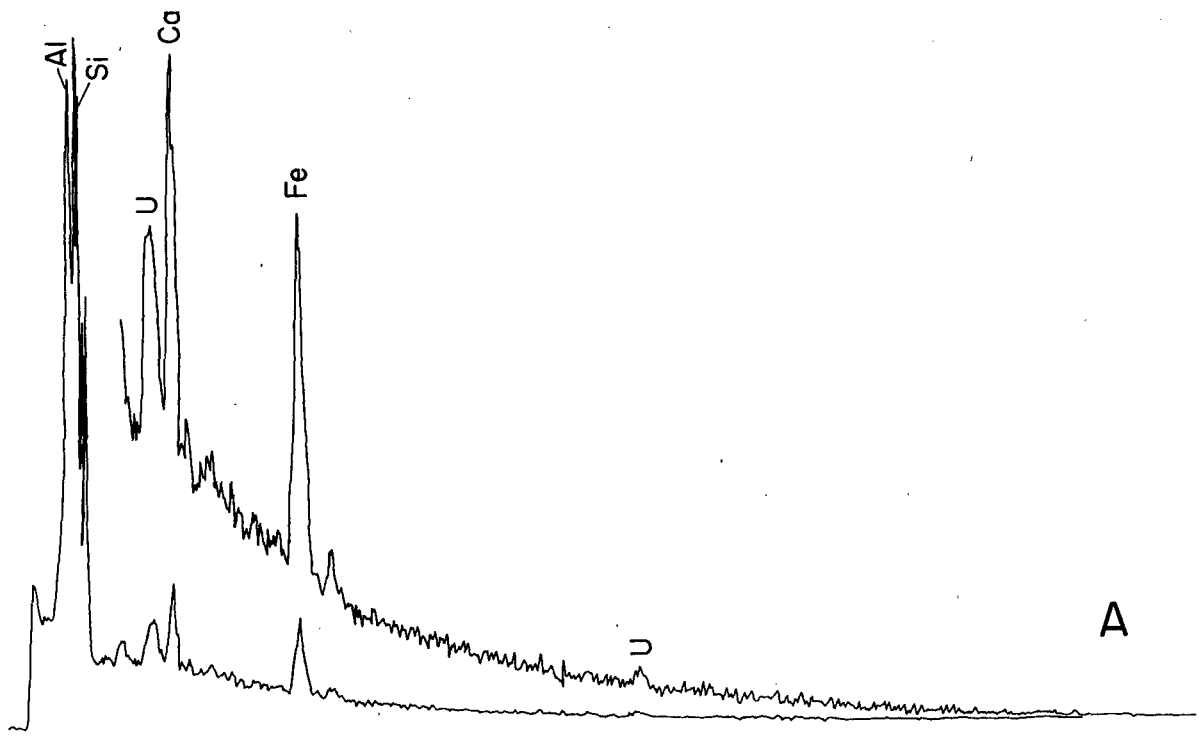
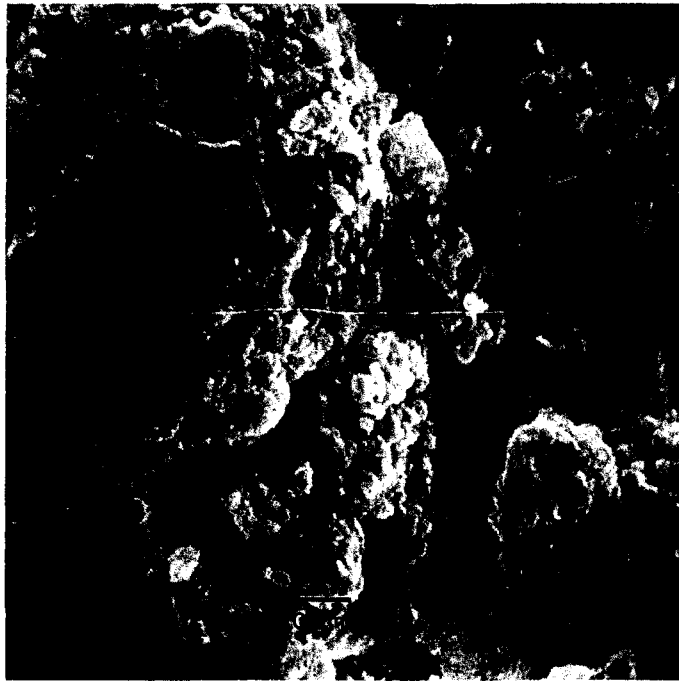
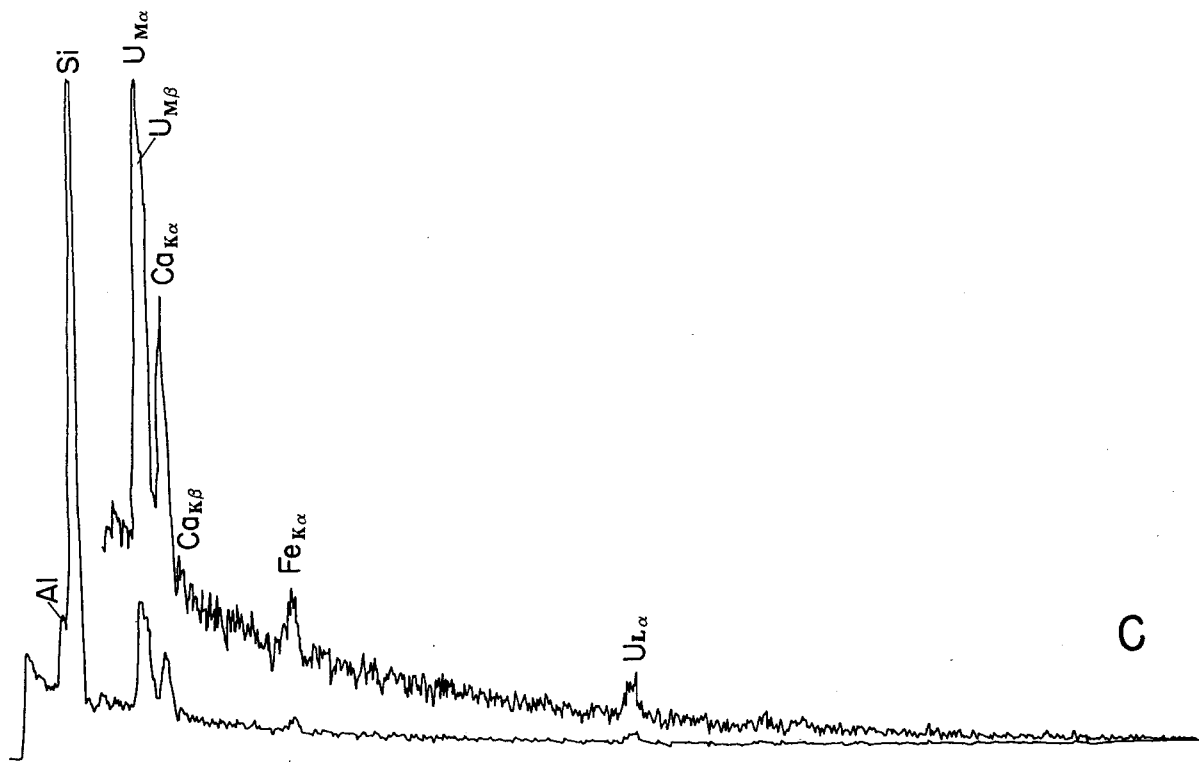


Figure 26. Scanning electron microscope spectra (A, B, C) and micrograph (D) of uranium-bearing mineral, House-Seale deposit.



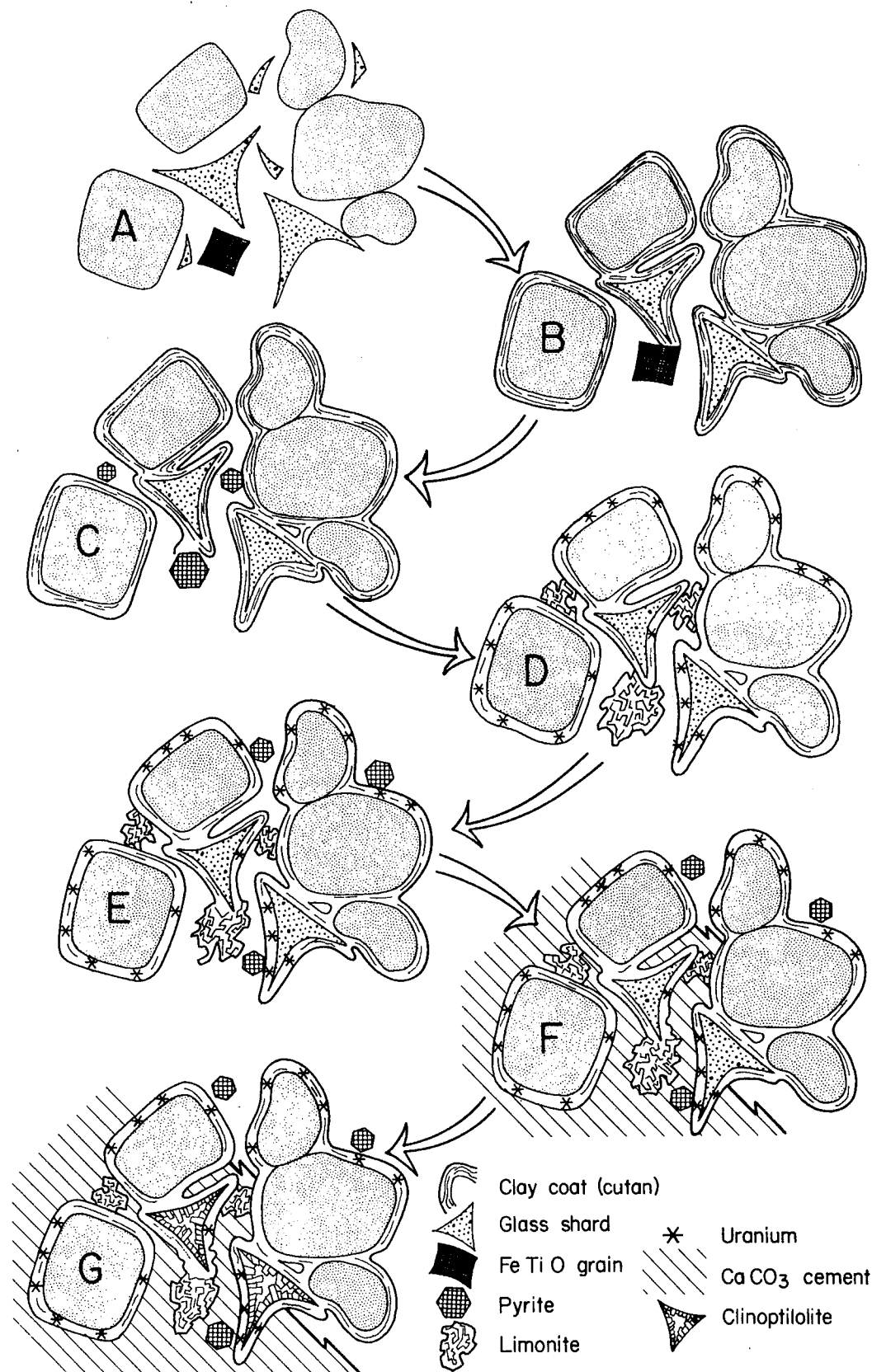


Figure 27. Paragenetic sequence displayed by tuffaceous host sands of Brunu deposit. A. Deposition of framework grains. B. Pedogenesis. C. Reduction. D. Mineralization and oxidation. E. Re-reduction. F. Calcite cementation. G. Open hydrologic system zeolitization.

3. A premineralization phase of reduction and sulfidization analogous to that at Bruni probably ensued during early burial. Reducing solutions presumably migrated updip from a major fault zone (fig. 23).

4. Flux of uranium-charged, oxidizing ground water into the reduced, semi-confined aquifer produced local alteration tongues. Water entered the crevasse facies through the genetically associated channel sand belt that lay northwest, up regional hydrodynamic gradient (fig. 24). Uranium was concentrated along active margins of the alteration tongues by sorption onto early-formed Ca-montmorillonite cutans, and associated trace metals (Mo and Se) were zoned according to the decreasing Eh as waters traversed active fronts.

Concentration of uranium in a typically highly depleted, pedogenically altered host obviously occurred because of the local presence of the oxidation front and postdates shallow leaching in the vadose zone. Thus environmentally and diagenetically analogous sediments may serve as both a source and host for uranium at different times in their hydrologic history.

5. Additional pulses of highly reducing waters re-reduced the epigenetically oxidized interior of portions of the alteration tongue. Abundance of sulfide is highest in porous, permeable units as would be expected if dissolved sulfide were introduced with an invading water mass. Sample distribution is inadequate to determine possible epigenetic reduction zonation as described by Shmariovich (1973).

6. Much of the sparry calcite replacement and pore fill was precipitated. Spar completely encloses many pyrite grains and greatly modified facies-controlled porosity patterns.

7. With sufficient burial, advanced open-hydrologic-system diagenesis of the abundant volcanic glass resulted in dissolution of glass shards and pumice, and precipitation of clinoptilolite pore fill. Dissolved shards commonly leave open molds within spar blebs, indicating glass leaching and zeolitization postdated carbonate cementation. Concomitantly, thorough argillation destroyed most of the remaining permeability, totally modifying original permeability patterns and insulating the earlier formed uranium deposit from further flushing.

8. Minor late-phase calcite precipitated as isolated microspar crystals in leached pores.

The deposit now occurs in a hydrologically stagnant environment. Original high permeability of the section has been severely restricted by the extensive postmineralization diagenesis. Consequently, the ore is generally in radiometric equilibrium.

Washington-Fayette Deposit

A small deposit in the Washington-Fayette Counties area provides an example of a very different style of mineralization, but one that may be representative of deposits in the Chita-Corrigan fluvial system of East Texas. Mineralization occurs along an arcuate alteration front within a crevasse splay sand body lying on the downdip margin of channel-fill sand (fig. 28). The oxidized interior of the front is preserved and displays a complex cross-sectional geometry commensurate with the heterogeneous composition and permeability of the splay host (fig. 28). Polarity of the front is consistent with regional hydrodynamic gradient, and modern ground waters in the area are fresh, suggesting continued active flushing of the shallow aquifer.

Uranium and Trace Metal Distribution

Ore occurs as discontinuous pods within a matrix of diffusely mineralized ground along the periphery of the alteration front. Maximum concentration occurs in or closely adjacent to lenses or pockets of carbonaceous trash or humate-like material that is dispersed in clay. The deposit resembles the classic trash pile accumulations of the Colorado Plateau, but accumulation occurs only proximal to a well-defined alteration front. Uranium probably occurs as urano-organic complexes or adsorbed cations and possibly as discrete reduced mineral phases (Doi and others, 1975; Breger, 1974). It is interesting to speculate that this deposit would probably be interpreted as a tabular ore body if subsequent geologic changes were to obscure the obvious oxidation front (as has occurred in the House-Seale deposit).

Comparison of chemical uranium distribution with the gamma-ray logs indicates local disequilibrium along margins of the pods. Flux of oxidizing ground water, probably rejuvenated during the recent phase of outcrop incision, is redistributing uranium along the periphery of the front.

Molybdenum is concentrated along the periphery of the mineralized pods, commonly on the side farthest removed from the oxidation front. Selenium, on the other hand, is locally enriched within the oxidized section (fig. 29, table 4). Thus, trace metal zonation supports inferred alteration front polarity. Brooks and Campbell (1976) described a similar zonation in tabular uranium deposits in the Salt Wash Member of the Morrison Formation.

Copper and lead show varying degrees of local concentration in and around argillaceous or organic-rich sediments (fig. 29, table 4). Both appear to be slightly depleted in the altered ground. Arsenic averaged 480 ppm in seven samples. Two uraniferous, carbonaceous samples contained 1510 and 1160 ppm arsenic.

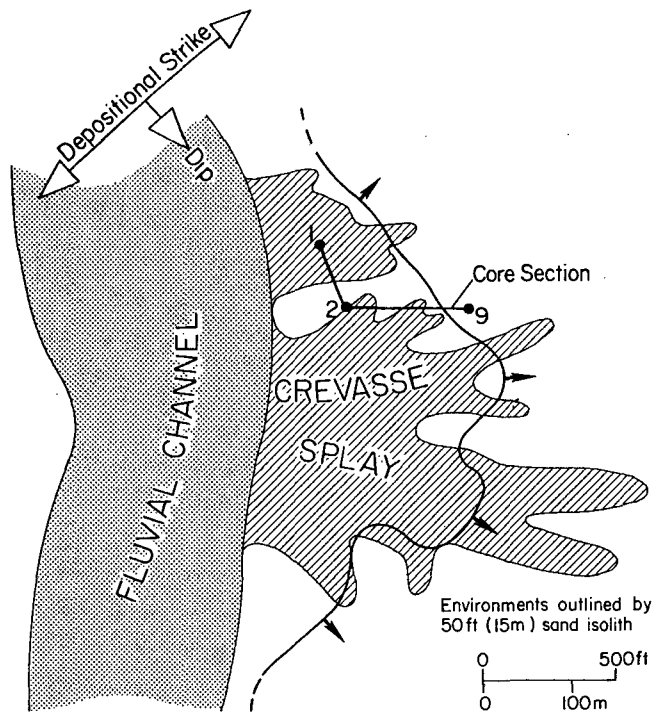


Figure 28. Geologic setting of the Washington-Fayette deposit. Ore-grade mineralization occurs along the portion of the alteration front that extends into the crevasse splay sand body.

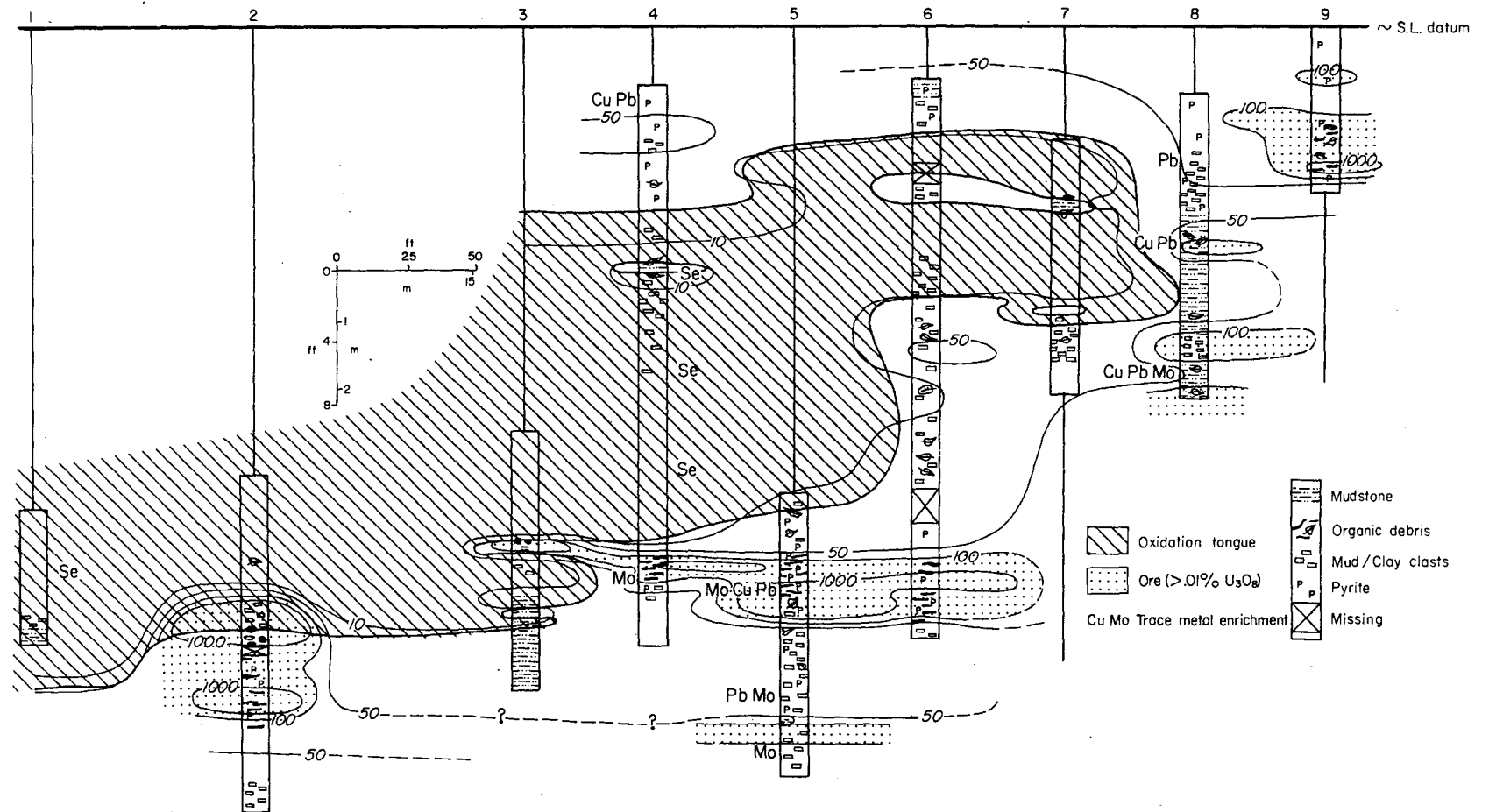


Figure 29. Uranium and trace element distribution in cores of the Washington-Fayette oxidation/alteration tongue. Uranium of ore grade ($>0.01\%$ or $100 \text{ ppm } \text{U}_3\text{O}_8$) occurs as isolated pods directly downflow from the preserved oxidation interface. Anomalous concentrations of trace metals are indicated by appropriate symbols. Contours are ppm U_3O_8 . For location of core section see figure 28.

Table 4. Analytical and petrologic data, Washington-Fayette deposit.

Sample No.	Fe Ox. state o= Ox. r= Re.	Metals (ppm)					Major Components (percent by weight)					Mineralogy				
		U ₃ O ₈	Mo	Se	Cu	Pb	Fe ₂ O ₃	FeS ₂	Pyritic S	SO ₄	CO ₃	Organic C	Clinopt.	Kaol.	Montmorillonite Na Ca	
1-167	o	2	1	3	3	4	0.80	0.02	<0.01	<0.03	6	0.08	Ab	R	R	D
1-169	o	3	1	10	3	20	1.04	0.03	<0.01	<0.03	5	-	-	-	-	-
1-171	o	1	1	38	3	1	0.93	0.03	<0.01	<0.03	8	0.07	Ab	R	Ab	D
1-173	o	4	1	19	3	1	0.90	0.03	<0.01	<0.03	9	0.01	Ab	R	R	D
1-174	o	3	1	15	5	5	1.76	0.02	<0.01	<0.03	2	0.01	Ab	R	R	D
5-165	o/r	45	-	8	6	6	0.71	0.18	<0.01	<0.03	5	0.51	Ab	Ab	R	D
5-167	o/r	34	-	0.8	3	5	0.54	0.12	0.12	0.06	9	-	-	-	-	-
5-168	r	750	370	<0.1	15	6	2.66	3.92	0.68	3.38	4	1.10	-	-	-	-
5-170	r	3,600	361	1	14	8	1.06	2.51	<0.01	4.00	4	-	-	-	-	-
5-171	r	4,000	17	0.3	2	3	0.41	0.54	0.48	0.18	5	0.25	-	-	-	-
5-173	r	23	8	3	6	9	0.34	1.32	0.30	0.09	10	-	-	-	-	-
5-175	r	18	11	12	7	8	0.45	1.23	0.31	0.03	11	0.19	-	-	-	-
5-177	r	19	8	4	6	8	0.51	1.91	0.34	0.12	13	-	-	-	-	-
5-178	r	800	16	0.2	4	4	0.26	1.87	0.95	0.60	24	0.24	-	-	-	-
5-179	r	75	25	0.3	5	4	0.27	1.04	0.51	0.45	21	-	-	-	-	-
2-166	o	3	-	-	-	-	-	-	<0.01	<0.03	5	-	Ab	R	C	D
2-169	o	5	-	-	-	-	-	-	<0.01	<0.03	7	-	-	-	-	-
2-171	o	10	-	-	-	-	-	-	<0.01	<0.03	4	-	-	-	-	-
2-173	o	2,600	-	-	-	-	-	-	<0.01	<0.03	13	-	Ab	R	Ab	D
2-174	o/r	2,900	-	-	-	-	-	-	0.05	0.66	6	-	Ab	R	Ab	D
2-176	r	2,900	-	-	-	-	-	-	0.96	0.54	11	-	-	-	-	-
2-177	r	500	-	-	-	-	-	-	0.47	0.24	6	-	Ab	R	Ab	D
2-179	r	500	-	-	-	-	-	-	0.51	0.39	8	-	Ab	R	R	D
2-180	o/r	75	-	-	-	-	-	-	0.47	0.27	7	-	Ab	R	Ab	D
2-184	o	35	-	-	-	-	-	-	0.04	0.06	2	-	Ab	R	C	D
2-186	r	135	-	-	-	-	-	-	0.17	0.09	6	-	-	-	-	-

75

Table 4. (Cont'd)

Sample No.	Fe Ox. state	Metals (ppm)					Major Components (percent by weight)					Mineralogy				
	o= Ox. r= Re.	U ₃ O ₈	Mo	Se	Cu	Pb	Fe ₂ O ₃	FeS ₂	Pyritic S	SO ₄	CO ₃	Organic C	Clinopt.	Kaol.	Montmorillonite Na	Ca
9-141	r	60	-	-	-	-	-	-	0.15	0.03	6	-	-	-	-	-
9-143	r	100	-	-	-	-	-	-	0.34	< 0.03	11	-	-	-	-	-
9-145	r	60	-	-	-	-	-	-	0.13	< 0.03	7	-	-	-	-	-
9-146	r	115	-	-	-	-	-	-	0.90	< 0.03	9	-	-	-	-	-
9-147	r	280	-	-	-	-	-	-	0.38	< 0.03	13	-	-	-	-	-
9-148	r	1,000	-	-	-	-	-	-	0.48	< 0.03	13	-	-	-	-	-
9-149	r	46	-	-	-	-	-	-	0.04	< 0.03	7	-	-	-	-	-
76 3-161	o	5	-	-	-	-	-	-	< 0.01	< 0.03	5	-	-	-	-	-
3-164	o	4	-	-	-	-	-	-	< 0.01	< 0.03	4	-	-	-	-	-
3-165	o	2	-	-	-	-	-	-	< 0.01	< 0.03	12	-	-	-	-	-
3-166	r	6,700	-	-	-	-	-	-	0.06	4.71	10	4.7	-	-	-	-
3-167	o	11	-	-	-	-	-	-	< 0.01	< 0.03	5	-	-	-	-	-
3-168	o	9	-	-	-	-	-	-	0.08	0.18	21	-	-	-	-	-
3-169	o	20	-	-	-	-	-	-	< 0.01	< 0.03	8	-	-	-	-	-
3-171	o	7	-	-	-	-	-	-	< 0.01	< 0.03	11	-	-	-	-	-
3-172	r	47	-	-	-	-	-	-	0.12	< 0.03	4	-	-	-	-	-
3-174	r	28	-	-	-	-	-	-	0.11	< 0.03	3	-	-	-	-	-
7-146	o	7	-	-	-	-	-	-	< 0.01	< 0.03	7	-	-	-	-	-
7-148	o	5	-	-	-	-	-	-	< 0.01	< 0.03	10	-	-	-	-	-
7-149	r	9	-	-	-	-	-	-	0.26	< 0.03	15	-	-	-	-	-
7-150	o	5	-	-	-	-	-	-	< 0.01	< 0.03	8	-	-	-	-	-
7-152	o	3	-	-	-	-	-	-	< 0.01	< 0.03	14	-	-	-	-	-
7-154	o	4	-	-	-	-	-	-	< 0.01	< 0.03	13	-	-	-	-	-
7-155	o	35	-	-	-	-	-	-	0.25	< 0.03	10	-	-	-	-	-
7-157	r	9	-	-	-	-	-	-	0.29	< 0.03	8	-	-	-	-	-
7-159	r	21	-	-	-	-	-	-	0.07	< 0.03	6	-	-	-	-	-

Table 4. (Cont'd)

Sample No.	Fe Ox. state	Metals (ppm)					Major Components (percent by weight)					Mineralogy				
	o= Ox. r= Re.	U ₃ O ₈	Mo	Se	Cu	Pb	Fe ₂ O ₃	FeS ₂	Pyritic S	SO ₄	CO ₃	Organic C	Clinopt.	Kaol.	Montmorillonite Na	Ca
4-135	o/r	5	2	98	6	1	0.36	0.23	< 0.01	< 0.03	4	-	-	-	-	-
4-138	o	7	2	11	6	1	0.25	0.44	0.06	< 0.03	6	0.08	Ab	R	C	D
4-140	o	14	1	6	9	8	1.31	1.23	0.09	< 0.03	8	-	Ab	R	C	D
4-141	r	60	2	0.4	17	10	0.31	1.53	0.36	< 0.03	10	0.02	Ab	R	R-C	D
4-144	r	22	2	0.2	7	7	0.31	1.52	0.31	< 0.03	9	-	-	-	-	-
4-146	o/r	48	2	0.7	6	5	1.66	1.32	0.58	0.30	11	-	-	-	-	-
4-147	o	39	2	13	5	1	0.62	0.03	< 0.01	< 0.03	7	-	-	-	-	-
4-149	o	4	2	10	5	4	0.41	0.02	< 0.01	< 0.03	7	0.03	Ab	R	C	D
4-151	o	11	0.9	154	4	4	2.01	0.15	< 0.01	< 0.03	9	-	Ab	R	C	D
4-154	o	6	1	108	4	4	2.23	0.22	< 0.01	< 0.03	<1	-	-	-	-	-
4-157	o	8	1	70	6	5	1.74	0.14	< 0.01	< 0.03	<1	0.05	-	-	-	-
4-158	o	3	1	4	2	2	0.41	0.09	< 0.01	< 0.03	<1	-	Ab	R	C	D
4-160	o	4	1	14	3	3	0.48	0.07	< 0.01	< 0.03	<1	0.00	Ab	R	C	D
4-165	r	2	2	13	2	3	0.14	0.04	< 0.01	< 0.03	<1	5.02	Ab	R	T	D
4-167	r	1,000	194	2	7	7	0.84	1.45	0.02	2.82	6	7.8	Ab	Ab	Ab	D
4-169	r	60	12	0.4	3	4	0.27	0.84	0.53	0.27	8	-	Ab	R	Ab	D
4-171	r	38	3	0.4	4	12	0.39	1.68	0.16	< 0.03	3	0.07	Ab	R	Ab	D
6-140	r	35	-	-	-	-	-	-	0.42	< 0.03	10	-	-	-	-	-
6-142	r	28	-	-	-	-	-	-	0.22	< 0.03	10	-	-	-	-	-
6-144	o	5	-	-	-	-	-	-	< 0.01	< 0.03	6	-	-	-	-	-
6-149	o	3	-	-	-	-	-	-	< 0.01	< 0.03	8	-	-	-	-	-
6-152	o	3	-	-	-	-	-	-	< 0.01	< 0.03	12	-	-	-	-	-
6-154	r	36	-	-	-	-	-	-	0.25	< 0.03	8	-	-	-	-	-
6-156	r	50	-	-	-	-	-	-	0.24	< 0.03	7	-	-	-	-	-
6-158	r	9	-	-	-	-	-	-	0.24	< 0.03	7	-	-	-	-	-
6-160	r	29	-	-	-	-	-	-	0.01	< 0.03	6	-	-	-	-	-
6-162	r	29	-	-	-	-	-	-	0.10	< 0.03	6	-	-	-	-	-
6-167	r	38	-	-	-	-	-	-	0.26	< 0.03	8	-	-	-	-	-
6-169	r	1,900	-	-	-	-	-	-	0.15	1.65	5	4.7	-	-	-	-
6-171	r	370	-	-	-	-	-	-	1.35	0.15	5	-	-	-	-	-
6-172	r	30	-	-	-	-	-	-	0.32	< 0.03	6	-	-	-	-	-

Table 4. (Cont'd)

Sample No.	Fe Ox. state	Metals (ppm)					Major Components (percent by weight)					Mineralogy				
	o= Ox. r= Re.	U ₃ O ₈	Mo	Se	Cu	Pb	Fe ₂ O ₃	FeS ₂	Pyritic S	SO ₄	CO ₃	Organic C	Clinopt.	Kaol.	Montmorillonite Na Ca	
8-145	r	87	2	0.1	3	4	0.67	0.39	0.14	< 0.03	7	0.06	-	-	-	-
8-147	r	55	2	< 0.01	3	6	0.28	0.42	0.06	< 0.03	5	-	Ab	R	Ab	D
8-148	r	55	3	0.1	5	11	1.53	0.83	0.40	< 0.03	9	0.01	Ab	R	Ab	D
8-150	r	47	3	0.1	3	5	0.82	0.24	0.12	< 0.03	8	-	Ab	R	R	D
8-152	r	100	3	7	13	19	2.06	0.87	0.34	< 0.03	14	0.04	-	-	-	-
8-154	r	18	3	0.2	10	12	2.17	0.97	0.48	< 0.03	20	-	-	-	-	-
8-156	r	30	4	< 0.1	9	8	0.97	0.48	0.03	< 0.03	29	0.01	-	-	-	-
8-159	r	650	4	0.4	4	4	0.34	0.17	0.08	< 0.03	6	-	Ab	R	Ab	D
8-160	r	56	10	0.4	8	12	1.72	1.03	0.49	< 0.03	13	0.14	-	-	-	-
8-162	r	140	8	0.4	9	14	1.56	1.02	0.38	< 0.03	12	-	-	-	-	-

78

- = not analyzed
Ab = absent
Tr = trace

R =rare
C = common
A = abundant
D = dominant

Major Element Distribution

In contrast to the other deposits studied, total iron appears to be depleted in altered ground (average content 1.2 percent by weight, compared with 2.1 percent in unaltered ground). However, a comparison of argillaceous samples reveals no significant difference in the two settings; thus iron distribution may be controlled in part by lithology as well as by alteration environment.

Sulfide is thoroughly depleted in altered ground and shows considerable variation in reduced ground (fig. 30). Highest total sulfide and FeS_2 values occur in and around the organic-rich and uranium-rich pods. However, the association is only general; highest uranium enrichment rarely coincides with maximum sulfide content within any set of core samples (table 4).

Sulfate is locally abundant in and around sulfide, organic-rich and uranium-rich pods (fig. 30), suggesting oxidation of sulfide as an early stage in encroachment of the alteration front. Sulfur in all forms is thoroughly depleted in oxidized ground and probably has been enriched along the periphery of the alteration tongue.

Carbonate is present in all cores and exceeds 20 percent by weight in a few samples (table 4). Carbonate distribution suggests irregular pods (fig. 31) and shows no relationship to ore zones. Possible enrichment along the margin of the alteration tongue is suggested by the cross section, but the strongest correlation is with lithology. Carbonate is most abundant in muddy samples (where it partially replaces matrix) or in clast-rich sands, where it occurs as reworked nodules and grains.

Analyses of total organic carbon substantiate the megascopic association of organic debris and uranium and further indicate that (1) reduced samples have variable organic content, ranging from a few hundredths of a percent to several percent, and (2) altered samples are uniformly depleted in organic carbon, averaging at most a few hundredths of a percent (table 4).

Mineralogy and Diagenesis

Host sands are typical Chita-Corrigan chert and carbonate rock fragment-bearing quartzose lithic arkoses and feldspathic litharenites (fig. 32). Volcanic rock fragments and glass are minor components of some samples. Clay minerals are dominantly Ca-montmorillonite with minor Na-montmorillonite. Most samples contain a trace of kaolinite.

In contrast to Gueydan deposits, the Washington-Fayette deposit has a simple diagenetic history. It includes formation of pedogenic clay cutans and rims on detrital grains, micrite matrix replacement and nodules, and local selenite crystals and sheets.

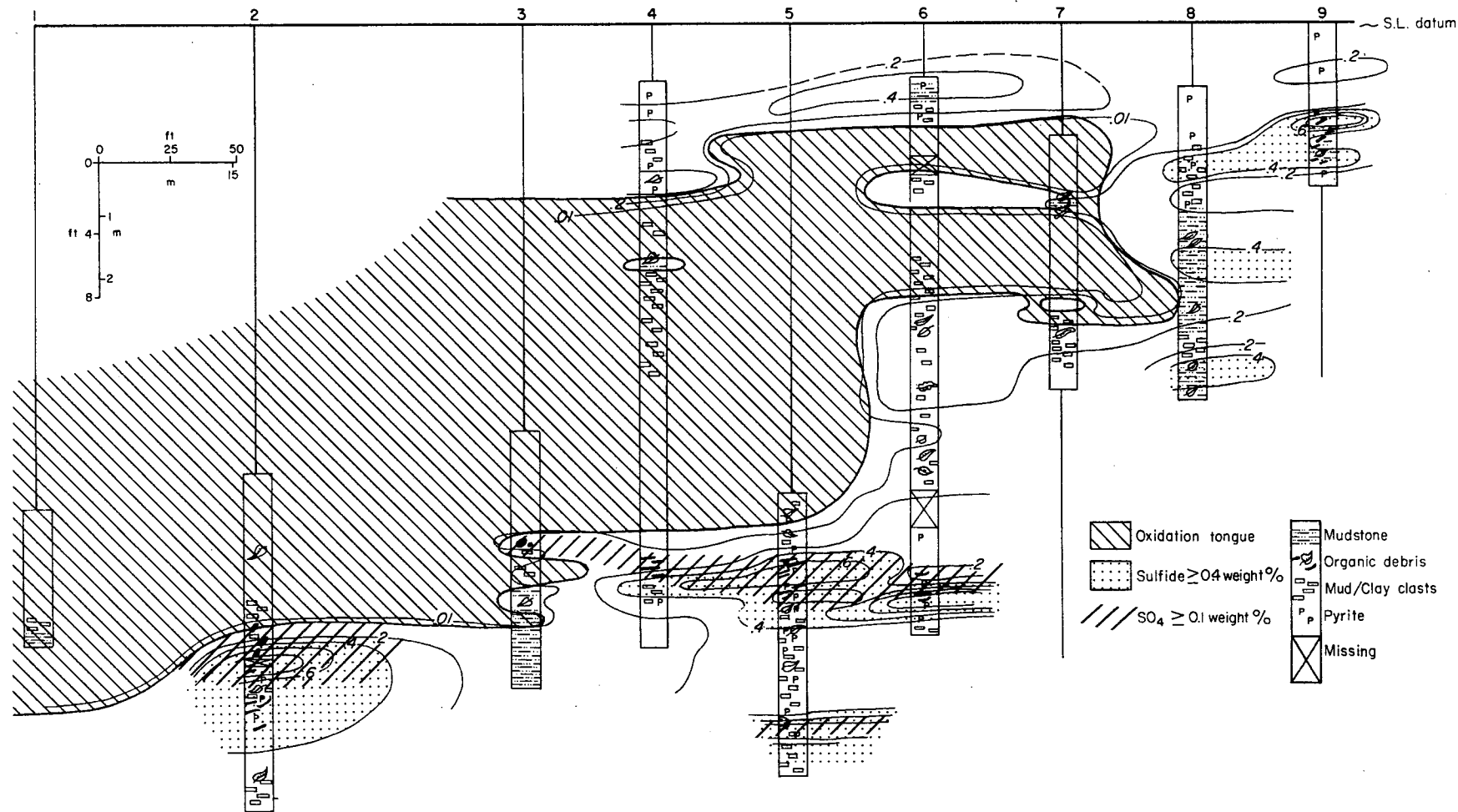


Figure 30. Distribution of sulfide and sulfate around the periphery of the Washington-Fayette oxidation/alteration tongue. Sulfide is most abundant in isolated pods that closely correspond to zones of uranium enrichment. Sulfate occurs along the margin of sulfide pods proximate to the oxidation front. Sulfur is thoroughly depleted in the oxidized interior.

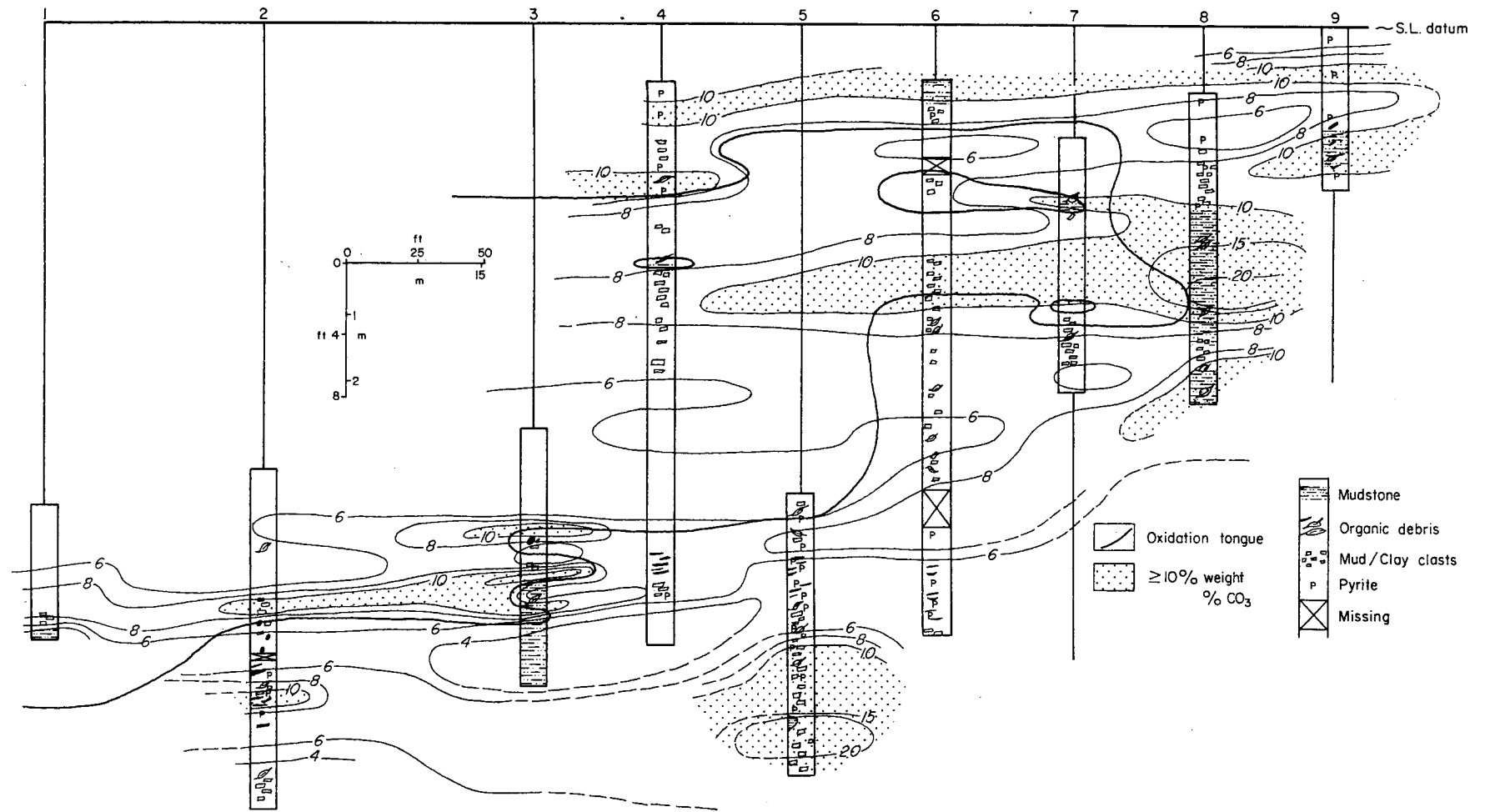


Figure 31. Distribution of carbonate around the periphery of the Washington-Fayette oxidation/alteration tongue. Carbonate occurs principally in pedogenic micrite or as reworked carbonate rock fragments and shows no relationship to mineralization.

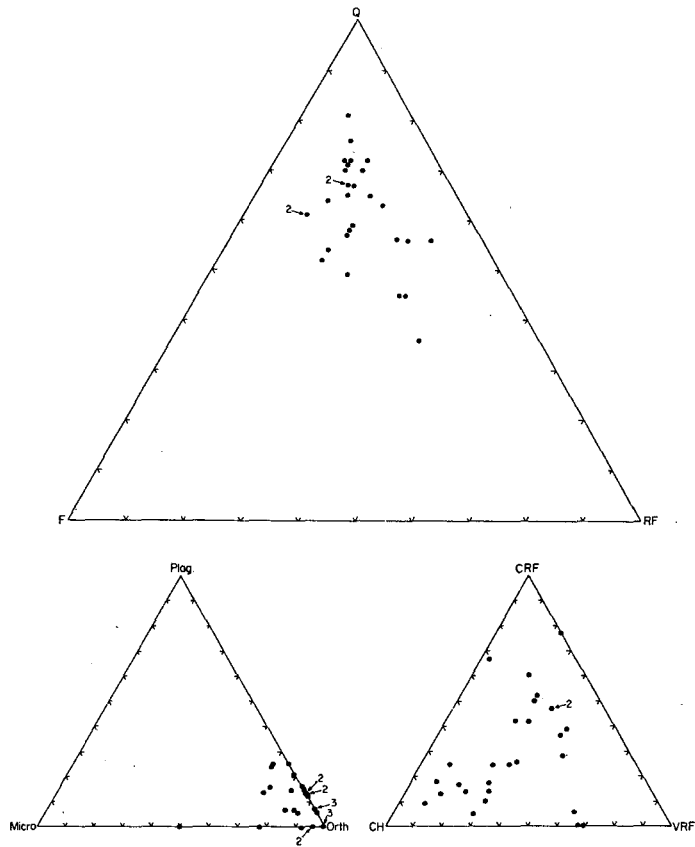


Figure 32. Petrographic composition of the Washington-Fayette host sand. Samples range from quartzose feldspathic litharenite to lithic arkose. Classification after Folk (1974). For explanation of abbreviations see figure 22.

Following deposition of the host crevasse splay sediments, pedogenesis produced mobile aluminosilicate gels, which washed onto grains to form cutanic coats; additional clay probably precipitated around grains below the water table. Micrite cement and replacement was precipitated in vadose or shallow phreatic zones. Early diagenetic marcasite or pyrite formed locally below the water table in slightly reducing environments supported by the abundant detrital organic debris present within the splay and interbedded floodplain deposits. Mineralizing ground water entered the splay from the genetically equivalent channel fill sand after an organized, semi-confined flow system developed. Alteration phenomena induced by the reactive waters included oxidation and leaching of organic carbon, oxidation of iron sulfide with local remobilization of iron and thorough leaching of sulfur, and deposition of uranium and associated trace metals along the Eh gradient at the periphery of the alteration tongue. Renewed or continued ground-water flux has redistributed some uranium or daughter products during the last 300,000 years, causing local radiometric disequilibrium.

Summary Comparison of Deposits

All of the deposits examined possess several common characteristics, despite their broad geographic and stratigraphic distribution.

1. All are associated with a definable mineralization front, which was emplaced as one product of the development of a tongue of epigenetically altered sediment within a regionally reduced, semi-confined aquifer.

2. All mineralization fronts retain in their consistent zonation of selenium, uranium, and molybdenum, a definite polarity indicative of downflow decrease in oxidation potential (Eh) of the mineralizing ground water.

3. Mineralogical and geochemical phenomena that appear to be genetically related to epigenetic alteration include oxidation of iron sulfide with thorough leaching of sulfur and minor redistribution of iron, leaching of uranium and molybdenum, destruction of organic material, and precipitation of an iron sulfide phase at the distal margin of the alteration tongue. Similar phenomena characterize most alteration front deposits (Harshman, 1974)

4. In all deposits, localization of uranium at both macroscopic and microscopic scales is consistent with a model requiring initial concentration of uranium by adsorption on a reactive substrate present at or near oxidation/reduction boundary. Positively identified substrates include titanium oxides, montmorillonite, and organic debris. Once concentrated by sorption, some uranium may have reacted to form

uranous minerals. However, identification of discrete uranium minerals remains the exception rather than the rule.

5. The uranium mineralization phase occurred early, and predates all but earliest diagenetic or pedogenic phenomena. Pedogenesis becomes the favored mechanism to account for such early uranium release into shallow aquifers. Where glass is present, uranium mineralization demonstrably predates open-system leaching and zeolitization, further ruling out this form of glass diagenesis as important in uranium mobilization.

6. All the sampled deposits occur in fluvial channel-margin crevasse splay facies. However, all are small, shallow deposits. Although the channel-margin setting is obviously favorable, larger, more deeply buried deposits can be emplaced by similar epigenetic processes within more massive channel-fill sand facies.

The deposits also illustrate some significant differences indicative of the range of manifestations of the basic epigenetic alteration/mineralization process in different geological and geochemical environments.

1. Reductants necessary to develop the sharp Eh gradient, which defines the mineralization front, may be either intrinsic organic material or iron sulfides, or may be pyrite produced during intrusion of highly reactive, reducing sulfide-rich waters following deposition of the host. Distribution of intrinsic reductants within a fluvial system will be facies related and localized. Extrinsic sulfide will, in contrast, be pervasively concentrated in permeable portions of the aquifer, and commonly will be spatially associated with conduits for vertical fluid migration such as fault zones. The active dissolved sulfur species may be HS^- rather than dissolved or gaseous H_2S because Gueydan subsurface waters are uniformly basic.

2. A wide range of postmineralization diagenetic events can superimpose mineralogical and geochemical patterns (such as carbonate content, sulfide content, or zeolitization) on the host. These patterns may mask or obscure patterns developed during primary mineralization, but may not be totally unrelated to mineralization patterns, however. Many different diagenetic processes, such as zeolitization in confined tuffaceous aquifers, reflect permeability distribution in the same way that mineralizing alteration does. Diagenetic processes, which share common controls with alteration epigenesis, may provide general guides for localization and extent of alteration, but are not direct mineralization indicators. Likewise, their products must be separated from those of primary mineralization if the mineralizing process is to be understood. This has too rarely been the case in published interpretations of ore genesis.

The hydrochemical and mineralogic evidence for the volumetric and geochemical importance of the discharge of deeper ground or formation waters into shallow, uranium host aquifers partially validates the theory that vertically discharged basinal brines might be a contributing or main source of the uranium (Gableman, 1977, p. 104-106). To date, however, the geology of all described deposits of the Coastal Plain emphasizes the importance of meteoric flow systems in determining the distribution, mineralogy, and stratigraphic position of ore-forming epigenesis. An adequate uranium source is certainly present in the Catahoula tuffs.

URANIUM CONCENTRATION II: MINERALIZATION GEOCHEMISTRY

Uranium mineralization in the Catahoula Formation is discussed in terms of the physical and chemical factors that control accumulation. Adsorption is an important concentration mechanism, probably a necessary first step to uranium fixation. The important chemical factors are pH, Eh, uranium and bicarbonate activities, and SiO₂ concentration. The availability of dissolved SiO₂ controls the ultimate formation of coffinite or uraninite.

In the context of Catahoula deposit mineralogy, trace metal associations, organic matter content, and uranium concentration in general, the hydrochemistry of the mineralizing waters can be characterized. Uranium ores are essentially low-grade sulfide deposits; thus, sulfide mineralogy and geochemistry provide important clues to the Catahoula geochemical environment. The paragenetic sequence, specifically the timing of montmorillonite, calcite, and clinoptilolite formation versus mineralization, provides additional clues about the geochemistry. Key thermodynamic data are presented in Appendix A.

Concentration Mechanisms

Physical

Adsorption may be the critical first step in concentration of uranium from dilute solutions (Katayama and others, 1974; Doi and others, 1975; Kochenov and others, 1977). Maximum adsorption of uranium by different sorbents occurs at approximately pH 6 (Dement'yev and Syromyatnikov, 1968). The majority of natural sorbents adsorb positively charged uranium species and do not adsorb negatively charged uranyl

carbonate ion complexes (Lisitsin and others, 1967). The boundary between neutral and anionic forms of uranium in carbonate-rich water occurs at about pH 6 (fig. 33). At slightly alkaline pH about 10 percent of the dissolved uranium is present as cationic species (Lisitsin and others, 1967).

Adsorption of uranium is operative in waters with positive Eh; it is reversible in an oxidizing medium and irreversible under strongly reducing conditions (Kochenov and others, 1965). Adsorption by inorganic compounds such as clay minerals and zeolites occurs in oxidizing and reducing waters, whereas adsorption by organic matter is most likely at low Eh and pH. Soluble organic compounds in carbonate-rich waters have Eh-pH stability fields that are small and only stable at low Eh and pH (fig. 34). Benzoic acid, a degradation product of fulvic acid, is used as a model humic material in figure 34 (Gamble and Schnitzer, 1973). Humic acids are capable of breaking down uranyl carbonate ions. Adsorption of UO_2^{2+} takes place on insoluble humic acids (Szalay and Szilagyi, 1969). Spectroscopic studies on the binding of uranium by organic matter points to complexing of UO_2^{2+} by carboxylate groups which act as bidentate ligands (Koglin and others, 1978).

Chemical

The role of Eh and pH in uranium precipitation is well known (Hostetler and Garrels, 1962; Langmuir, 1978). The importance of reducing conditions (low Eh) is generally recognized. Until recently (Huang, 1977) the role of pH has been little discussed by South Texas uranium workers. Low pH favors precipitation of uranium compounds, whereas high pH promotes their dissolution, as shown in figure 35 by the expanded fields of stability for UO_2 and USiO_4 at pH 6 and decreased fields at pH 8. High pH and low uranium activity require more powerful reducing conditions (lower Eh) for uranium precipitation. Likewise, in the presence of strong complexing agents lower Eh is required. To characterize conditions more closely at the time of deposition the initial precipitate is shown as amorphous UO_2 and USiO_4 . The precursors of many mineral species are similarly precipitated.

A SiO_2 concentration of 60 mg/l ($\text{H}_4\text{SiO}_4^\circ$ activity of 10^{-3}) was assumed for the UO_2 - USiO_4 equilibrium concentration, a value above the average in ground water (17 mg/l or ppm) and below saturation with amorphous SiO_2 (120 mg/l) (Langmuir, 1978). Coincidentally, 60 mg/l SiO_2 is the equilibrium saturation with silica glass. Earlier published equilibrium values (a few $\mu\text{g/l}$ or ppb SiO_2) would have made coffinite the stable form in almost all natural, reducing waters (Brookins, 1975a; Huang, 1977). In

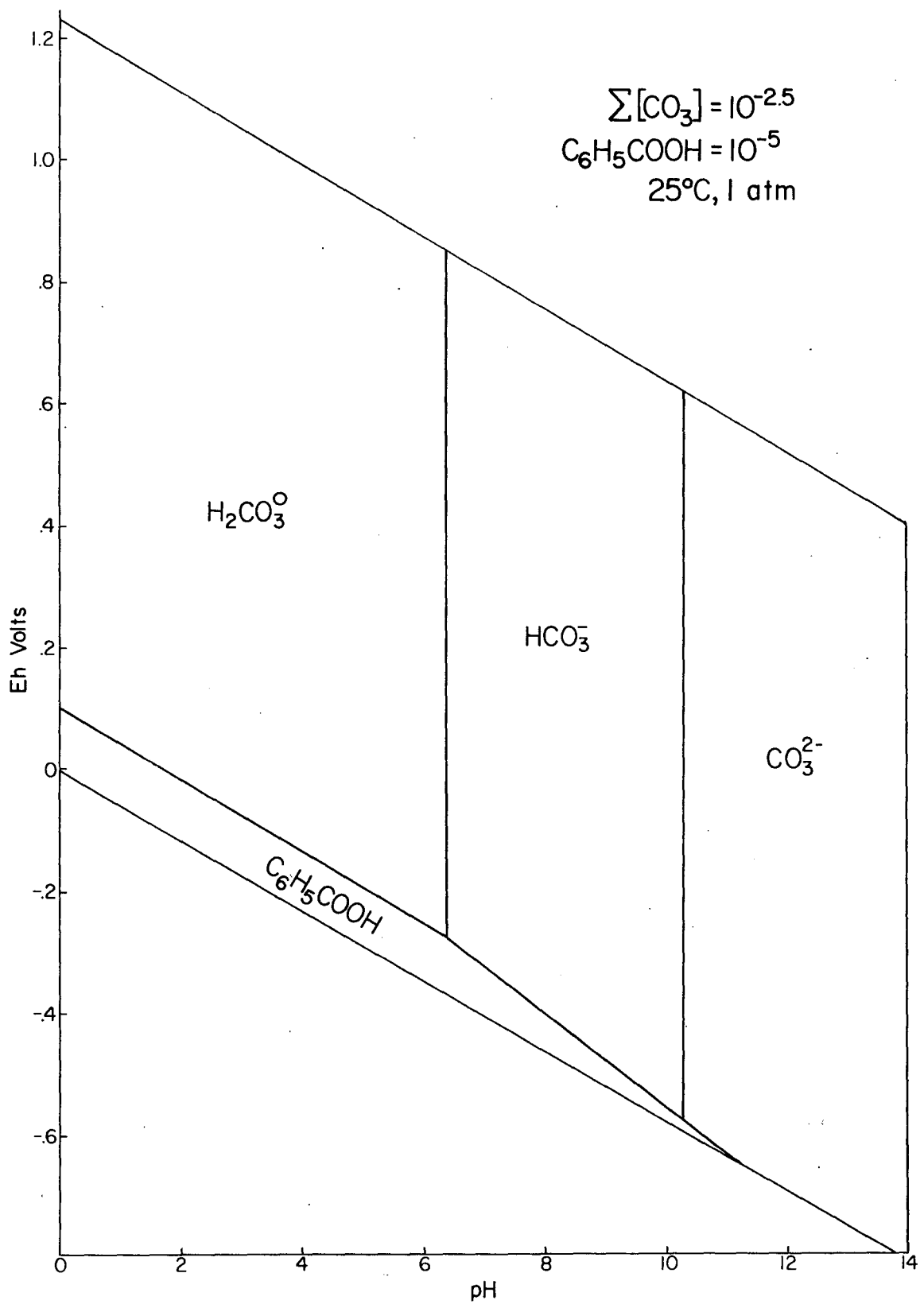


Figure 34. Eh-pH diagram showing the stability of benzoic acid in carbonate-rich water (10^{-5} $\text{C}_6\text{H}_5\text{COOH} = 1$ mg/l).

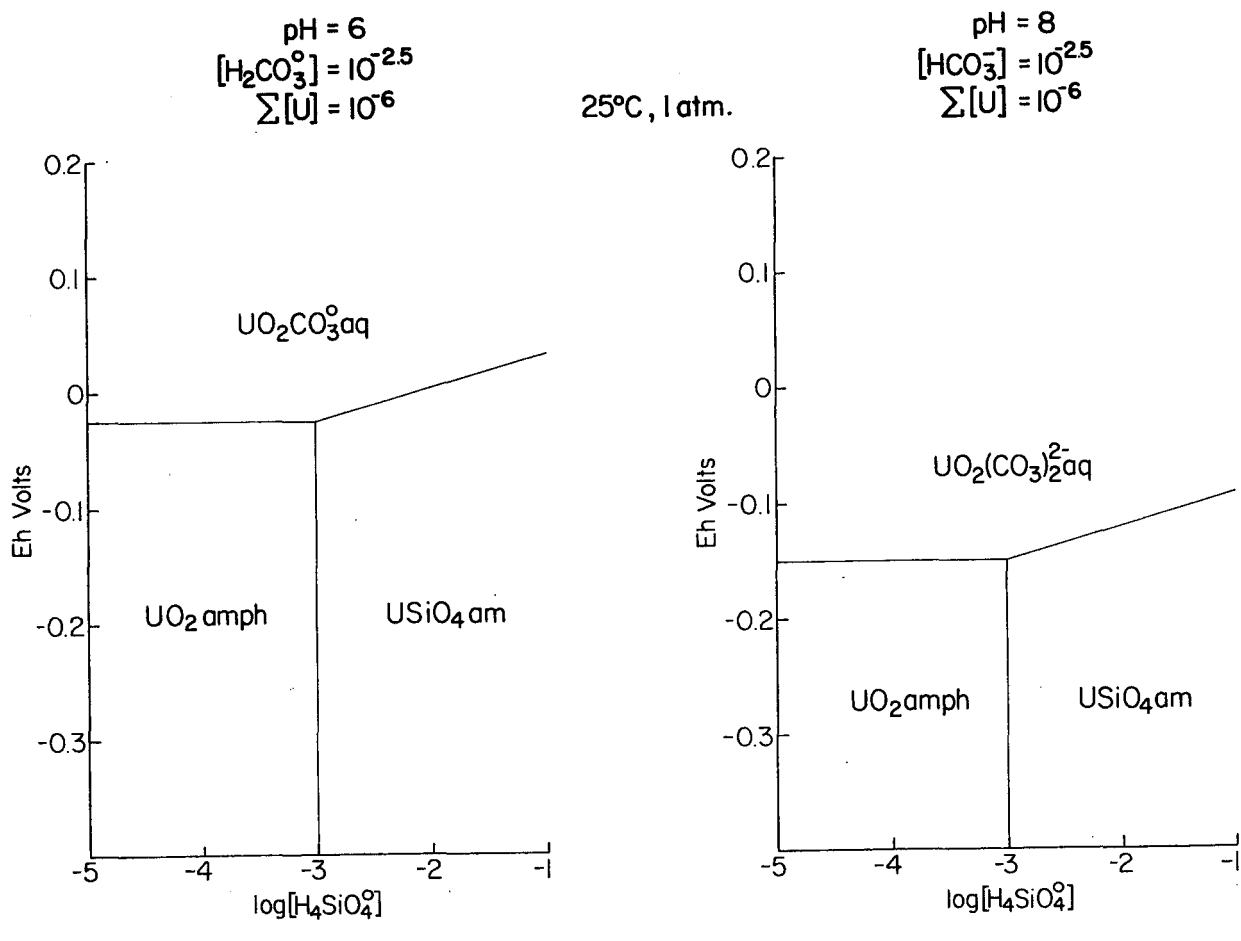


Figure 35. The effect of pH on the stability of UO_2 and $USiO_4$ amorphous in carbonate-rich waters.

the Whitsett and Oakville Formations of South Texas uraninite and coffinite are found coexisting (Eargle and others, 1975) in ground waters containing 20 to 120 mg/l SiO_2 giving indirect support to an intermediate SiO_2 equilibrium value.

The Eh-pH stability fields for coffinite and uraninite are nearly identical (Brookins, 1976); which mineral forms is a function of dissolved SiO_2 concentration (fig. 35). Coffinite (or uraninite) has a large field of stability (fig. 33) suggesting it can precipitate from ground waters far more dilute than previously assumed, perhaps containing only a few $\mu\text{g/l}$ uranium. Experimental work (Kochenov and others, 1977) indicates that uranium cannot be precipitated from solutions containing less than 100 $\mu\text{g/l}$ uranium in the absence of an adsorbent. Since the initial precipitate is commonly an amorphous phase, the amorphous USiO_4 field (fig. 33) best characterizes the Eh-pH conditions favoring uranium precipitation from waters containing abundant uranium and carbonate species. Those favorable conditions are zero Eh or less and acid pH.

Deposit Mineralogy

Dominant clay minerals in the Catahoula are Ca-montmorillonite and Na-montmorillonite. Clinoptilolite is the only zeolite and of secondary abundance; calcite is abundant. Ca-montmorillonite is dominant in the Bruni and Washington-Fayette deposits, Na-montmorillonite in the House-Seale deposit. Pyrite and marcasite are abundant in the Bruni deposit; data are unavailable for other deposits. Distribution of trace metals parallels that reported from other roll-type uranium deposits.

Iron Sulfides

In the Bruni deposit marcasite is dominant at the mineralization front (fig. 21). Pyrite-rich sediments extend from downdip toward the front. Pathways of marcasite and pyrite formation are shown in figure 36. The formation of marcasite requires the presence of elemental sulfur (S^0) and is dependent on the reaction of S^0 and a pre-existing iron monosulfide, such as mackinawite (Rickard, 1969b; Berner, 1970). Only in the presence of excess S^0 will pyrite form via $\text{FeS} + \text{S}^0$ at neutral pH or less and low temperature (Berner, 1970).

The Eh-pH stability fields of mackinawite and S^0 against thermodynamically unstable sulfur species are shown in figure 37. Unstable species were chosen because their consideration yields geologically significant information about oxidation-reduction reactions at low temperature (Granger and Warren, 1969). The field for elemental

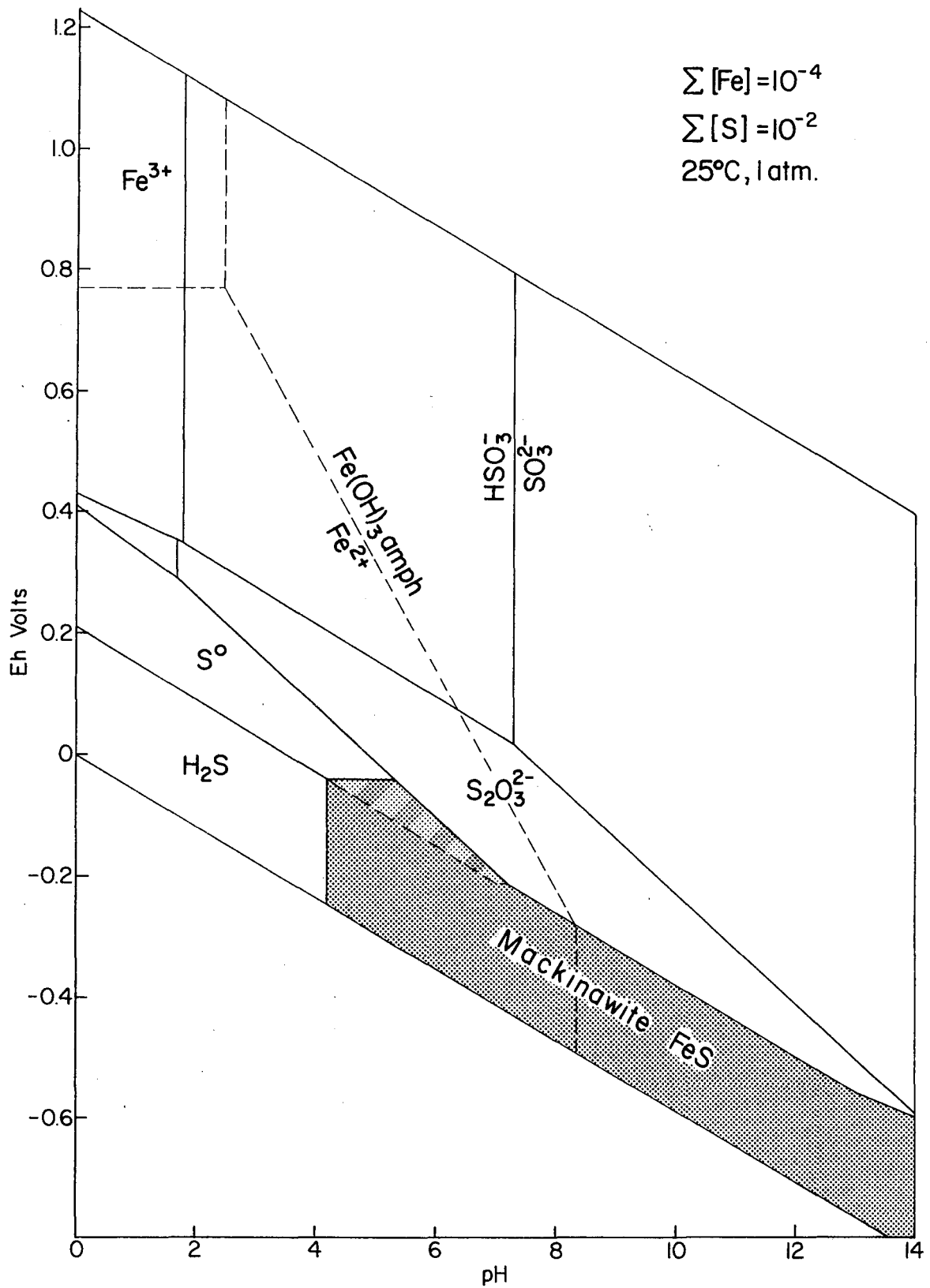


Figure 37. Eh-pH diagram showing the stability of mackinawite and elemental sulfur (10^{-4} iron species = 5.6 mg/l, 10^{-2} sulfur species = 320 mg/l).

sulfur at the total sulfur activity shown (10^{-2} , equivalent to 960 mg/l SO_4^{2-}) extends to pH 7.2 and expands with decreasing pH. At a sulfur activity of 10^{-3} the S^0 field contracts and extends to pH 6. The area of overlap of the S^0 and mackinawite stability fields represents the pH condition most favorable for marcasite formation. The formation of marcasite is obviously favored by acid conditions; however, its presence alone is inconclusive proof of acid conditions since S^0 can exist metastably under a variety of pH conditions (Rickard, 1969b). In the Bruni deposit marcasite is linked to uranium mineralization; its precipitation spans the time of roll-front development and uranium emplacement (Goldhaber and Reynolds, 1977). Thus, the presence of marcasite and uranium together at the roll-front strongly supports an acid pH during mineralization.

Trace Metals and Organic Matter

The zoned distribution of Se, U, and Mo reflects a decreasing Eh gradient with each metal in turn requiring a lower Eh for precipitation (Harshman, 1974). Joint precipitation of U and Mo is possible in weakly acidic media (Lisitsin, 1969). Thus, the extent of U and Mo overlap may be a pH indicator. Some overlap is found in the Bruni, House-Seale, and Washington-Fayette deposits; however, peak concentrations more closely match in the latter deposit, possibly reflecting a more acidic environment (tables 2, 3, 4, figs. 20 and 29).

In the South Texas deposits there is no direct correlation between uranium and organic carbon, indicating that organic carbon was not directly involved in uranium accumulation (Harshman, 1974). Low levels of organic carbon in the Bruni (Goldhaber and Reynolds, 1977) and House-Seale (table 3) deposits suggest that organic matter did not play an important role in uranium concentration. On the other hand, in the Washington-Fayette deposit of Central Texas there is a correlation between organic carbon and uranium (table 4). The higher organic matter content of this deposit may have generated a lower pH which in turn accounts for the greater degree of U and Mo overlap.

Paragenetic Sequence

Relative to mineralization the paragenesis of montmorillonite, calcite, and clinoptilolite are most instructive (table 5). Montmorillonite precedes mineralization and thus was available to play a role in the concentration of uranium, probably through adsorption on cutans (see p. 62-66, fig. 26D, fig. 27). Doi and others (1975) report a distribution coefficient of montmorillonite for uranium of about 10,000 in uranyl

Table 5. Summary of Paragenetic Sequence *

	Deposition	Pedogenesis	Shallow burial	Back-flux	Semi-confined meteoric circulation	Pleistocene rejuvenation of aquifer	Present
Montmorillonite cutans (argillation)		-----	-----				
Micrite replacement and nodules		-----	-----				
Hematitic oxidation		-----	-----				
Microcrystalline clinoptilolite		-----	-----				
Solution of feldspar		-----	-----				
Authigenic montmorillonite and alteration of glass		-----	-----		-----	-----	-----
Sulfidization of detrital FeTiO to pyrite				-----			
Limonic oxidation					-----	-----	-----
Marcasite formation					-----		?
Mineralization							
Calcite mosaic spar pore-fill and replacement		-----	-----		-----	-----	?
Solution of glass					-----	-----	?
Pore-fill clinoptilolite					-----	-----	?

solution or approximately 10 times that of clinoptilolite. From uranyl solutions the greatest adsorption on montmorillonite occurs at pH 6. Montmorillonite's large-surface free energy enables nucleation to take place with smaller free energies of activation than are required for nucleation of a solute in saturated solution. This means that in the presence of an adsorbent like montmorillonite uranium can be concentrated from solutions far more dilute than required for direct precipitation. Montmorillonite also possesses a high electrokinetic force and may have competed with bicarbonate and carbonate ions for the uranyl ion promoting enrichment (Brookins, 1975b). The overwhelming mass of montmorillonite relative to clinoptilolite gives montmorillonite the preeminent role in adsorption. Furthermore, clinoptilolite, at least in the Bruni (fig. 20) and House-Seale deposits, was precipitated in significant amounts following mineralization and is negatively correlated with uranium mineralization.

The distribution of calcite is pervasive throughout the roll fronts (figs. 23 and 31) and shows no relationship to mineralization. Significantly, calcite is paragenetically late and as a high-pH indicator it would preclude the formation of marcasite during mineralization.

Summary

Whether uranium concentration occurs by adsorption and/or precipitation, both mechanisms are favored by weakly acidic conditions. Maximum adsorption and minimum solubility of uranium occur at pH 6 in carbonate waters (Dement'yev and Syromyatnikov, 1968). Adsorption can take place in waters with positive Eh, whereas precipitation and reduction require negative Eh. If reduction does not follow adsorption, uranyl can be desorbed and remobilized easily by increased alkalinity at constant pH or raising pH (Langmuir, 1978). Montmorillonite was the principal sorbent. Fixation requires uranyl reduction to U^{4+} , probably in amorphous $USiO_4$ (see p. 66).

Lowering the pH of weakly alkaline uranyl transporting waters is probably achieved by a combination of factors--oxidization of pre-ore pyrite (Harshman, 1966; Goldhaber and Reynolds, 1977), decomposition and oxidation of organic matter (Boström, 1967), and bacterial activity (Zobell, 1964; Lisitsin and Kuznetsnova, 1967).

The oxidation potential of the system is supplied mainly by dissolved free oxygen at concentrations of approximately 5 ppm (Granger and Warren, 1978). Pyrite oxidation is an extremely effective mechanism for reducing pH as shown by low-pH waters (less than 6 is common) draining from coal-mine spoil piles.

URANIUM CONCENTRATION III: DEPOSIT HYDROCHEMISTRY

To evaluate the potential use of geochemistry in exploration and to further understand uranium concentration, Catahoula waters associated with uranium mineralization were analyzed. Data for this analysis come from permit applications for in situ leach mining filed by industry with the Texas Department of Water Resources. Four deposits were studied: Holiday-El Mesquite, Bruni, O'Hern, and Piedre Lumbré (fig. 3). Solution and mineral equilibria were used to test activities and mineral saturation against the occurrence of uranium. Activities were calculated by computer (Truesdell and Jones, 1974). In all calculations an assumed aluminate (Al(OH)_4^-) activity of 10^{-6} was used. Equilibrium pH values calculated using 10^{-6} are within a few tenths of a pH unit of observed pH.

Mineral equilibria for montmorillonite and clinoptilolite were emphasized because of their presumed role in mineralization. Lacking analyses of solid phases, formulas for montmorillonite and clinoptilolite were chosen based on the work of Ross and Hendricks (1945) and Mumpton (1977). Free energies of formation were estimated for montmorillonite following the method of Tardy and Garrels (1974) and for clinoptilolite using the method of Chen (1975). The methods are outlined in Appendix B.

Mineral-Solution Equilibria

The average concentrations and activities for major ionic species for waters associated with the uranium deposits are shown in tables 6 and 7. Fresh river water, the world average river water reported by Hem (1970), is included for comparison. Ionic strengths (I) are high enough so that deviations of chemical activity from concentration must be considered; activity coefficients of divalent ions may be as low as 0.45. The effect is illustrated by sulfate concentration in Bruni and O'Hern where concentration in Bruni waters exceeds that in O'Hern waters, whereas the reverse is the case for activity.

Table 6. Average concentration mg/l.

Deposit	Ca ²⁺	Mg ²⁺	Na ⁺	K ⁺	SO ₄ ²⁻	HCO ₃ ⁻	Cl ⁻	SiO ₂	I
Holiday	23	8.1	358	7.6	87	266	408	20	0.0193
El Mesquite	8.7	1.8	306	4.6	105	340	200	20	0.0151
Bruni	307	62	483	20	187	164	992	17	0.0564
O'Hern	15	3.2	322	9.3	123	328	244	43	0.0170
Piedre Lumbre	45	7.8	1984	50	91	466	2838	49	0.0934
House-Seale	169	25	1900	58	810	360	2486	NA	0.103
River Water	15	4.1	6.3	2.3	11	58	7.8	13	0.00211

Table 7. Negative log average activity.

Deposit	Ca ²⁺	Mg ²⁺	Na ⁺	K ⁺	SO ₄ ²⁻	HCO ₃ ⁻	H ₄ SiO ₄ ⁰	pH
Holiday	3.53	3.77	1.86	3.77	3.30	2.44	3.49	8.2
El Mesquite	3.95	4.40	1.93	3.98	3.19	2.34	3.51	8.5
Bruni	2.52	2.96	1.77	3.38	3.29	2.65	3.57	7.7
O'Hern	3.72	4.15	1.88	3.68	3.11	2.34	3.18	8.2
Piedre Lumbre	3.40	3.72	1.17	3.02	3.53	2.25	3.09	8.1
River Water	3.51	3.85	3.59	4.22	4.05	3.05	3.66	7

These waters are below the assumed $\text{UO}_2\text{-USiO}_4$ equilibrium value for dissolved SiO_2 (60 mg/l). O'Hern and Piedre Lumbre averages exceed 40 mg/l and many individual analyses exceed 60 mg/l. In Live Oak County abundant volcanic glass persists today and silica values above 60 mg/l are common, reaching 112 mg/l in some cases. Presumably diagenesis of the volcanic-rich sediments is not advanced and the silica values of these waters are more representative of earlier Catahoula waters.

With respect to the average deposit waters (table 8) montmorillonite, clinoptilolite, calcite, and cristobalite are all supersaturated. Relative to fresh river water montmorillonite and clinoptilolite are less highly supersaturated, whereas calcite is undersaturated and cristobalite is at saturation. Deposit waters are more highly supersaturated with respect to Ca-montmorillonite than Na-montmorillonite indicating that Ca-montmorillonite should be the dominant montmorillonite in equilibrium with these waters. All deposit waters plot in the Ca-montmorillonite field, even the sodium-rich Piedre Lumbre water (fig. 38). The House-Seale is a sodium-rich water similar to Piedre Lumbre, but with high calcium activity that would certainly plot in the Ca-montmorillonite field; however, Na-montmorillonite is dominant (table 3) in it and Piedre Lumbre. A possible explanation, assuming the thermodynamic data are approximately correct, is disequilibrium of these sodium-rich waters caused by mixing of vertically discharged sodium chloride brines and meteoric calcium-rich water (see figure 13C and p. 33-39).

Based on the deposit waters' high degree of supersaturation with respect to clinoptilolite, it should be far more abundant than it is; however, relative to Ca-montmorillonite only Piedre Lumbre water plots in the clinoptilolite field (fig. 39). Only in the House-Seale deposit with its sodium-rich water is appreciable clinoptilolite known to be present (table 3). Tested against Na-montmorillonite Piedre Lumbre, O'Hern, and El Mesquite waters plot in the clinoptilolite field (fig. 40).

Sequencing of montmorillonite and clinoptilolite precipitation inferred from mineral-solution equilibria (figs. 39 and 40) parallels an evolving hydrochemical system proceeding from calcium-rich to sodium-rich waters and is consistent with the observed paragenetic sequence (table 5). Montmorillonite cutans are postulated to be dominantly Ca-montmorillonite, whereas authigenetic montmorillonite may be either the calcium or sodium variety. Prior to mineralization Ca-montmorillonite was

Table 8. Saturation ratios, average log IAP/Ksp values.

<u>Deposit</u>	<u>Silica glass</u>	<u>Cristobalite</u>	<u>Calcite</u>	<u>Clinoptilolite</u>	<u>Ca-montmorillonite</u>	<u>Na-montmorillonite</u>
Holiday	-0.48	0.18	0.25	7.05	7.52	6.96
El Mesquite	-0.50	0.16	0.23	6.78	6.99	6.47
Bruni	-0.56	0.10	0.55	6.64	7.89	7.20
O'Hern	-0.17	0.49	0.16	8.88	8.53	8.00
Piedre Lumbre	-0.08	0.58	0.47	9.64	9.20	8.84
River Water	-0.65	0.01	-1.43	4.39	7.14	6.00

66

<u>Reaction</u>	<u>log Ksp</u>
$\text{SiO}_2 \text{ glass} + 2\text{H}_2\text{O} = \text{H}_4\text{SiO}_4^\circ$	-3.01
$\text{SiO}_2 \text{ cristobalite} + 2\text{H}_2\text{O} = \text{H}_4\text{SiO}_4^\circ$	-3.67
$\text{CaCO}_3 \text{ calcite} + \text{H}^+ = \text{Ca}^{2+} + \text{HCO}_3^-$	1.98
$\text{NaAlSi}_5\text{O}_{12} \cdot 4\text{H}_2\text{O} \text{ clinoptilolite} + 8\text{H}_2\text{O} = \text{Na}^+ + 5\text{H}_4\text{SiO}_4^\circ + \text{Al}(\text{OH})_4^-$	-32.26
$\text{Ca}_{0.16}(\text{Al}_{1.56}\text{Mg}_{0.5})\text{Si}_4\text{O}_{10}(\text{OH})_2 \text{ Ca-montmorillonite} + 10.24\text{H}_2\text{O} =$ $0.16\text{Ca}^{2+} + 1.56\text{Al}(\text{OH})_4^- + 0.5\text{Mg}^{2+} + 4\text{H}_4\text{SiO}_4^\circ + 0.24\text{H}^+$	-35.26
$\text{Na}_{0.33}(\text{Al}_{1.56}\text{Mg}_{0.5})\text{Si}_4\text{O}_{10}(\text{OH})_2 \text{ Na-montmorillonite} + 10.24\text{H}_2\text{O} =$ $0.33\text{Na}^+ + 1.56\text{Al}(\text{OH})_4^- + 0.5\text{Mg}^{2+} + 4\text{H}_4\text{SiO}_4^\circ + 0.24\text{H}^+$	-34.75

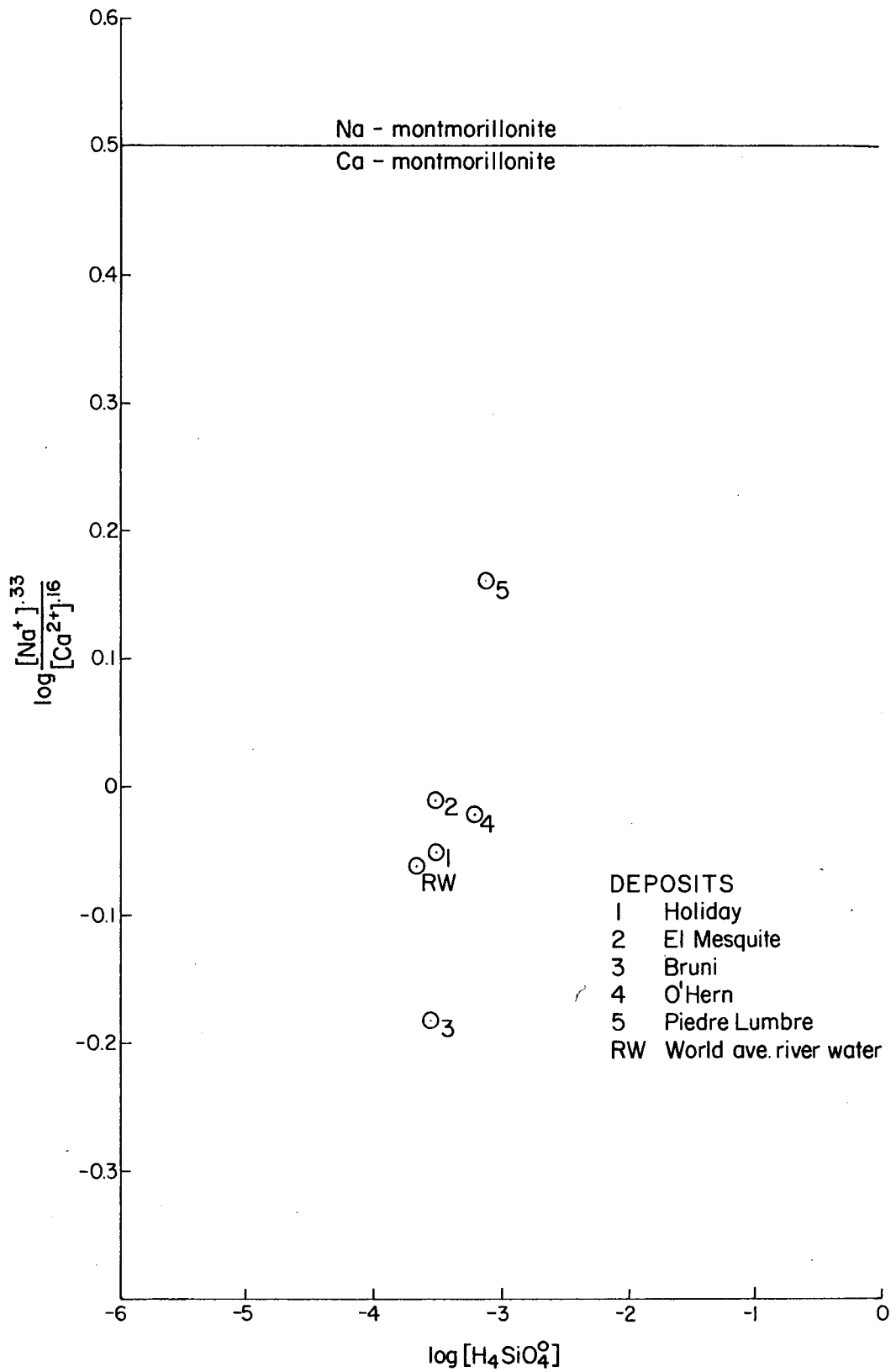


Figure 38. Plot of average deposit waters on Ca-montmorillonite - Na-montmorillonite activity diagram, defined by the reaction $\text{Na-montmorillonite} + 0.16 \text{Ca}^{2+} = \text{Ca-montmorillonite} + 0.33 \text{Na}^+$ and $\log K = 0.5$.

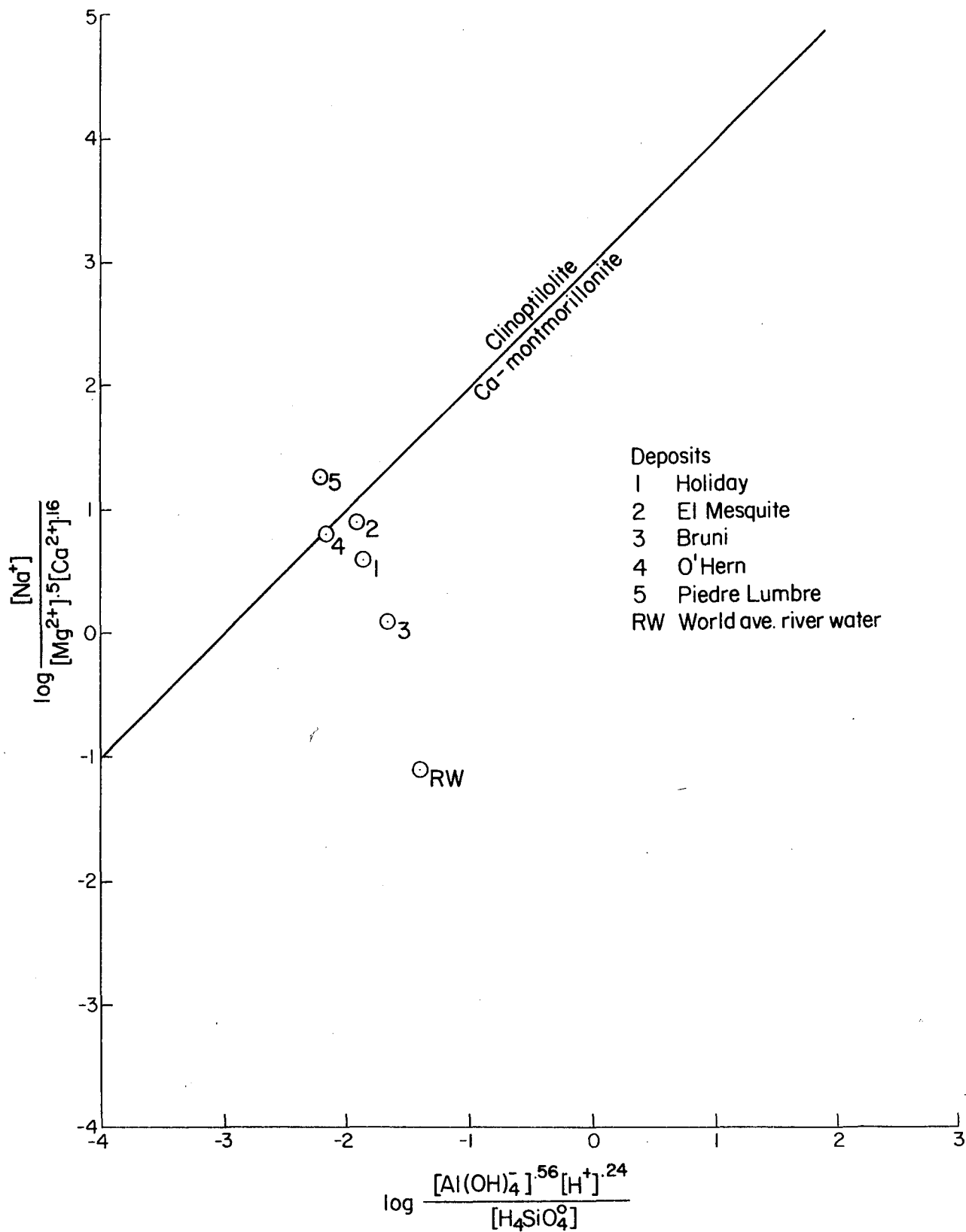


Figure 39. Plot of average deposit waters on Ca-montmorillonite-clinoptilolite activity diagram, defined by the reaction $\text{Ca-montmorillonite} + \text{Na}^+ + \text{H}_4\text{SiO}_4 + 2.24 \text{H}_2\text{O} = \text{clinoptilolite} + 0.56 \text{Al(OH)}_4^- + 0.5 \text{Mg}^{2+} + 0.16 \text{Ca}^{2+} + 0.24 \text{H}^+$ and $\log K = -3.0$.

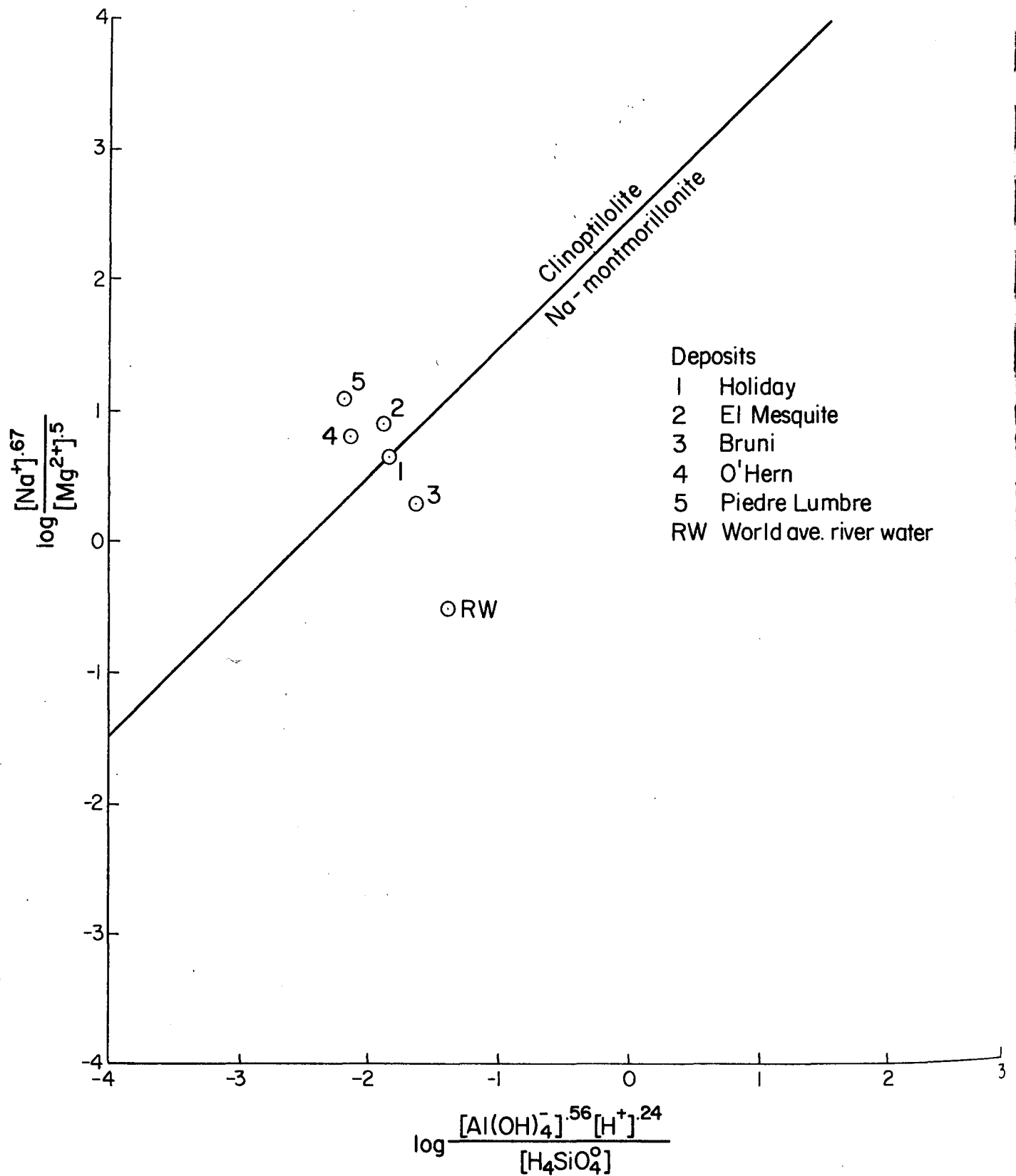


Figure 40. Plot of average deposit waters on Na-montmorillonite-clinoptilolite activity diagram, defined by the reaction $\text{Na-montmorillonite} + 0.67 \text{Na}^+ + \text{H}_4\text{SiO}_4 + 2.24 \text{H}_2\text{O} = \text{clinoptilolite} + 0.56 \text{Al}(\text{OH})_4^- + 0.5 \text{Mg}^{2+} + 0.24 \text{H}^+$ and $\log K = -2.5$.

probably favored. Calcite is later, and in view of its undersaturation in fresh water a longer evolution is implied before reaching supersaturation. Porefill clinoptilolite forms well after mineralization in sodium-silica-rich waters such as those of the Piedre Lumbre and House-Seale deposits.

Uranium Occurrence

Montmorillonite is a major mineral phase in the Catahoula and is presumed to have played an important role in uranium accumulation. As a primary mineral of huge mass and tremendous surface area it exerts significant influence on past and present hydrochemistry. Therefore, the compositions of present waters were plotted on montmorillonite-clinoptilolite activity diagrams, and their positions tested against the occurrence of uranium by mapping log activity ratios. Log Ionic Activity Product/-Equilibrium solubility product (IAP/Ksp) values or saturation ratios for montmorillonite and calcite were mapped as well as other combinations of saturation ratios. Salient diagrams and maps are presented from the four deposits discussed above (figs. 41 to 55).

Holiday-El Mesquite

The Ca-montmorillonite-clinoptilolite activity diagram (fig. 41) shows an obvious trend of individual analyses parallel to the Y-axis, $\log \frac{[\text{Na}^+]}{[\text{Mg}^{2+}]^{.5}[\text{Ca}^{2+}]^{.16}}$; therefore, values of this log ratio were mapped. Mapped values show a positive correlation between small values, those deeper into the montmorillonite field or more highly supersaturated with respect to montmorillonite, and the 50-percent oxidized-reduced line which is presumed to approximate the average mineralization-front position (fig. 42). Finger-like projections of low values approximately parallel to equipotential lines may represent recent uranium mobilization or ghost fronts. Log IAP/Ksp values for Ca-montmorillonite display a trend normal to the 50-percent line (fig. 43) and parallel to the direction of ground-water flow postulated during mineralization (fig. 19). Values for calcite show no correlation with the 50-percent line (fig. 44).

Bruni

Small Y-axis values of figure 45 coincide almost exactly with the production boundary or presumed locus of uranium mineralization (fig. 46). Mapping the ratio Y/X axis gave an anomaly offset downflow from the production boundary. Maps of log

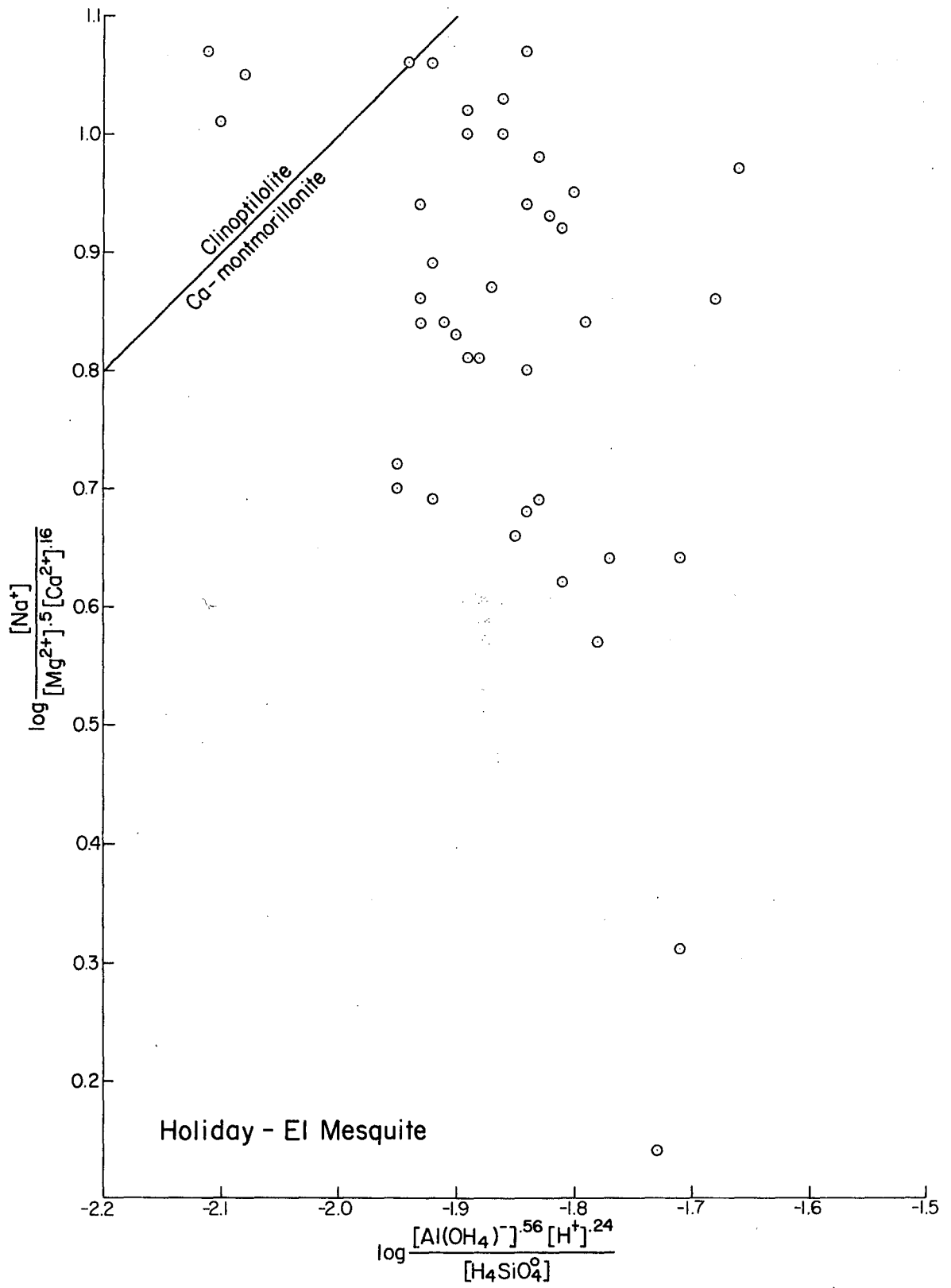


Figure 41. Plot of Holiday-El Mesquite waters on Ca-montmorillonite-clinoptilolite activity diagram.

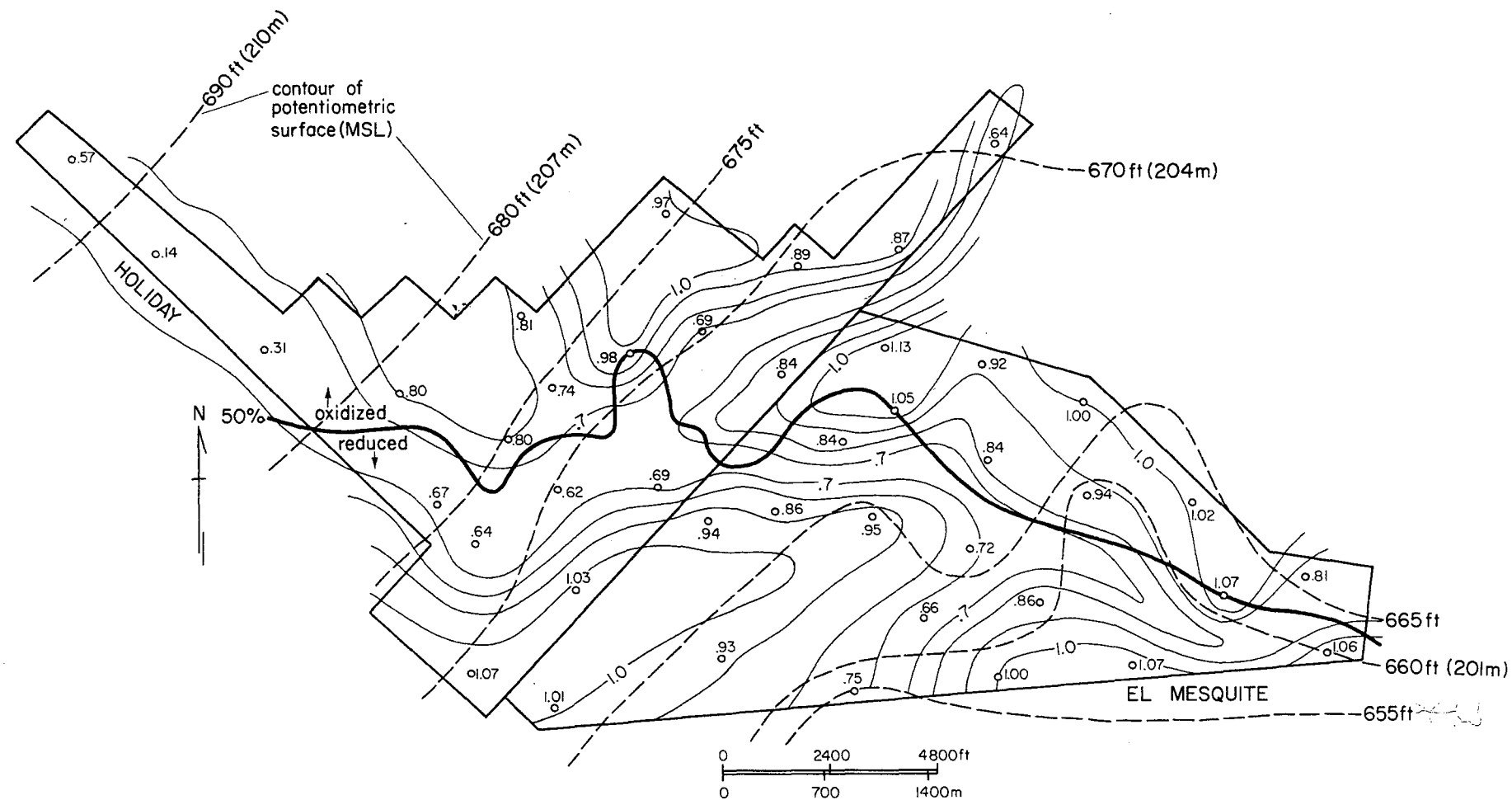


Figure 42. Map of Y-axis values, $\log \frac{[Na^+]}{[Mg^{2+}]^5 [Ca^{2+}]^{16}}$, from Holiday-El Mesquite Ca-montmorillonite-clinoptilolite activity diagram, figure 41. Fifty-percent line based on sediment color (oxidized is yellow, orange, and red; reduced is gray) and the presence or absence of sulfide minerals.

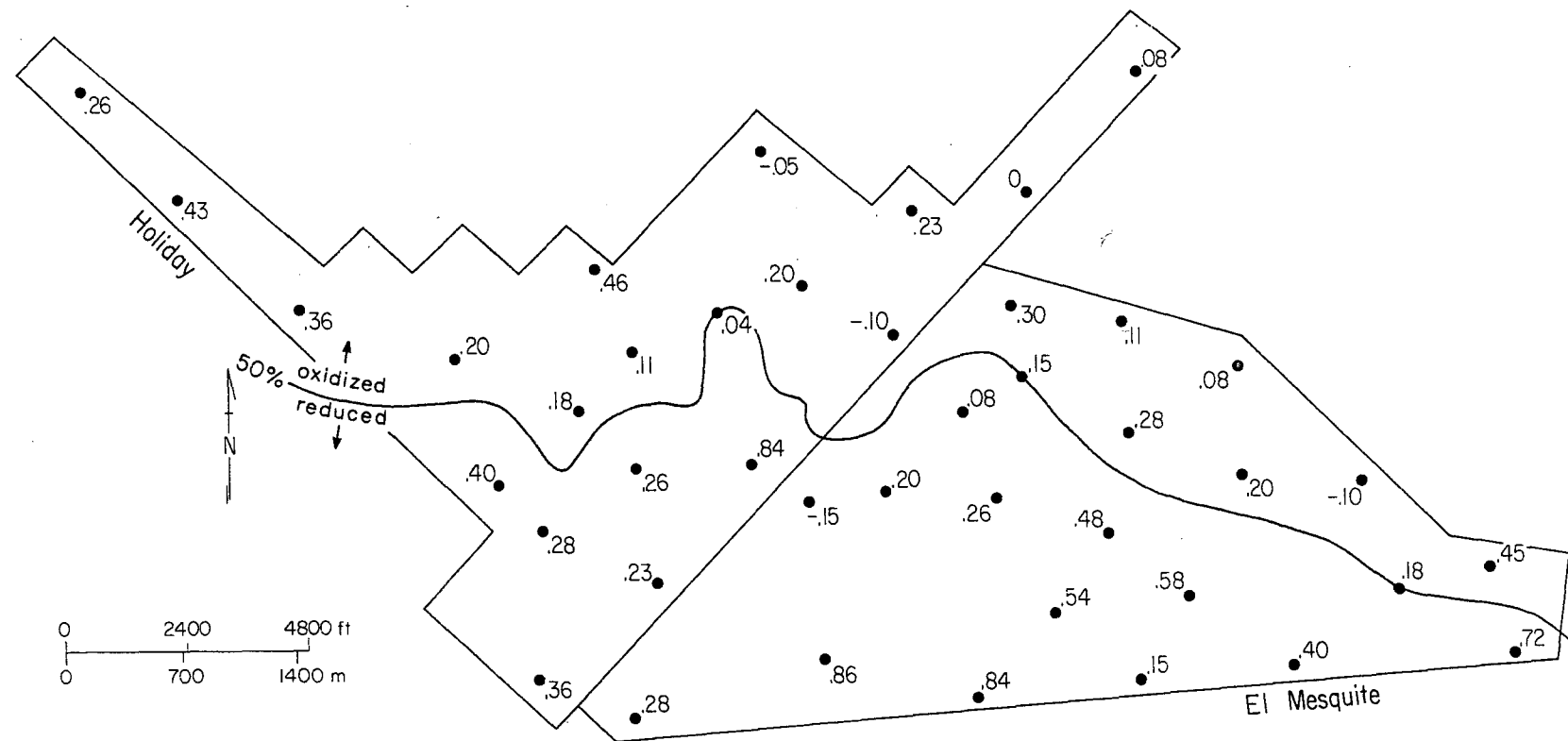


Figure 44. Map of Holiday-El Mesquite log IAP/Ksp values for calcite.

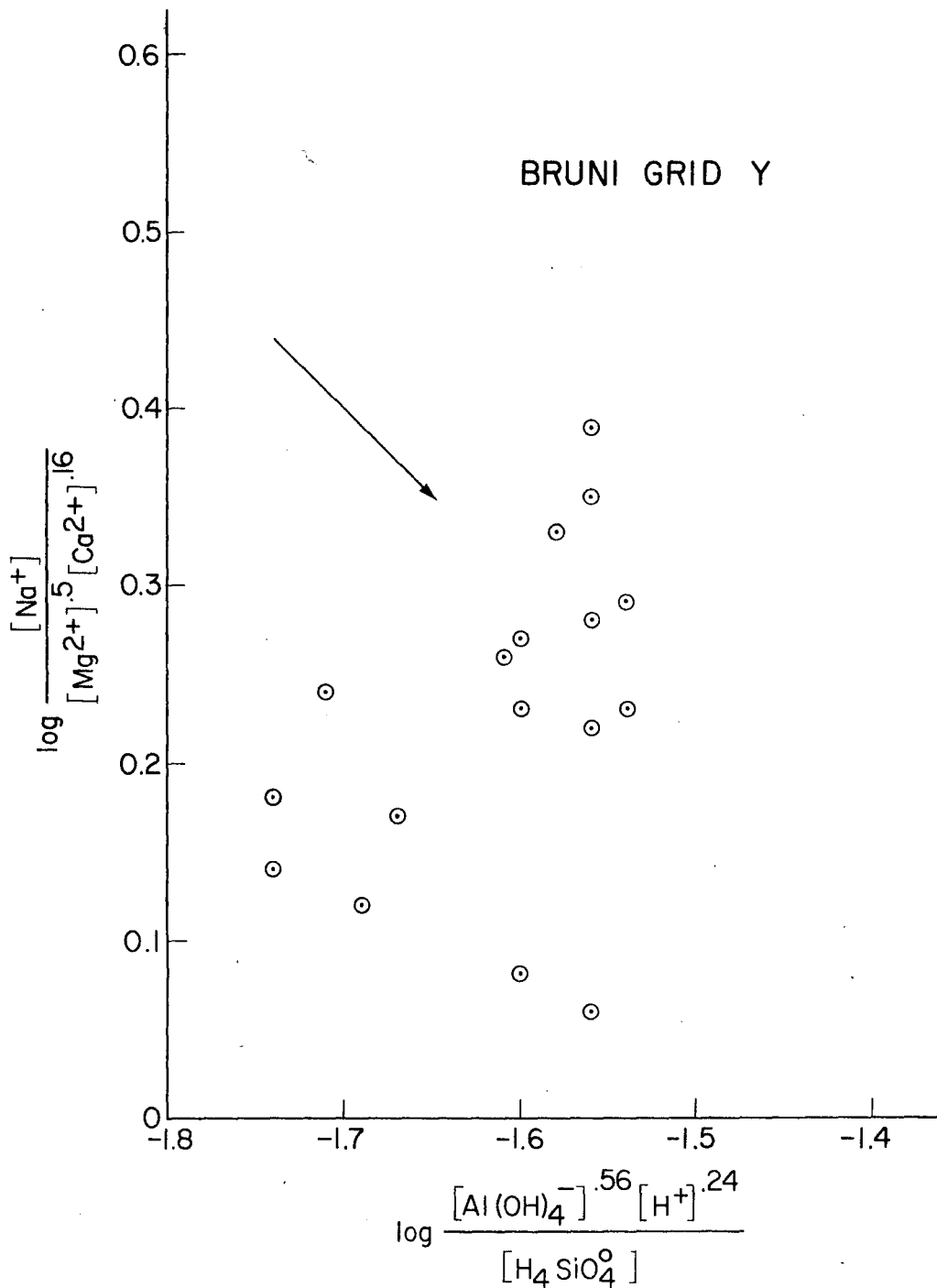


Figure 45. Plot of Bruni waters on Ca-montmorillonite - clinoptilolite activity diagram. All waters plot in Ca-montmorillonite field, arrow points deeper into Ca-montmorillonite field or away from clinoptilolite field.

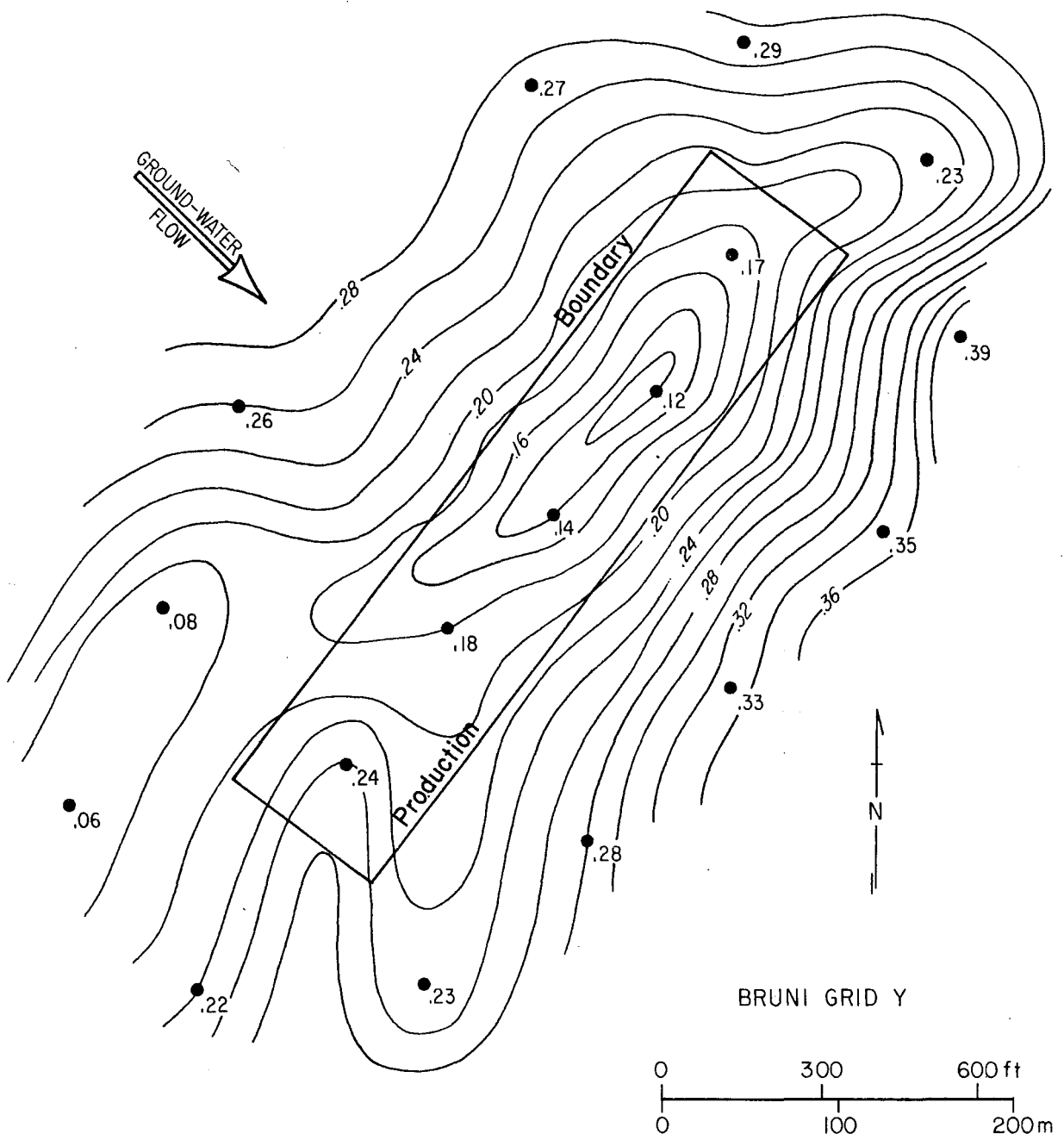


Figure 46. Map of Y-axis values, $\log [Na^+]/[Mg^{2+}]^5[Ca^{2+}]^{16}$, from Bruni (Grid Y) Ca-montmorillonite-clinoptilolite activity diagram, figure 45. Small values deeper into the montmorillonite field or more highly supersaturated with respect to montmorillonite.

IAP/Ksp values for Ca-montmorillonite and calcite show high values within the production boundary (figs. 47 and 48).

O'Hern

Mapped in figure 49 is the ratio Y/X axis; it was chosen because the plot of individual analyses on the Ca-montmorillonite-clinoptilolite activity diagram showed no obvious trend of data points parallel to either axis (fig. 50). Again there is a positive correlation between small values or those more highly supersaturated with respect to Ca-montmorillonite and the production boundary. A fair correlation was found between high log IAP/Ksp values for Ca-montmorillonite and the production boundary (fig. 51), whereas no correlation was found for log IAP/Ksp calcite (fig. 52). In fact, the highest and lowest calcite ratios calculated are found within the production area.

Piedre Lumbré

Waters in this deposit are sodium-rich and individual analyses were therefore first plotted on a Na-montmorillonite-clinoptilolite activity diagram (fig. 53). In this case the obvious trend of the data points is parallel to the X-axis, $\log [Al(OH)_4^-]^{.56} [H^+]^{.24} / [H_4SiO_4^0]$; mapped values are shown in figure 54. Less negative values, those not as deep into the clinoptilolite field or less highly supersaturated with respect to clinoptilolite and closer to the montmorillonite field, skirt the edges of production blocks 199, 202, and 205, split 201, and bifurcate through 106. The map pattern of Y-axis values (fig. 55) from the Ca-montmorillonite-clinoptilolite activity diagram is almost identical to figure 54. Without data between production blocks the correlation between log activity ratios and uranium occurrence could not be thoroughly tested.

The map patterns (figs. 54 and 55) are analogous to the geometry of the deposit's host ancient fluvial channel sands displaying the same northeast-southwest trending linear and bifurcating geometries. Patterns of values more highly supersaturated with respect to montmorillonite (less negative values of fig. 54 and smaller values of fig. 55) are linear and flank or trend across production blocks (uranium mineralization). The relation of log activity ratios to mineralization parallels that of host channel sands and mineralization front where ore commonly occurs flanking and axial to channels.

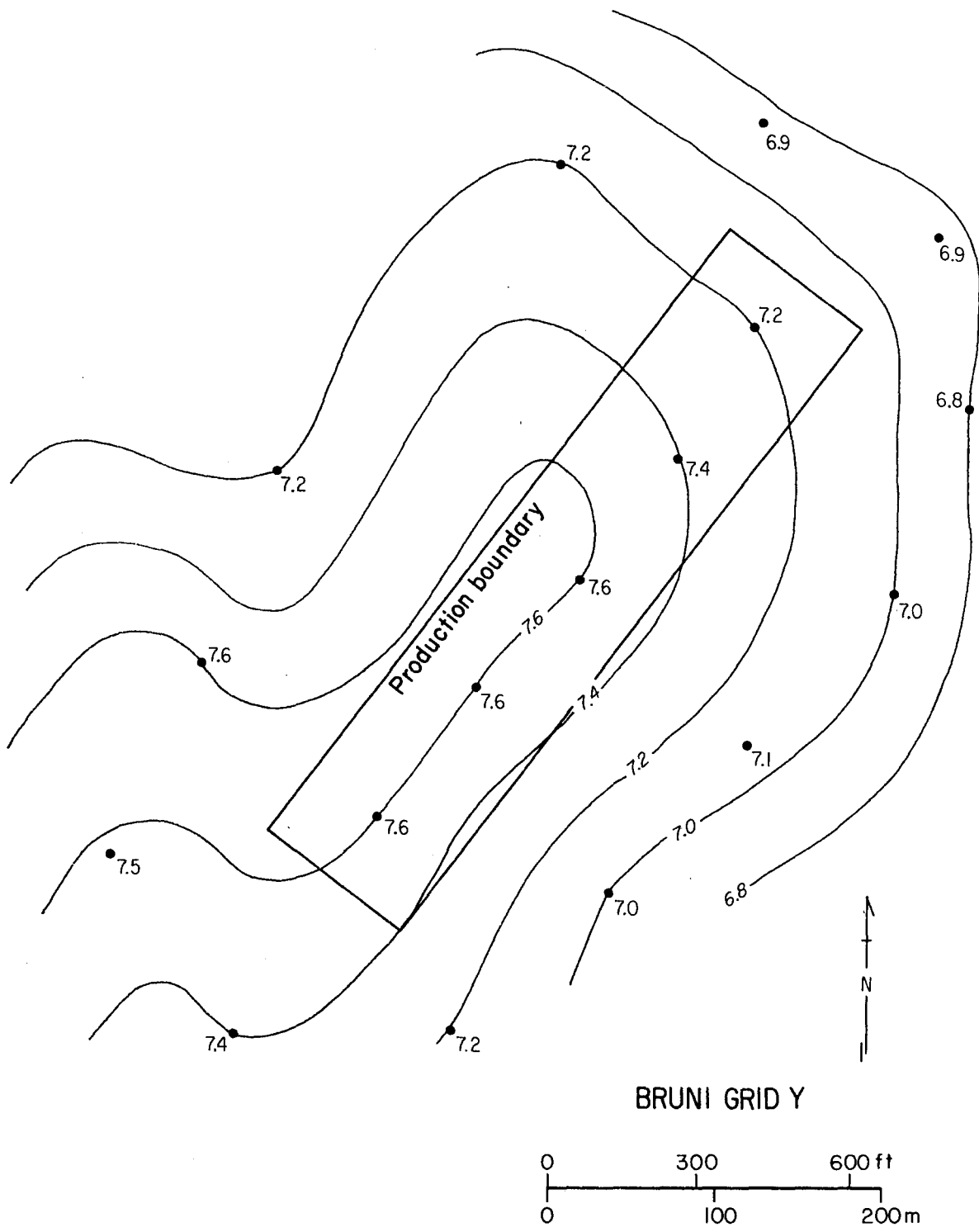


Figure 47. Map of Bruni log IAP/Ksp values for Ca-montmorillonite.

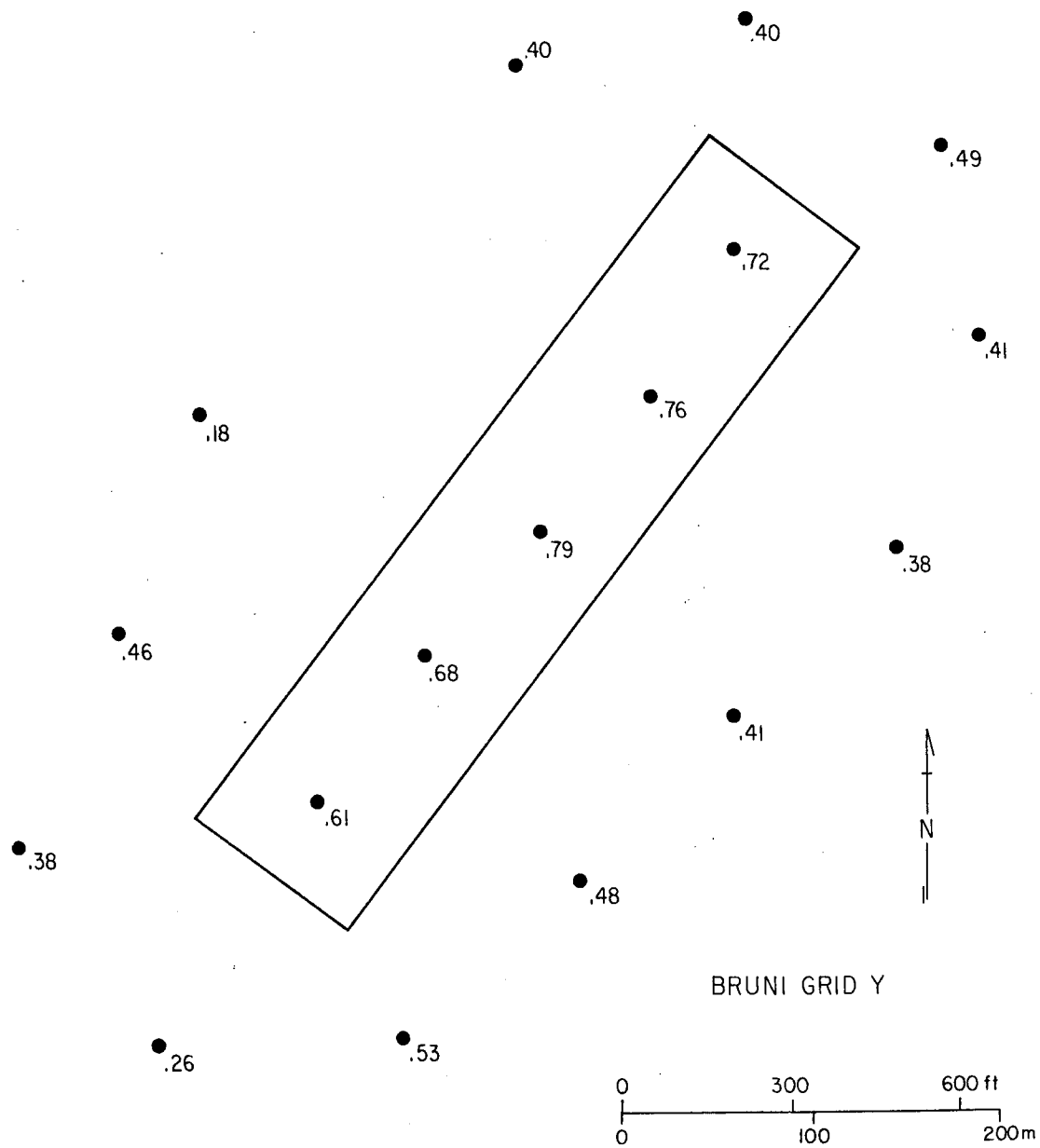


Figure 48. Map of Bruni log IAP/Ksp values for calcite.

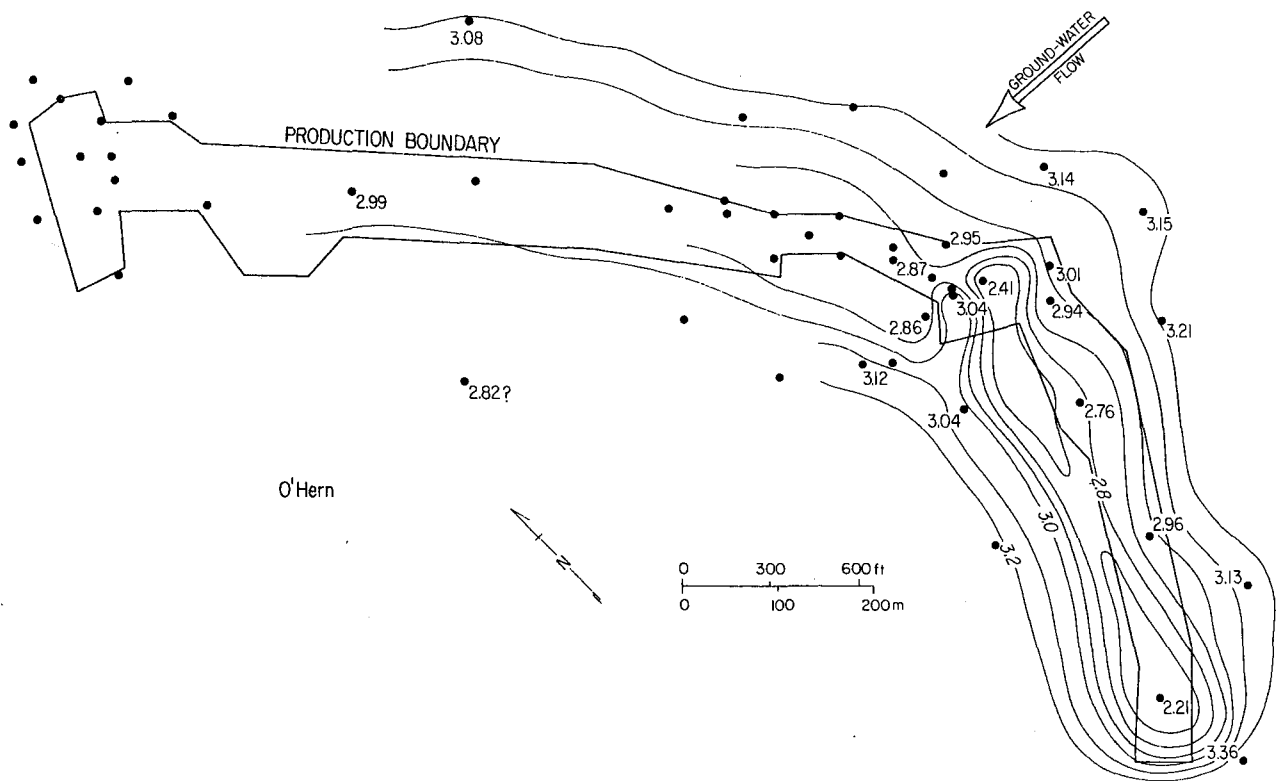


Figure 49. Map of the ratio Y/X axis, $\log \frac{[\text{Na}^+]}{[\text{Mg}^{2+}]^5 [\text{Ca}^{2+}]^{16}}$ over $\log \frac{[\text{Al}(\text{OH})_4]^{-56} [\text{H}^+]^{24}}{[\text{H}_4\text{SiO}_4]}$, from O'Hern Ca-montmorillonite - clinoptilolite activity diagram, figure 50.

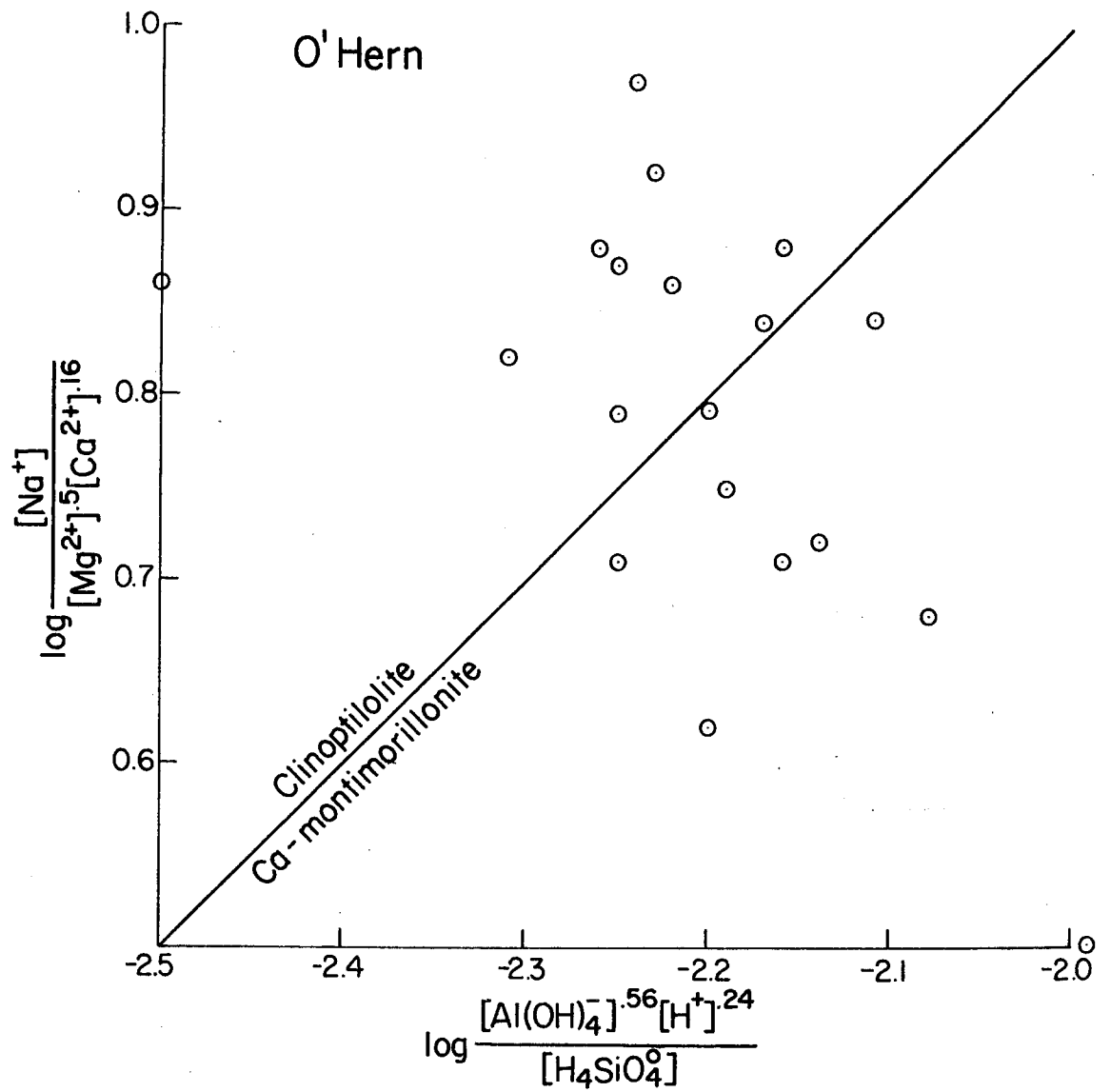


Figure 50. Plot of O'Hern waters on Ca-montmorillonite - clinoptilolite activity diagram.

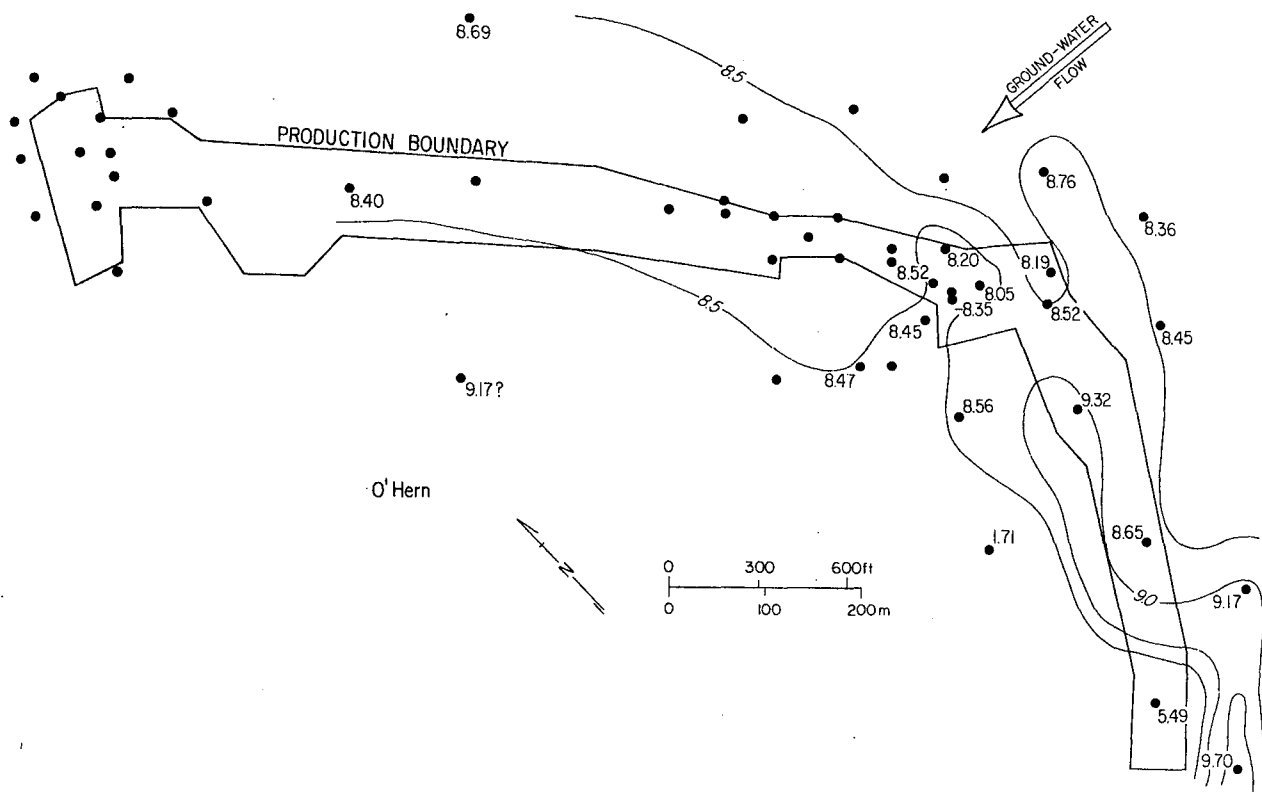


Figure 51. Map of O'Hern log IAP/Ksp values for Ca-montmorillonite.

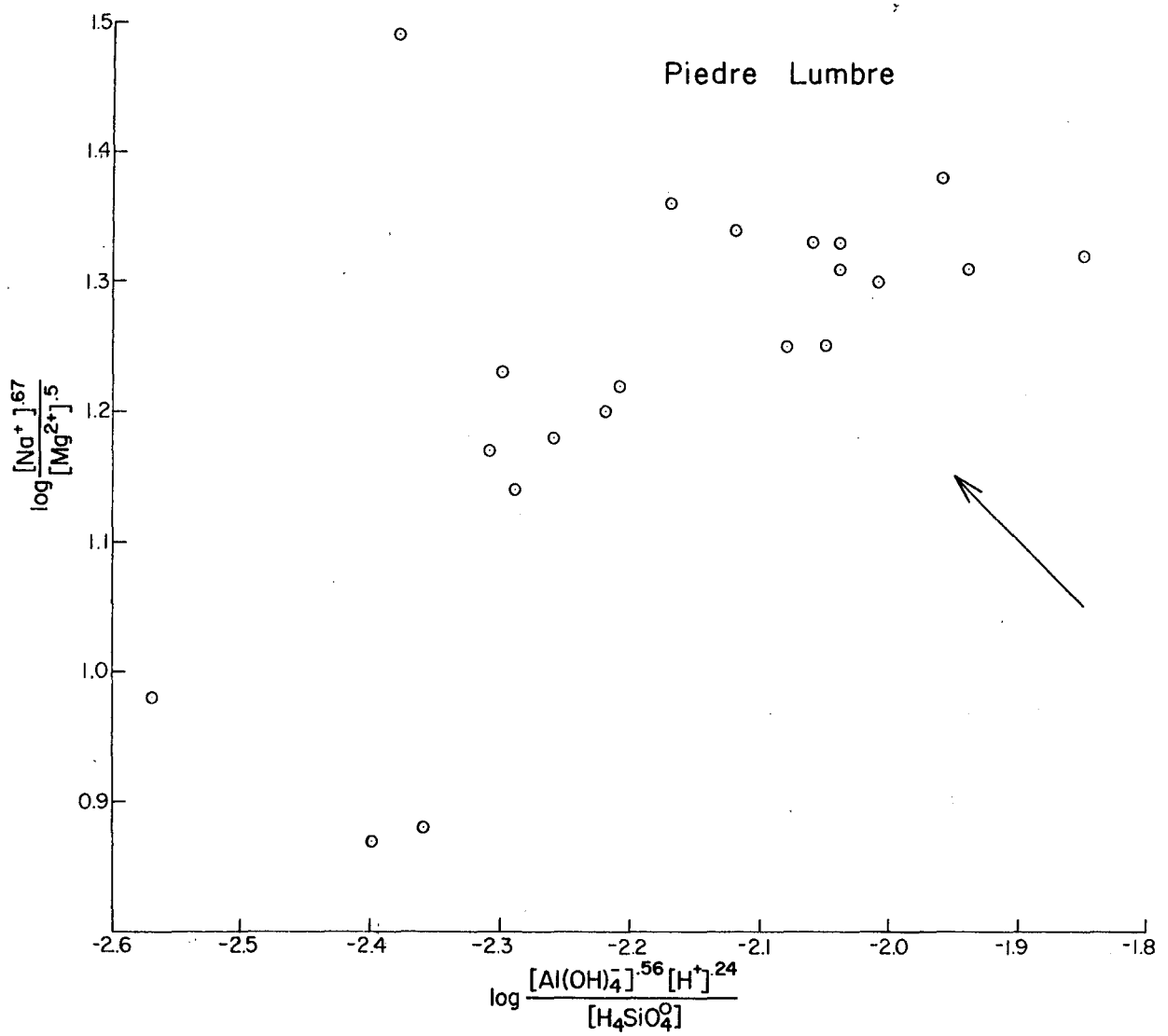


Figure 53. Plot of Piedre Lumbre waters on Na-montmorillonite - clinoptilolite activity diagram. All waters plot in clinoptilolite field; arrow points deeper into clinoptilolite field, or away from Na-montmorillonite field.

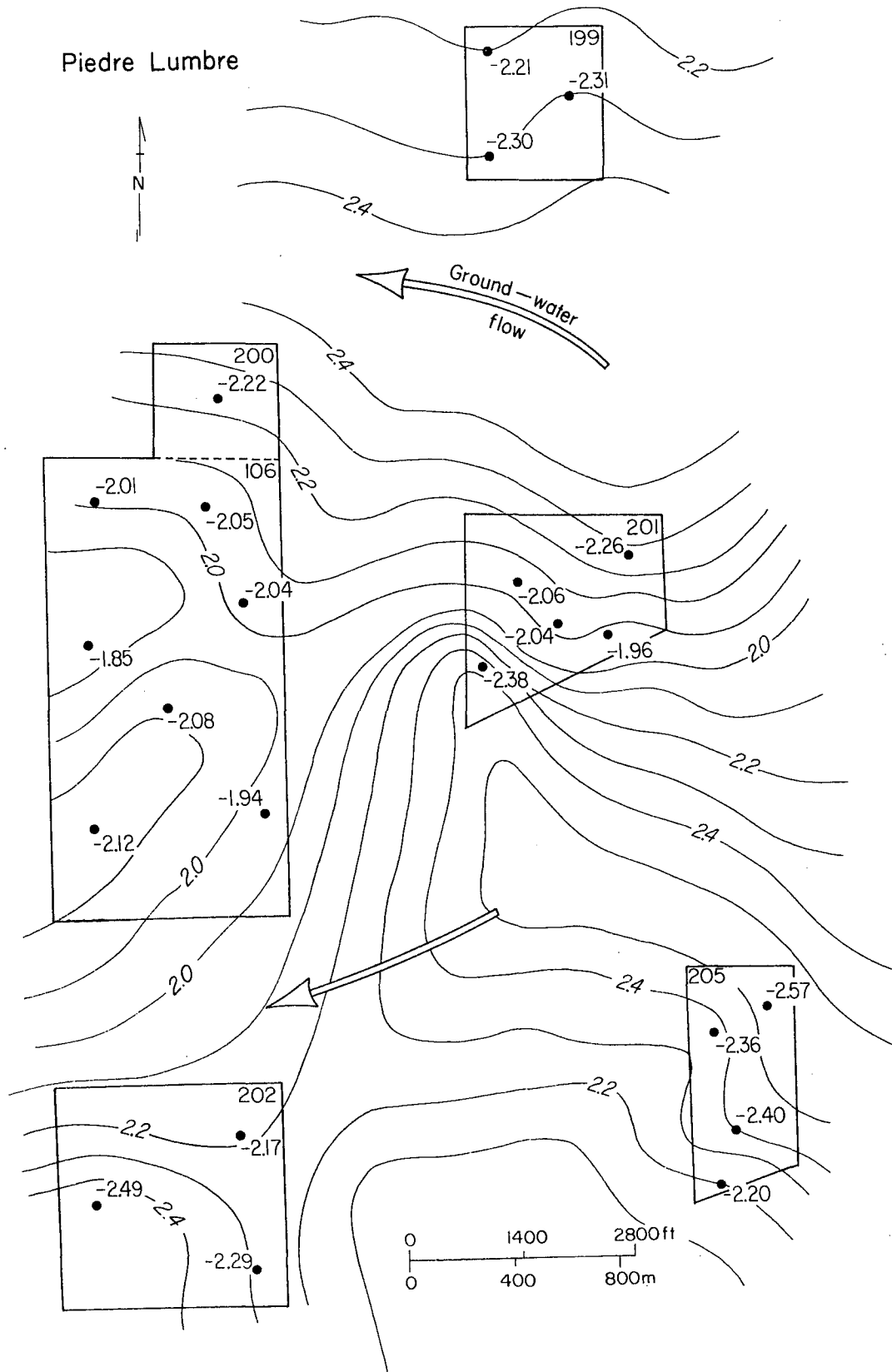


Figure 54. Map of X-axis values, $\log \frac{[Al(OH)_4]^{56}[H^+]^{24}}{[H_4SiO_4]}$, from Piedre Lumbre Na-montmorillonite - clinoptilolite activity diagram, figure 53. Less negative values are closer to Na-montmorillonite field or more highly supersaturated with respect to Na-montmorillonite.

Summary and Exploration Implications

Individual waters most closely associated with uranium mineralization plot on montmorillonite-clinoptilolite activity diagrams deepest into the montmorillonite field, or if in the clinoptilolite field closer to montmorillonite. In other words, waters more highly supersaturated with respect to montmorillonite show a positive correlation with uranium mineralization, whereas those more highly supersaturated with respect to clinoptilolite show little or no correlation. Implied is an important role for montmorillonite in uranium concentration and an unimportant role for clinoptilolite. High Ca^{2+} , Mg^{2+} , $\text{Al}(\text{OH})_4^-$, and H^+ ion activities favor the formation of montmorillonite relative to clinoptilolite (see log activity ratios figs. 39 and 40). Among these, low pH directly favors uranium concentration, as discussed above. Moreover, low pH might indirectly promote the formation of montmorillonite by increasing Ca^{2+} and Mg^{2+} activities through dissolution of carbonates and hydrolysis of silicates. High Na^+ and H_4SiO_4^0 activities promote the formation of clinoptilolite relative to montmorillonite; high activities for these species provide no special conditions advantageous to uranium accumulation. The negative correlation of clinoptilolite and uranium mineralization inferred from mineral-solution equilibria is the same as that seen in field and petrographic evidence. High log IAP/Ksp values for montmorillonite show fair positive correlation with uranium mineralization. Erratic and unpredictable distribution of log IAP/Ksp values for calcite relative to uranium occurrence implies an unimportant role for it in accumulation and supports a postmineralization origin for most calcite.

The mineral-solution equilibria approach, at the scale of individual deposits, has revealed positive geochemical correlations and trends with uranium mineralization. These are empirical relationships that are poorly understood at this time. To begin to understand their meaning requires, at a minimum, specific knowledge of the major uranium and associated solid phases, compositional data for those phases, representative analyses for dissolved aluminum, surface water analyses for comparison with deposit waters, and more precise location of mineralization fronts. Good compositional data are essential to writing representative reactions and to making better free energy estimates. Montmorillonite and clinoptilolite free energy values are the most uncertain part of this analysis and are more important than analytical errors in individual water analyses.

Geochemistry has a role to play in an integrated exploration effort of lithofacies mapping and geophysical logging. Applicability of mineral-solution equilibria to regional analysis remains to be demonstrated. One technique might be regional

mapping of log activity ratios taken from activity diagrams for major mineral species or of log IAP/Ksp values. Exploration priority should be given to those ratios and trends favoring the formation of minerals known to be associated with uranium ore. Statistical analysis of regional mineral-solution equilibria data, for example, trend surface analysis or mapping of factor scores, might be a way to locate anomalies for more detailed study (Hitchon, 1976).

The use of hydrochemistry in exploration requires computer capability to calculate activities; mapping of concentrations was singularly unsuccessful. Reliable sampling and analysis of waters is very important. Analytical accuracy and precision must be compatible with sophisticated computer programs now available for calculating mineral-solution equilibria. Analyses almost never include dissolved aluminium, which is essential for equilibria information about aluminosilicates, or reliable values for SiO₂, pH, temperature, Eh, and dissolved oxygen.

Trace metals were not reported at sensitivity levels low enough ($\mu\text{g/l}$) to reveal any meaningful relationships. Uranium, regarded as the best pathfinder element for uranium deposits, was reported in mg/l at a detection level of 0.1 mg/l in our data. In the Holiday-El Mesquite and Piedre Lumbre deposits, almost all the analyses were reported as less than 0.1 mg/l. Bruni and O'Hern have a halo of low values (less than 0.1 mg/l) around the ore; and within the ore values range from 0.1 to 1.0 mg/l. Unfortunately, accuracy and precision of the data do not permit evaluation of uranium as a pathfinder in the diverse hydrogeologic settings represented by the deposits studied: 1) ground-water flow from oxidized interior to reduced ground, 2) flow from reduced ground to oxidized interior, 3) flow approximately parallel to the front, and 4) vertical discharge of brines and re-reduction.

The high uranium concentrations in and about the deposits studied are compatible with the present hydrochemistry. As predicted from the Eh-pH diagram (fig. 33), uranium is mobile under conditions representative of the deposit waters: Eh of +240 to +300 mV, average pH 8.1, and HCO₃⁻ concentration of 200 to 500 mg/l. Furthermore, they are high-ionic strength waters more concentrated than waters believed necessary to form roll-type uranium deposits (Granger and Warren, 1978). Reducing and acid waters of any ionic strength might serve as models for Catahoula mineralization as long as they are supersaturated with respect to montmorillonite. Clearly, modern Catahoula waters are far different chemically from those favoring accumulation of uranium. They should never serve as a model for the primary mineralizing waters.

CONCLUSIONS

Uranium in the Catahoula aquifers was derived from early pedogenic and vadose alteration and leaching of newly deposited glass. Ground water circulating through surficial tuffaceous beds recharged shallow permeable units, initiating a coherent flux of oxidizing uranium-charged water through the semi-confined aquifers. Ash-rich crevasse and lacustrine margin units that had released uranium during earliest stages of diagenesis later became conduits for migration of uranium-charged waters originating in younger ash, and locally produced the geochemical environment suitable for efficient uranium concentration. Waters moving through the semi-confined aquifers evolved geochemically through reaction with the aquifer matrix and mixing with water masses discharged from underlying aquifers. A variety of geochemical and mineralogical changes, collectively described as epigenetic alteration, accompanied influx of the mineralizing waters. Uranium and associated trace metals were reduced and then concentrated, primarily by adsorption, along the relatively sharp Eh-pH gradient that developed at the margin of the alteration tongue where oxidants were rapidly consumed by reactions with sulfide and organic material. Either mechanism is favored by weakly acidic reducing media. Geometry as well as vertical and lateral extent of alteration is largely controlled by physical flow phenomena induced by the three-dimensional permeability framework of the host depositional system and principal recharge and discharge boundaries. Reductants included intrinsic organic debris, humate, or syngenetic iron sulfide; or pyrite formed from extrinsic sulfide dissolved in waters discharged from the underlying sediment pile. Significantly, both efficient release of uranium from its source and formation of primary uranium deposits occurred early in the history of the Catahoula aquifers, and by geologic standards were contemporaneous and rapid events. Processes responsible for ore formation neither had nor required millions of years to operate and the commonly accepted model of a mineralization front slowly marching through an aquifer is inappropriate.

Postmineralization changes in the ground-water flow system have superimposed a variety of geochemical and diagenetic trends not directly related to mineralization, and which locally obscure primary alteration patterns. For instance, calcite and clinoptilolite played an unimportant role in mineralization and are diagenetically late. The visually oxidized interior of alteration fronts is particularly fragile; especially in portions of the aquifer system where vertical discharge of deeper waters continues. Durable indicators of epigenetically altered strata include (1) the uniform near-absence of organic carbon, (2) lateral increase in the Fe^{+2}/Fe^{+3} ratio or in total sulfur

content, and (3) variation in gamma ray log signature or trace uranium content (ppm levels) of possible host units. Leaching and zeolitization of ash or a high proportion of Ca-montmorillonite in the clay fraction of a possible host indicate ground-water flushing, but neither appears to be directly correlative with mineralization.

In many areas modern ground-water flow dynamics and chemistry differ significantly from those of systems extant during primary mineralization. Modern waters associated with the deposits studied are not models for mineralizing waters. Recognition of this fact has considerable significance for understanding the origin of the deposits, as well as interpretation of drill data and results of hydrogeochemical surveys. Unraveling the geochemical environment of roll-type uranium deposits requires an understanding of the dynamic equilibrium of water-rock interaction. Advanced statistical techniques such as factor analysis are no substitute for calculated mineral-solution equilibria data. The mineral-solution equilibria approach is a potential method of geochemical exploration.

A simplified flow chart (fig. 56) illustrates the range of known and probable types of mineralization present in the Catahoula, and in other Coastal Plain uranium hosts as well. Gueydan deposits are found in a depositional environment conducive to early oxidation and subsequent, possibly ongoing intrusion of deep-seated, sulfide-rich waters. Reductants are dominantly extrinsic and the potential for re-reduction is high. Reduction is concentrated around fault zones, but extensive, updip migration of the intruded sulfidizing water masses means that mineralization need not be exclusively proximal to faulting. Widespread distribution of extrinsic sulfide favors laterally extensive, relatively uniform mineralization fronts. The Chita-Corrigan deposits will most commonly be associated with intrinsic reductants. Only deeply buried sections intersect fault zones, and modern ground-water chemistry does not indicate major intrusion of deeper waters along these zones. Large-scale epigenetic re-reduction is less likely. The preservation and abundance of early diagenetic or syngenetic iron sulfide and detrital organic material result from the shallower paleo-water table and greater organic productivity of the more humid upper Texas Oligocene Coastal Plain. Surplus recharge was likely discharged from shallow water-table portions of the aquifer system directly into surface drainage. Consequently a portion of the available uranium was lost, or accumulated as low-grade, syngenetic deposits in local lacustrine basins. Less total uranium and less extensive alteration tongues can be expected within the Chita-Corrigan. Mineralization will likely be erratic in grade because of the variable distribution of intrinsic reductants. Shmariovich (1977) describes changes in uranium deposit morphology resulting from increasingly dilute

URANIUM FLOW CHART – CATAHOULA FORMATION

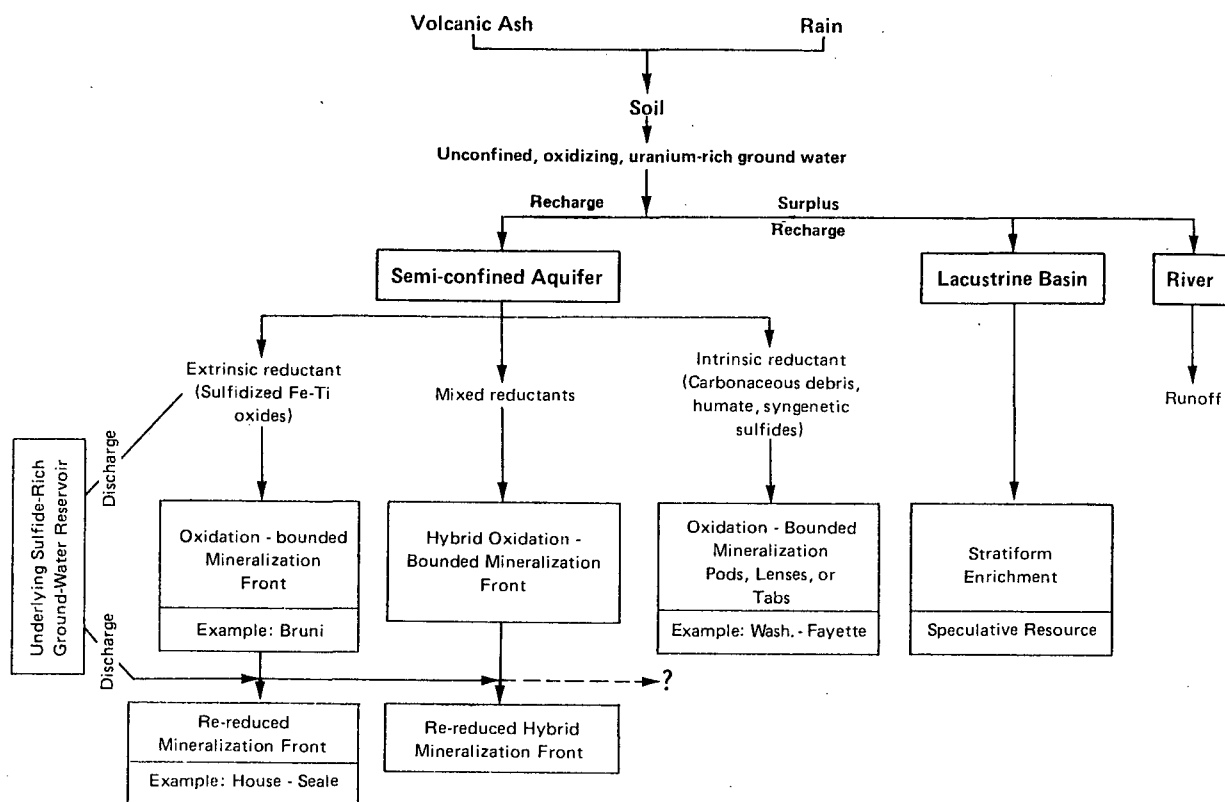


Figure 56. Family tree of Catahoula uranium deposits based on the various likely geochemical histories. Uranium dissolved from fresh glass by meteoric water that was rejected by semi-confined aquifers was discharged to the surface. Some syngenetic or very early epigenetic concentration occurred in organic-rich lacustrine sediments; however, most uranium entering the through-flowing surface drainage was lost. Uranium-charged waters recharging semi-confined aquifers encountered a reducing subsurface environment produced by intrinsic reductants, such as organic debris or syngenetic sulfides, or by previously intruded extrinsic reductants in the form of authigenic sulfide minerals. A mix of intrinsic and extrinsic reductants is possible, but has not been encountered in studied deposits. The superimposed oxidation/alteration pattern may be obscured if additional reducing waters discharge into the mineralized aquifer. Such re-reduction is a common feature of many Coastal Plain uranium deposits.

concentrations of uranium in the water. Pod-shaped ore bodies such as those present in the Washington-Fayette deposit form from dilute waters, further suggesting the diluting effect of rejected recharge in a wetter climate. Pod-shaped or tabular deposits will likely prove typical of the Chita-Corrigan system. Finally, the ready supply of meteoric water, rapid recharge, and continued active flushing of permeable parts of the aquifer have likely moderated the possible range of water chemistry, reducing abundance of postmineralization diagenetic features.

REFERENCES

- Ahschuler, Z. S., Dwornik, E. J., and Kramer, H., 1963, Transformation of montmorillonite to kaolinite during weathering: *Science*, v. 141, p. 148-152.
- Austin, S. R., 1970, Some patterns of sulfur isotope distribution in uranium deposits: *Wyoming Geological Association Earth Science Bulletin*, v. 3, no. 2, p. 5-20.
- Back, W., 1960, Origin of hydrochemical facies of ground water in the Atlantic Coastal Plain: 21st International Geological Congress, Copenhagen 1960, Report, pt. 1, p. 87-95.
- Berner, R. A., 1967, Thermodynamic stability of sedimentary iron sulfides: *American Journal of Science*, v. 265, p. 773-785.
- _____, 1970, Sedimentary pyrite formation: *American Journal of Science*, v. 268, p. 1-23.
- Boström, K., 1967, Some pH-controlling redox reactions in natural waters, in *Equilibrium concepts in natural water systems*: Washington, D. C., American Chemical Society Advances in Chemistry Series 67, p. 286-311.
- Breger, I. A., 1974, The role of organic matter in the accumulation of uranium: The organic geochemistry of the coal-uranium association, in *Formation of uranium ore deposits*: International Atomic Energy Agency, Panel Proceedings Series No. STI/PUB/374, p. 99-124.
- Brookins, D. G., 1975a, Coffinite-uraninite stability relations in Grants mineral belt, New Mexico (abst): *American Association of Petroleum Geologists*, v. 59, p. 905.
- _____, 1975b, Uranium deposits of the Grants, New Mexico mineral belt: Grand Junction, Colo., U. S. Energy Research and Development Administration, contract No. AT(05-1)-1636-1, 143 p.
- _____, 1976, The Grants mineral belt, New Mexico: comments on the coffinite-uraninite relationship, probable clay mineral reactions, and pyrite formation, in Woodward, L. A., and Northrop, S. A., eds., *Tectonics and mineral resources of southwestern North America*: New Mexico Geological Society Special Paper No. 6., p. 158-166.
- Brooks, R. A., and Campbell, J. A., 1976, Preliminary investigation of the elemental variation and diagenesis of a tabular uranium deposit, La Sal Mine, San Juan County, Utah: U. S. Geological Survey Open-File Report 76-287, 30 p.
- Chebotarev, I. I., 1955, Metamorphism of natural waters in the crust of weathering: *Geochimica et Cosmochimica Acta*, v. 8, p. 22-48, 137-170, 198-212.

- Chen, Chao-Hsia, 1975, A method of estimation of standard free energies of formation of silicate minerals at 298.15°K: *American Journal of Science*, v. 275, p. 801-817.
- Cheney, E. S., and Trammell, J. W., 1973, Isotopic evidence for inorganic precipitation of uranium roll ore bodies: *American Association of Petroleum Geologists Bulletin*, v. 57, No. 7, p. 1297-1304.
- Davies, D. K., and Almon, W. R., 1977, Diagenesis of Tertiary volcanoclastics, Guatemala (abstract): *American Association of Petroleum Geologists-Society of Economic Paleontologists and Mineralogists, Rocky Mountain Sections, 26th Annual Meeting, Denver, Abstracts with Program*, p. 50
- Dement'yev, V. S., and Syromyatnikov, N. G., 1968, Conditions of formation of a sorption barrier to the migration of uranium in an oxidizing environment: *Geochemistry International*, v. 5, p. 394-400.
- Doi, K., Hironi, S., and Sakamaki, Y., 1975, Uranium mineralization by ground water in sedimentary rocks, Japan: *Economic Geology*, v. 70, p. 628-646.
- Dooley, J. R., Jr., 1958, The radioluxograph: A fast, simple type of autoradiograph, *in Proceedings of the 2d United Nations International Conference on the Peaceful Use of Atomic Energy*, v. 3, Processing of Raw Materials: Geneva, United Nations, Paper 1762, p. 550-553.
- Dooley, J. R., Jr., Conwell, C. N., Berendsen, P., Otton, J. K., Pierson, C. T., Hoisington, W. D., Lindsey, D. A., and Rosholt, J. N., 1977, Examples of uranium distribution in geologic rock specimens illustrated with the radioluxograph, induced fission tracks and other tracks methods, *in Campbell, J. A., ed., Short papers of the U. S. Geological Survey uranium-thorium symposium: U. S. Geological Survey Circular 753*, p. 32.
- Eargle, D. H., Dickinson, K. A., and Davis, B. O., 1975, South Texas uranium deposits: *American Association of Petroleum Geologists Bulletin*, v. 59, No. 5, p. 766-779.
- Eugster, H. P., and Chou, I-Ming, 1973, The depositional environments of Precambrian banded iron-formations: *Economic Geology*, v. 68, p. 1144-1168.
- Fitz Patrick, E. A., 1971, *Pedology*: Edinburgh, Oliver and Boyd, 306 p.
- Folk, R. L., 1974, *Petrology of sedimentary rocks*: Austin, Hemphill Publishing Co., 182 p.
- Gabelman, J. W., 1977, Migration of uranium and thorium: exploration significance: *American Association of Petroleum Geologists Studies in Geology No. 3*, 168 p.

- Galloway, W. E., 1977, Catahoula Formation of the Texas Coastal Plain: depositional systems, composition, structural development, ground-water flow history, and uranium distribution: The University of Texas at Austin, Bureau of Economic Geology Report of Investigations No. 87, 59 p.
- Galloway, W. E., Kreitler, C. W., and McGowen, J. H., 1979, Depositional and ground-water flow systems in the exploration for uranium--A research colloquium: The University of Texas at Austin, Bureau of Economic Geology.
- Gamble, D. S., and Schnitzer, M., 1973, The chemistry of fulvic acid and its reactions with metal ions, *in* Singer, P. C., ed., Trace metals and metal-organic interactions in natural waters: Ann Arbor Science Publication, p. 265-302.
- Garrels, R. M., and Christ, C. L., 1965, Solutions, Minerals, and Equilibria: Harper and Row, New York,, 450 p.
- Gavshin, V. M., Bobrov, V. A., Pyalling, A. O., and Reznikov, N. V., 1973, The two types of uranium accumulation in rocks by sorption: *Geochemistry International*, v. 10, No. 3, p. 682-690.
- Goldhaber, M. B., and Reynolds, R. L., 1977, Geochemical and mineralogical studies of a South Texas roll front uranium deposit: U. S. Geological Survey Open-File Report 77-821, 34 p.
- Goldhaber, M. B., Reynolds, R. L., and Rye, R. O., 1978, Origin of a South Texas roll-type uranium deposit: 2. petrology and sulfur isotope studies: *Economic Geology*, v. 73, no. 8, p. 1690-1705.
- Granger, H. C., and Warren, C. G., 1969, Unstable sulfur compounds and the origin of roll-type uranium deposits: *Economic Geology*, v. 64, p. 160-171.
- _____ 1978, Some speculations on the genetic geochemistry and hydrology of roll-type uranium deposits, *in* Guidebook 13th Annual Field Conference: Wyoming Geological Association, p. 349-361.
- Gronvold, F., and Westrum, E. F., Jr., 1976, Heat capacities of iron disulfides, thermodynamics of marcasite from 5 to 700 K, pyrite from 300 to 780 K, and the transformation of marcasite to pyrite: *Journal of Chemical Thermodynamics*, v. 8, p. 1039-1048.
- Harshman, E. N., 1966, Genetic implications of some elements associated with uranium deposits, Shirley basin, Wyoming: U. S. Geological Survey Professional Paper 550-C, p. 167-173.

- 1974, Distribution of elements in some roll-type uranium deposits; in Formation of uranium ore deposits: International Atomic Energy Agency Panel Proceedings No. STI/PUB 374, p. 169-183.
- Hay, R. L., 1977, Geology of zeolites in sedimentary rocks, in Mumpton, F. A., ed., Mineralogy and geology of natural zeolites: Mineralogical Society of America, Short Course Notes, v. 4, p. 53-64.
- Hay, R. L., and Sheppard, R. A., 1977, Zeolites in open hydrologic systems; in Mumpton, F. A., ed., Mineralogy and geology of natural zeolites: Mineralogical Society of America, Short Course Notes, v. 4, 93-102.
- Hem, J. D., 1970, Study and interpretation of the chemical characteristics of natural water: U. S. Geological Survey Water-Supply Paper 1473, 358 p.
- Henry, C. D., and Tyner, G. N., 1978, Alteration and uranium release from rhyolitic igneous rocks: examples from the Mitchell Mesa Rhyolite, Santana Tuff, Chinati Mountains Group, and Allen Complex, Trans-Pecos Texas, in Henry, C. D., and Walton, A. W., principal investigators, Formation of uranium ores by diagenesis of volcanic sediments: Grand Junction, Colo., Bendix Field Engineering Corporation Rept. GJBX-22 (79), 440 p.
- Hitchon, B., 1976, Hydrogeochemical aspects of mineral deposits in sedimentary rocks (ch. 3), in Wolf, K. H., ed., Handbook of strata-bound and stratiform ore deposits, v. 2: New York, Elsevier Scientific Publishing Company, p. 53-66.
- Hostetler, P. B., and Christ, C. L., 1968, Studies in the system $MgO-SiO_2-CO_2-H_2O(l)$: the activity-product constant of chrysotile: *Geochimica et Cosmochimica Acta*, v. 32, p. 485-497.
- Hostetler, P. B., and Garrels, R. M., 1962, Transportation and precipitation of uranium and vanadium at low temperatures, with special reference to sandstone-type uranium deposits: *Economic Geology*, v. 57, p. 137-167.
- Huang, W. H., 1977, Stability relations of uraninite and coffinite in sedimentary environment: *Geological Society of America Abstracts with Programs*, v. 9, no. 7, p. 1029.
- Huang, W. H., and Keller, W. D., 1972, Organic acids as agents of chemical weathering of silicate minerals: *Nature*, v. 239, p. 149-151.
- Jonas, E. C., and Roberson, H. E., 1965, Structural charge density as indicated by montmorillonite hydration: *Clays and Clay Minerals*, v. 13, p. 223-230.

- Katayama, N., Kubo, K., and Hironi, S., 1974, Genesis of uranium deposits of the Tono mine, Japan, in *Proceedings of Formation of Uranium Ore Deposits Symposium: Vienna, International Atomic Energy Agency, STI/PUB/374, Paper IAEA-SM-183/11, p. 437-452.*
- Kittrick, J. A., 1966, Free energy formation of kaolinite from solubility measurements: *American Mineralogist*, v. 51, p.1457-1466.
- Kochenov, A. V., Korolev, K. G., Dubinchuk, V. T., and Medvedev, Yu. L.; 1977, Experimental data on the conditions of precipitation of uranium from aqueous solutions: *Geochemistry International*, v. 14, p. 82-87.
- Kochenov, A. V., Zinev'yev, V. V., and Lovaleva, S. A., 1965, Some features of the accumulation of uranium in peat bogs: *Geochemistry International*, v. 2, no. 1, p. 65-70.
- Koglin, E., Schenk, H. J., and Schwochau, K., 1978, Spectroscopic studies on the binding of uranium by brown coal: *Applied Spectroscopy*, v. 32, no. 5, p. 486-488.
- Langmuir, D., 1978, Uranium solution-mineral equilibria at low temperatures with applications to sedimentary ore deposits: *Geochimica et Cosmochimica Acta*, v. 42, no. 6, p. 547-569.
- Lindemann, W. L., 1963, Catahoula Formation, Duval County, Texas: University of Texas, Master's thesis, 192 p.
- Lisitsin, A. K., 1969, Conditions of molybdenum and selenium deposition in exogenous epigenetic uranium deposits: *Lithology and Mineral Resources*, no. 5, p. 541-548.
- Lisitsin, A. K., Kruglov, A. I., Panteleev, V. M., and Sidel'nikova, V. D., 1967, Conditions of uranium accumulation in low-moor oxbow peat bogs: *Lithology and Mineral Resources*, No. 3, p. 360-370.
- Lisitsin, A. K., and Kuznetsnova, E. C., 1967, Role of microorganisms in development of geochemical reduction barriers where limonitization bedded zones wedge-out: *International Geology Review*, v. 9, no. 9, p. 1180-1191.
- Mumpton, F. A., 1977, Natural zeolites, in Mumpton, F. A., ed., *Mineralogy and geology of natural zeolites*: Washington, D. C., Mineralogical Society of America, Short Course Notes, v. 4, p. 1-17.
- Nichols, C. E., Butz, T. R., Cagle, G. W., and Kane, V. E., 1977, Uranium geochemical survey in the Crystal City and Beeville Quadrangles, Texas: Union Carbide Oak Ridge Gaseous Diffusion Plant, Uranium Resources Evaluation Project, prepared for U. S. Energy Research and Development Administration, under contract W-7405 eng 26, 111 p.

- Payne, J. N., 1970, Geohydrologic significance of lithofacies of the Cockfield Formation of Louisiana and Mississippi and of the Yegua Formation of Texas: U. S. Geological Survey Professional Paper 569-B, p. B1-B14.
- _____ 1975, Geohydrologic significance of lithofacies of the Carrizo Sand of Arkansas, Louisiana, and Texas, and the Meridian Sand of Mississippi: U. S. Geological Survey Professional Paper 569-D, 11 p.
- Reynolds, R. L., and Goldhaber, M. B., 1978, Origin of a South Texas roll-type uranium deposit: 1. Alteration of iron-titanium oxide minerals: *Economic Geology*, v. 73, no. 8, p. 1677-1689.
- Reynolds, R. L., Goldhaber, M. B., and Granch, R. I., 1977, Uranium associated with iron-titanium oxide minerals and their alteration products in a South Texas roll-type deposit: U. S. Geological Survey Circular 753, p. 37-39.
- Rickard, D. T., 1969a, The microbiological formation of iron sulphides: *Stockholm Contributions in Geology*, v. 20, no. 3, p. 49-66.
- _____ 1969b, The chemistry of iron sulphide formation at low temperatures: *Stockholm Contributions in Geology*, v. 20, no. 4, p. 67-95.
- Robie, R. A., Hemingway, B. S., and Fisher, J. R., 1978, Thermodynamic properties of minerals and related substances at 298.15K and 1 bar (10^5 Pascals) pressure and at higher temperatures: U. S. Geological Survey Bulletin 1452, 456 p.
- Rose, W. I., Jr., 1977, Scavenging of volcanic aerosol by ash: atmospheric and volcanologic implications: *Geology*, v. 5, p. 621-624.
- Ross, C. S., and Hendricks, S. B., 1945, Minerals of the montmorillonite group, their origin and relation to soils and clays: U. S. Geological Survey Professional Paper 205-B, p. 23-79.
- Shmariovich, Ye. M., 1973, Identification of epigenetic oxidation and reduction as impositions on sedimentary rock: *International Geology Review*, v. 15, no. 11, p. 1333-1340.
- _____ 1977, The mechanism of layer-infiltration ore-deposition: *International Geology Review*, v. 19, p. 137-144.
- Spirakis, C. S., Goldhaber, M. B., and Reynolds, R. L., 1977, Thermoluminescence of sand grains around a South Texas roll-type deposit: U. S. Geological Survey Open-File Report 77-640, 13 p.
- Szalay, A., and Szilagy, M., 1969, Accumulation of micro-elements in peat humic acids and coal, in Schenck, P. A., and Havenaar, eds., *Advances in organic geochemistry 1968*: Oxford, Pergamon Press, p. 567-578.

- Tardy, Y., and Garrels, R. M., 1974, a method of estimating the Gibbs energies of formation of layer silicates: *Geochimica et Cosmochimica Acta*; v. 38, p. 1101-1116.
- Taylor, P. S., and Stoiber, R. E., 1973, Soluble material on ash from active Central American volcanoes: *Geological Society of America Bulletin*, v. 84, p. 1031-1042.
- Tóth, József, 1972, Properties and manifestations of regional ground-water movement: *International Geological Congress, 24th, 1972, Proceedings*, p. 153-163.
- Truesdell, A. H., and Jones, B. F., 1974, WATEQ, a computer program for calculating chemical equilibria of natural waters: *U. S. Geological Survey Journal of Research*, v. 2, no. 2, p. 233-248.
- Turcan, A. N., Jr., 1966, Calculation of water quality from electrical logs: theory and practice: Louisiana Department of Conservation, Louisiana Geological Survey and Louisiana Department of Public Works, in cooperation with the U. S. Geological Survey, Water Resources Pamphlet no. 19, 23 p.
- Vasil'eva, E. G., 1972, Simulation of depositional processes of uranium, selenium, and molybdenum during the interaction between metal-bearing oxygenated waters and a counterflow of gaseous reducing agents: *Lithology and Mineral Resources*, v. 7, no. 6, p. 703-713.
- Wagman, D. D., Evans, W. H., Parker, V. B., Halow, I., Bailey, S. M., and Schumm, R. H., 1968, Selected values of chemical thermodynamic properties: National Bureau of Standards Technical Note 270-3, 264 p.
- _____ 1969, Selected values of chemical thermodynamic properties: National Bureau of Standards Technical Note 270-4, 152 p.
- Walker, T. R., Waugh, B., and Grove, A. J., 1978, Diagenesis in first-cycle desert alluvium of Cenozoic age, southwestern United States and northwestern Mexico: *Geological Society of America Bulletin*, v. 89, p. 19-32.
- Walton, A. W., 1975, Zeolitic diagenesis in Oligocene volcanic sediments, Trans-Pecos Texas: *Geological Society of America Bulletin*, v. 86, p. 615-624.
- _____ 1978, Release of uranium during alteration of volcanic glass, in Henry, C. D., and Walton, A. W., principal investigators, Formation of uranium ores by diagenesis of volcanic sediments: Grand Junction, Colo., Bendix Field Engineering Corporation Rept. GJBX-22 (79), 440 p.
- Zielinski, R. A., 1977, Uranium mobility during interaction of rhyolitic glass with alkaline solutions: dissolution of glass: U. S. Geological Survey Open-File Report 77-744, 36 p.

Zobell, C. E., 1964, Geochemical aspects of the microbial modification of carbon compounds, *in* Colombo, U., and Hobson, G. D., eds., *Advances in organic chemistry 1962*: Oxford, Pergamon Press, p. 339-356.

APPENDIX A

Key Free Energy Values

<u>Aqueous Species</u>	ΔG_f° (kcal/mole)	<u>Source</u>
U ⁴⁺	-126.9	Langmuir, 1978
UO ₂ ²⁺	-227.7	Langmuir, 1978
UO ₂ ⁺	-231.5	Langmuir, 1978
U(OH) ₂ ²⁺	-237.5	Langmuir, 1978
U(OH) ₅ ⁻	-392.4	Langmuir, 1978
UO ₂ (OH) ⁺	-276.5	Langmuir, 1978
UO ₂ CO ₃ ⁰	-367.6	Langmuir, 1978
UO ₂ (CO ₃) ₂ ²⁻	-503.2	Langmuir, 1978
UO ₂ (CO ₃) ₃ ⁴⁻	-635.4	Langmuir, 1978
UO _{2am}	-239.0	Langmuir, 1978
USiO _{4am}	-442.3	Langmuir, 1978
USiO _{4c}	-452.0	Langmuir, 1978
SiO _{2am}	-202.9	Langmuir, 1978
H ₄ SiO ₄ ⁰	-312.6	Hostetler and Christ, 1968
SiO ₂ glass	-203.3	Robie and others, 1978
H ₂ CO ₃ ⁰	-149.0	Garrels and Christ, 1965
HCO ₃ ⁻	-140.3	Garrels and Christ, 1965
CO ₃ ²⁻	-126.2	Garrels and Christ, 1965
H ₂ O _l	-56.7	Garrels and Christ, 1965

Key Free Energy Values (continued)

<u>Aqueous Species</u>	ΔG_f° (kcal/mole)	<u>Source</u>
S^{2-}	20.5	Wagman and others, 1968
S_2^{2-}	19.0	Wagman and others, 1968
H_2S	-6.7	Wagman and others, 1968
HS^-	2.9	Wagman and others, 1968
SO_4^{2-}	-178.0	Wagman and others, 1968
HSO_4^-	-180.7	Wagman and others, 1968
HSO_3^-	-126.2	Wagman and others, 1968
SO_3^{2-}	-116.3	Wagman and others, 1968
$H_2SO_3^0$	-128.6	Wagman and others, 1968
$S_2O_3^{2-}$	-127.2	Garrels and Christ, 1965
$HS_2O_3^-$	-129.5	Garrels and Christ, 1965
FeS, mackinawite	-22.3	Berner, 1967
FeS ₂ , pyrite	-38.3	Berner, 1967
FeS ₂ , marcasite	-37.9	Gronvold and Westrum, 1976
Fe ²⁺	-18.9	Wagman and others, 1969
Fe ³⁺	-1.1	Wagman and others, 1969
Fe(OH) ₂ ⁺	-104.7	Wagman and others, 1969
Fe(OH) ₃ am	-166.5	Wagman and others, 1969
Fe(OH) ²⁺	-54.4	Eugster and Chou, 1973
Fe(OH) ⁺	-64.2	Eugster and Chou, 1973
Fe(OH) ₃ ⁻	-145.3	Eugster and Chou, 1973
C ₆ H ₅ COOH, benzoic acid	-52.9 ^a	Wagman and others, 1968

^a estimated from gas/aqueous ratio for CH₃COOH and HCOOH

Key Free Energy Values (continued)

<u>Aqueous Species</u>	ΔG_f° (kcal/mole)	<u>Source</u>
Ca ²⁺	-132.2	Garrels and Christ, 1965
Mg ²⁺	-109.0	Garrels and Christ, 1965
Na ⁺	-62.6	Garrels and Christ, 1965
K ⁺	-67.5	Garrels and Christ, 1965
Al(OH) ₄ ⁻	-310.0	Kittrick, 1966
Ca _{0.16} (Al _{1.56} Mg _{0.5})Si ₄ O ₁₀ (OH) ₂ Ca-montmorillonite	-1277.2	Appendix B
Na _{0.33} (Al _{1.56} Mg _{0.5})Si ₄ O ₁₀ (OH) ₂ Na-montmorillonite	-1276.0	Appendix B
NaAlSi ₅ O ₁₂ · 4H ₂ O clinoptilolite	-1526.0	Appendix B

APPENDIX B

CALCULATION OF FREE ENERGIES OF FORMATION FOR MONTMORILLONITE AND CLINOPTILOLITE

Montmorillonite

The method of Tardy and Garrels (1974) permits estimation of the free energies of formation of compositionally complex layer silicates such as montmorillonite. It is based on the assumption that the oxide and hydroxide components of the layer silicates have fixed free energies of formation within the silicate. The general rule is that all components are treated as oxides, with the exception of Mg, which is treated as Mg(OH)_2 in all silicates. Tables B-1 and B-2 show the method of estimation of free energies of formation (ΔG_f°) of the Ca-montmorillonite and Na-montmorillonite used in this paper.

Clinoptilolite

The method of Chen (1975) permits estimation of the free energies of formation of framework silicates such as zeolite. The ΔG_f° of the mineral in question can be estimated by the limit of extrapolation of $\Sigma \Delta G_f^\circ$; that is, the sum of ΔG_f° of many different component compounds forming the mineral. Table B-3 is a series of reactions written with different compounds to form the clinoptilolite used in this paper. The resulting $\Sigma \Delta G_f^\circ$'s are ranked, plotted, and extrapolated to obtain ΔG_f° for clinoptilolite (fig. B-1).

Table B-1. Calculation of ΔG_f° of Ca-montmorillonite,
 $\text{Ca}_{.16}(\text{Al}_{1.56}\text{Mg}_{.50})\text{Si}_4\text{O}_{10}(\text{OH})_2$

<u>Component</u>	<u>Moles</u>	<u>$\Delta G^\circ_{\text{sil/mol}}$</u>	<u>ΔG° kcal/mole</u>
CaOex ^a	0.16	-182.8	-29.25
Al ₂ O ₃ sil ^b	0.78	-382.4	-298.27
Mg(OH) ₂ sil	0.50	-203.3	-101.65
SiO ₂ sil	4.00	-204.6	-818.40
H ₂ Osil	0.50	-59.2	-29.60
			-1277.17 = ΔG_f°

^aex refers to the ΔG_f° value of ions in exchange sites,
treating them as oxides

^bsil refers to the ΔG_f° value for elements within the
silicate structure, treating them as oxides

Table B-2. Calculation of ΔG_f° of Na-montmorillonite,
 $\text{Na}_{.33}(\text{Al}_{1.56}\text{Mg}_{.50})\text{Si}_4\text{O}_{10}(\text{OH})_2$

<u>Component</u>	<u>Moles</u>	<u>$\Delta G^\circ_{\text{sil/mol}}$</u>	<u>ΔG° kcal/mole</u>
Na ₂ Oex	0.16	-175.4	-28.06
Al ₂ O ₃ sil	0.78	-382.4	-298.27
Mg(OH) ₂ sil	0.50	-203.3	-101.65
SiO ₂ sil	4.00	-204.6	-818.40
H ₂ Osil	0.50	-59.2	-29.60
			-1275.98 = ΔG_f°

Table B-3. Reactions to form Clinoptilolite, $\text{NaAlSi}_5\text{O}_{12} \cdot 4\text{H}_2\text{O}$

	$\Sigma \Delta G_f^\circ$ (kcal/mole)	Rank
$\frac{1}{2}\text{Na}_2\text{O} + \frac{1}{2}\text{Al}_2\text{O}_3 + 5\text{SiO}_2 + 4\text{H}_2\text{O}$	-1484.13	0
$\frac{1}{2}\text{Na}_2\text{O} + \frac{1}{2}\text{Al}_2\text{SiO}_5 + 4\frac{1}{2}\text{SiO}_2 + 4\text{H}_2\text{O}$	-1484.84	
$\frac{1}{2}\text{Na}_2\text{SiO}_3 + \frac{1}{2}\text{Al}_2\text{SiO}_5 + 4\text{SiO}_2 + 4\text{H}_2\text{O}$	-1507.93	1
$\text{NaAlSiO}_4 + 4\text{SiO}_2 + 4\text{H}_2\text{O}$	-1515.02	2
$\text{NaAl}(\text{SiO}_3)_2 + 3\text{SiO}_2 + 4\text{H}_2\text{O}$	-1517.92	3
$\text{NaAlSi}_2\text{O}_6 \cdot \text{H}_2\text{O} + 3\text{SiO}_2 + 3\text{H}_2\text{O}$	-1518.28	
$\text{NaAlSi}_3\text{O}_8 + 2\text{SiO}_2 + 4\text{H}_2\text{O}$	-1520.05	4

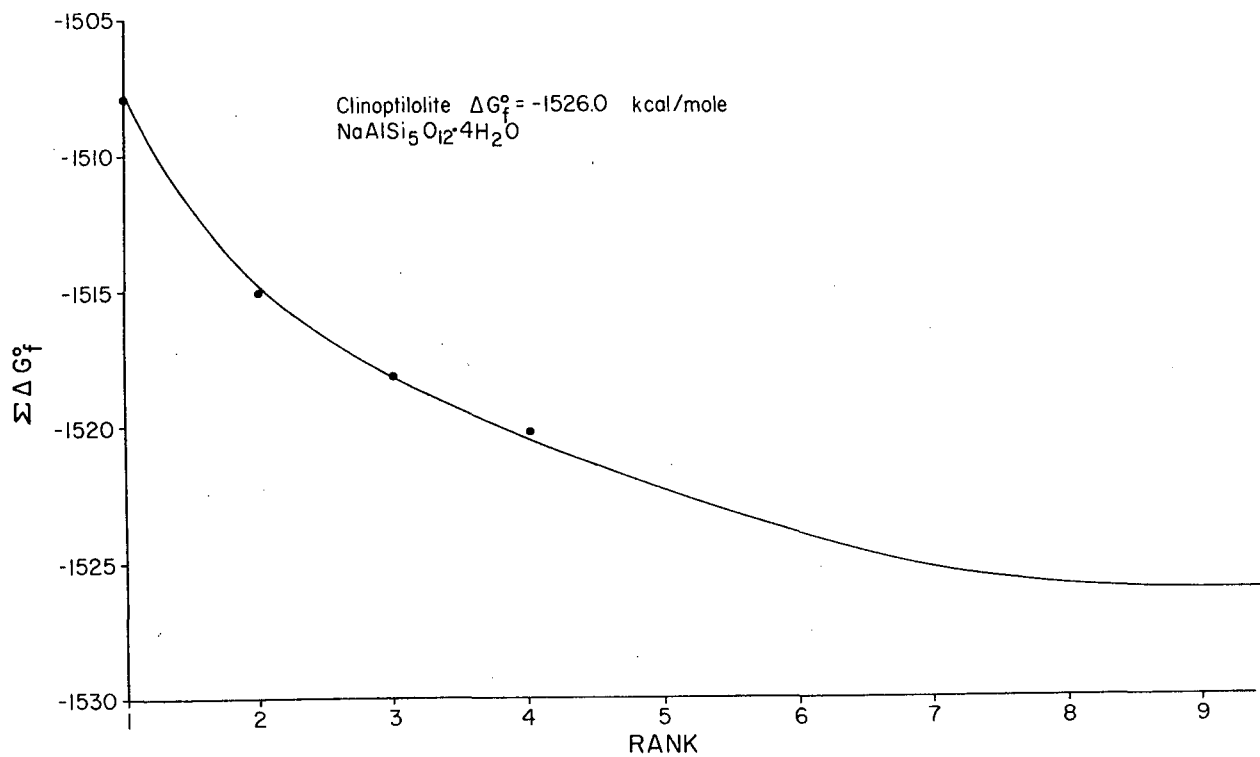


Figure B-1. Sum of ΔG_f° clinoptilolite versus rank.